AD-A094 575 MINNESOTA UNIV MINNEAPOLIS DEPT OF MECHANICAL ENGIN--ETC F/G 20/4
EXPERIMENTAL AND COMPUTATIONAL STUDIES OF HEAT TRANSFER IN COMP--ETC(U)
JAN 81 E M SPARROW, S V PATANKAR N00014-79-C-0621

UNCLASSIFIED NL

AD A094 575

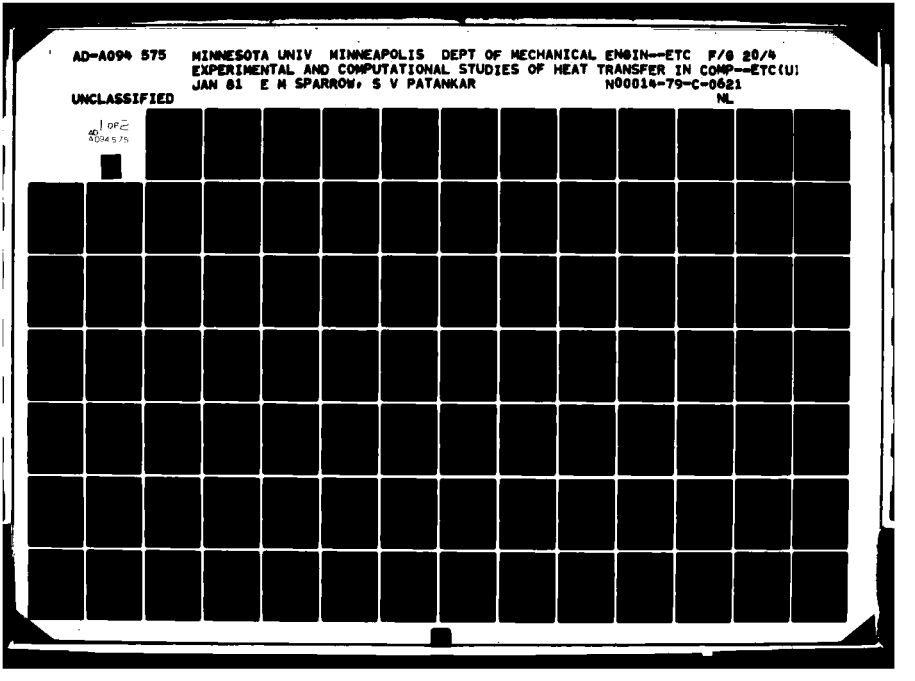

EXPERIMENTAL AND COMPUTATIONAL STUDIES OF HEAT TRANSFER IN COMPLEX INTERNAL FLOWS

E. M. Sparrow

S. V. Patankar

First Summary Report
Contract N00014-79-C-0621
Power Program, Office of Naval Research

January, 1981

Department of Mechanical Engineering
University of Minnesota
Minneapolis, Minnesota 55455

EXPERIMENTAL AND COMPUTATIONAL STUDIES OF HEAT TRANSFER IN COMPLEX INTERNAL FLOWS

E. M. Sparrow

S. V. Patankar

First Summary Report
Contract N00014-79-C-0621
Power Program, Office of Naval Research

January, 1981

Department of Mechanical Engineering
University of Minnesota
Minneapolis, Minnesota 55455

SECURITY CLASSIFICATION OF THIS PAGE *(When Data Entered)*

REPORT DOCUMENTATION PAGE

READ INSTRUCTIONS BEFORE COMPLETING FORM

1. REPORT NUMBER: N00014-79-C-0621-1981A
2. GOVT ACCESSION NO.: AD A094575
3. RECIPIENT'S CATALOG NUMBER:

4. TITLE (and Subtitle): EXPERIMENTAL AND COMPUTATIONAL STUDIES OF HEAT TRANSFER IN COMPLEX INTERNAL FLOWS
5. TYPE OF REPORT & PERIOD COVERED: Summary Report, No. 1, Sept 1979 to Dec 1980
6. PERFORMING ORG. REPORT NUMBER:

7. AUTHOR(s): E. M. Sparrow and S. V. Patankar
8. CONTRACT OR GRANT NUMBER(s): N00014-79-C-0621

9. PERFORMING ORGANIZATION NAME AND ADDRESS: Department of Mechanical Engineering, University of Minnesota, Minneapolis, MN 55455
10. PROGRAM ELEMENT, PROJECT, TASK AREA & WORK UNIT NUMBERS: Work Unit NR097-437

11. CONTROLLING OFFICE NAME AND ADDRESS: Power Program, Office of Research, 800 North Quincy Street, Arlington, Virginia 22217
12. REPORT DATE: January 1981
13. NUMBER OF PAGES: 119

14. MONITORING AGENCY NAME & ADDRESS *(if different from Controlling Office)*:
15. SECURITY CLASS. *(of this report)*: Unclassified
15a. DECLASSIFICATION/DOWNGRADING SCHEDULE:

16. DISTRIBUTION STATEMENT *(of this Report)*:
Approved for public release; distribution unlimited

17. DISTRIBUTION STATEMENT *(of the abstract entered in Block 20, if different from Report)*:

18. SUPPLEMENTARY NOTES:

19. KEY WORDS *(Continue on reverse side if necessary and identify by block number)*:
Heat exchangers, ducts, pressure drop, plenum, mixing, tees, fins, noncircular ducts, rectangular ducts, triangular ducts, heat transfer coefficients

20. ABSTRACT *(Continue on reverse side if necessary and identify by block number)*:
The details of five distinct pieces of research are set forth in this report. These research problems are interrelated in that they deal with various aspects of complex duct flows. Four of the research problems are experimental in nature. The first deals with the influence of plenum chamber geometry on the heat transfer and fluid flow characteristics in tubes situated downstream of the plenum. In the second experimental problem,

DD FORM 1 JAN 73 1473 EDITION OF 1 NOV 65 IS OBSOLETE
S/N 0102-LF-014-6601

Unclassified
SECURITY CLASSIFICATION OF THIS PAGE *(When Data Entered)*

the mixing of fluids of different temperatures in a tee is studied. The third experiment is focused on the fluid flow (without heat transfer) in arrays of longitudinal fins, while the last of the experiments treats a nonuniformly heated noncircular duct. The objective of the analytical work was to develop a turbulence model for rectangular passages, and one of the test cases for the model was to predict the friction factors that had been measured for the longitudinal fin arrays.

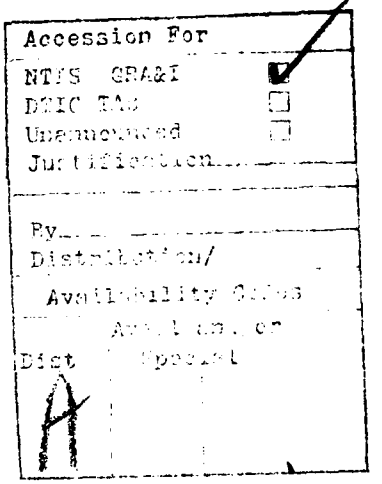

TABLE OF CONTENTS

INTRODUCTION TO THE REPORT

Power producing systems generally encompass a wide variety of complex fluid flows. The complexity of the flow may result from changes in cross section (both abrupt and gradual), partial blockages due to valves and other control devices, branching or merging of flow passages, changes of direction due to bends and elbows, and noncircular cross sections. The patterns of fluid flow which are caused by these geometrical features depart significantly from the flow patterns that are encountered in conventional ducts. Flow separation, recirculation (i.e., backflow), swirl, asymmetry, and maldistribution are among the ingredients which distinguish complex flows from conventional ones.

Among the external manifestations of these flow processes are increased pressure losses and possible unsteadiness. Perhaps of even greater significance are the heat transfer ramifications. For example, the heat transfer coefficients in a region of flow separation may either be substantially lower or substantially higher than that for a uniform flow, depending on the Reynolds number. In general, large variations of the local heat transfer coefficient can be expected in complex flows, in contrast to the relatively uniform coefficients that are characteristic of conventional flows. These variations may give rise to local hot spots. In addition, it can be expected that on the average, the general level of the transfer coefficient will be higher in complex flows. There is ample evidence that heat transfer coefficients for complex duct flows cannot be determined by extrapolating information for conventional duct flows.

The foregoing remarks provide the rationale for the research program whose initial results are set forth in this report. There are two complementary parts to the research. One part consists of a sequence of heat transfer and fluid flow experiments in which the effects of all the aforementioned complex flow processes are to be studied. These experiments are not aimed at reproducing specific applications; rather, they are designed to reproduce the flow and heat transfer

processes that are involved in the applications. It is planned to conduct the experiments with great care and attention to detail so that the results can serve as a standard for testing the efficacy of candidate analytical models. The other part of the research is analytical and numerical. Its thrust is to interact with the experiments in such a way as to provide predictions of the experimental results.

This report describes the research that was completed during the first funding period of the project, extending from September 15, 1979 to December 15, 1980. The details of five distinct pieces of research are set forth. These research problems are interrelated in that they deal with various aspects of complex duct flows.

Four of the research problems are experimental in nature. The first deals with the influence of plenum chamber geometry on the heat transfer and fluid flow characteristics in tubes situated downstream of the plenum. In the second experimental problem, the mixing of fluids of different temperatures in a tee is studied. The third experiment is focused on the fluid flow (without heat transfer) in arrays of longitudinal fins, while the last of the experiments treats a nonuniformly heated noncircular duct. The objective of the analytical work was to develop a turbulence model for rectangular passages, and one of the test cases for the model was to predict the friction factors that had been measured for the longitudinal fin arrays.

Each of the research problems is described in a separate chapter which is a fully self-contained report in itself.

Chapter 1

EFFECT OF PLENUM LENGTH AND DIAMETER ON TURBULENT HEAT TRANSFER IN A DOWNSTREAM TUBE AND ON PLENUM-RELATED PRESSURE LOSSES

ABSTRACT

A systematic experimental study was carried out to determine how the heat transfer characteristics of a turbulent tube flow are affected by the length and diameter of a cylindrical plenum chamber which delivers fluid to the tube. The net pressure loss due to the presence of the plenum was also measured. The experimental arrangement was such that the fluid experiences a consecutive expansion and contraction in the plenum before entering the electrically heated test section. Air was the working fluid, and the Reynolds number was varied over the range from 5,000 to 60,000. It was found that at axial stations in the upstream portion of the tube, there are substantially higher heat transfer coefficients in the presence of longer plenums. Thus, a longer plenum functions as an enhancement device. On the other hand, the plenum diameter appears to have only a minor influence in the range investigated (i.e., plenum diameters equal to three and six times the tube diameter). The fully developed Nusselt numbers are independent of the plenum length and diameter. With longer plenums in place, the thermal entrance length showed increased sensitivity to Reynolds number in the fully turbulent regime. The pressure loss coefficient, which compares the plenum-related pressure loss with the velocity head in the tube, increases more or less linearly with the plenum length. With regard to experimental technique, it was demonstrated that guard heating/cooling of the electrical bus adjacent to the tube inlet is necessary for accurate heat transfer results at low Reynolds numbers but, although desirable, is less necessary at higher Reynolds

numbers.

NOMENCLATURE

A_w cross-sectional area of tube wall

c_p specific heat of air

D inside diameter of plenum chamber

d inside diameter of tube

h local heat transfer coefficient, equation (4)

K pressure loss coefficient, equation (6)

k thermal conductivity of air

k_w thermal conductivity of stainless steel wall

L axial length of plenum chamber

$\dot{m}$ mass flow rate of air

Nu local Nusselt number, hd/k

ΔP_p net plenum-related pressure drop

Q_i rate of convective heat transfer from control volume i to the fluid

Re Reynolds number, $4\dot{m}/\mu\pi d$

T_b local bulk temperature

T_w local tube wall temperature

T_∞ temperature of surroundings

V mean air velocity in tube

x axial coordinate measured from tube inlet

x_e thermal entrance length

μ viscosity

ρ density

Subscript

fd thermally fully developed

Superscript

* at plenum inlet

INTRODUCTION

Turbulent heat transfer in circular tubes has been the subject of extensive study for many decades because the circular tube serves as a basic component in a wide variety of heat exchange devices. In general, fluid may be delivered to the tube from a broad range of sources, encompassing, for example, plenums of various geometric forms, upstream pipelines (either heated or unheated), and fittings of many types (e.g., tees, elbows). It may be expected that the tube heat transfer characteristics will be affected by the sources from which fluid is delivered, especially in the region of the tube adjacent to its inlet. The present research was undertaken to experimentally determine how the turbulent heat transfer characteristics of a heated tube respond to systematic variations of the length and diameter of an upstream plenum which delivers fluid to the tube. The pressure drop associated with the presence of the plenum was also measured, and flow visualization was employed for the observation of certain characteristics of the flow field.

In the heat transfer apparatus, a plenum chamber in the form of a circular cylinder is positioned immediately upstream of an electrically heated tube such that the tube and the plenum share the same axis. In turn, the working fluid, air, is delivered to the upstream end of the plenum via a tube which also shares the common axis of the plenum and the heated tube. Thus, the working fluid experiences a consecutive expansion and contraction prior to its entry into the heated test section tube.

The apparatus used for the pressure-drop studies is similar to that of the heat transfer experiments (and air is also the working fluid), except that the heated test section is replaced by an unheated tube instrumented with pressure taps. Flow visualization was conducted in an all-plexiglass apparatus with water as the working fluid.

Two plenums of different diameter D were employed during the experiments. Each plenum was designed and fabricated so that its streamwise length L could be varied.

Relative to the diameter d of the test section tube, the investigated plenum configurations encompassed the range $1/4 \leq L/d \leq 10$, respectively for $D/d = 3$ and 6. For each fixed plenum configuration investigated, experiments were conducted for Reynolds numbers ranging from 5,000 to 60,000.

The heated test section was heavily instrumented to enable local heat transfer coefficients to be determined and, thereby, to facilitate identification of the effects of plenum geometry. Furthermore, the presentation of results is structured to highlight these effects. The total heat transfer presentation includes the thermal entrance region, the thermally developed regime, entrance length, and comparisons with the literature. With regard to fluid-flow aspects, the plenum-related pressure drop is presented in terms of a dimensionless pressure loss coefficient for the same range of parameters as were employed in the heat transfer experiments. The flow visualization observations were of a qualitative nature and are reported as such.

The experimental apparatus was designed and fabricated to provide heat transfer results of impeccable quality which can serve both as a guide to design and as a standard against which to compare candidate analytical models. In recognition of the potential injurious role of extraneous heat losses in airflow systems, a number of measures were instituted to defend against such losses. These include: (a) near-zero contact between the heated test section and the plenum, (b) guard heating and cooling of the bus bars which deliver electrical power to the system, (c) suspension of the test section with thin nylon line, and (d) use of an insulation having a thermal conductivity less than that of air. In a sensitivity study, it was demonstrated experimentally that the absence of guard heating/cooling can have a substantial impact on the results in the thermal entrance region.

Attention will now be turned to the literature relevant to the subject under study. In general, a literature search failed to unearth any published research of the type reported in the present report. However, to provide perspective, the general state of affairs with regard to upstream hydrodynamic conditions for turbulent

tube-flow heat transfer will be briefly reviewed. With regard to analysis, it has been customary to avoid involvement with the actualities of the flow field upstream of the heated tube by imposing hydrodynamic boundary conditions at the tube inlet. Experiments have been reported in {1} and {2} for heated tubes to which flow is delivered via an abrupt or rounded contraction from a very large plenum, or via an adiabatic tube that is either straight (hydrodynamic development length) or curved (elbow or bend). In {2} and {3}, a tee was used to convey the working fluid to the heated tube.

The heat transfer characteristics of a heated tube situated downstream of either an abrupt expansion or an abrupt contraction of finite diameter ratio were investigated in {4 - 8}. In all cases, the tube situated upstream of the change of section was sufficiently long so that the hydrodynamically developed conditions prevailed prior to the expansion or contraction. The case of a successive expansion and contraction (i.e., a plenum of finite length) upstream of a heated tube does not appear to have been investigated.

THE EXPERIMENTS

Heat transfer apparatus. The heat transfer apparatus will be described in sufficient detail to convey its main features and novel design aspects. A more detailed description, including design drawings, is available in {9}.

The apparatus is an open-loop airflow system which is supplied by a dryer-equipped air compressor. Upon entering the loop, the air passes through a set of control valves, a filter, and a regulator, and then is ducted to a settling chamber which serves to damp the eddies induced by valves and elbows. From the setting chamber, the air enters and traverses a 65-diameters-long hydrodynamic development tube, the efflux of which discharges into the plenum chamber whose dimensions (length and diameter) are to be varied throughout the experiments. From the plenum, the air passes through the 76-diameters-long heated test section and the mixing chamber situated at its downstream end. The discharge from the mixing chamber is ducted to

a rotameter and then passes into the room.

Apparatus components. As noted earlier, the hydrodynamic development section, the plenum, and the test section all share a common axis. In addition, the development and test section tubes were cut from a single length of stainless steel tubing, the bore diameter of which, after internal honing to attain a smooth satin finish, was 2.36 cm (0.930 in.). The post-honing wall thickness of the test section tube (a parameter relevant to the ohmic heating) was 0.089 cm (0.035 in.) with a circumferential variation of $\pm$ 0.002 cm ($\pm$ 0.0008 in.). The two plenum chambers used in the experiments were made of plexiglass, with respective internal diameters equal to 2.96 and 5.91 times that of the test section tube (nominally, 3 and 6 times).

To enable the streamwise length of the plenum chamber to be varied during the course of the research, its upstream end-face was designed so that it could be moved axially within the cylindrical wall of the chamber. An air seal between the cylindrical wall and the contacting edge of the end-face was achieved with a pair of O-rings. The end-face was rigidly attached to the downstream end of the hydrodynamic development tube, so that the axial movement of the face required a corresponding axial movement of the development tube. This movement was accommodated by a flexible coupling at the upstream end of the development tube.

Two thermocouples threaded through the upstream end-face of the plenum served to measure the air temperature just downstream of the plenum inlet. The thermocouples were positioned 180° apart, with the junctions placed in the mixing region of the incoming jet.

At the downstream end of the plenum, special precautions were taken to minimize possible extraneous heat conduction from the test section tube to the plenum end-face. These precautions were motivated by the concern that the plenum airflow, either impinging against or recirculating adjacent to the end-face, would induce an extraneous flow of heat out of the test section.

The first of the defenses against such extraneous losses is in the adopted

structure of the end-face. The face consisted of two parts--an inner and an outer annular disk, of which only the former is relevant to the heat transfer loss issue because of its contact with the test section tube. This disk was fabricated from rigid fiberglass circuitboard whose thickness was only 0.043 cm (0.017 in.). The inner diameter of the disk was made identical to the outer diameter of the test section tube, so that the disk could just slip over the tube. They were positioned so that their upstream faces lay in a continuous plane. The only thermal path between the tube and the disk was through their 0.043 cm (0.017 in.) interface. This is believed to be the very minimum that is consistent with structural integrity, especially when a nonmetallic, relatively low thermal conductivity material such as fiberglass is employed. A small fillet of silicone rubber was inserted just downstream of the disk to seal against air leaks--other defenses against air leaks are described in {9}.

Immediately downstream of the fiberglass disk, a copper ring was soldered to the outer surface of the test section tube to serve as a distribution bus for the electric current used for the ohmic heating of the tube. The ring was beveled on its upstream face in such a way that it leaned away from the disk. To avoid ambiguity about the axial position where the ohmic heating began, the axial contact between the tube and the bus ring was kept as short as possible (axial contact length ≈ 1/4 tube diameter). The ring also served as a hub against which three sharp-tipped nylon screws were tightened to ensure the alignment of the plenum and the test section tube.

Electric current was supplied to the copper bus ring by six rod-like copper conductors, each 0.476 cm (3/16 in.) in diameter and about 5.08 cm (2 in.) long. The rods, canted toward the downstream to avoid conjestion adjacent to the plenum, emanated radially outward like the spokes of a wheel. The outer tip of each spoke was soldered to a heavy copper ring, which served as a terminal for a stranded copper cable from the power supply.

Each spoke was fitted with a differential thermocouple which enabled the existence

of extraneous heat conduction along the spokes to be detected. To null out such extraneous heat flows, the outer copper ring was fitted with a water-carrying copper tube. The water temperature could be precisely controlled by a thermostatically regulated heating/cooling bath. This guard heating/cooling capability constituted a very important defense against extraneous losses/gains and, as will be demonstrated later, it served to ensure the quality of the thermal entrance region results.

The test section tube itself was heavily instrumented with thermocouples. In an axial length extending eight diameters from the onset of heating, there were twelve thermocouple stations and, at each such station, four thermocouples were deployed at equal intervals around the circumference of the tube. Between the axial distances of eight and sixty-four diameters from the inlet, there were sixteen instrumented stations, each with two thermocouples. All thermocouples were of 30-gage, calibrated copper and constantan wire, applied to the tube via spot welding and oriented so that the lead wires lay along the expected isothermal directions.

The final thermocouple station was situated twelve tube diameters from the downstream bus-bar assembly. That assembly was similar in structure to that of the upstream bus but was not guard heated or cooled because there was no need to do so (because it was too remote from the nearest measurement station).

The mixing chamber was mated to the downstream end of the test section. It consisted of a length of pvc pipe which housed a series of copper baffle plates. An array of holes was machined in each plate, and the pattern and size of the holes in the respective plates were designed to induce both radial and circumferential fluid motions. Three thermocouples situated downstream of the last baffle were used to measure the temperature of the air. Flexible tubing served to couple the discharge end of the mixing chamber to the rotameter used for flow metering.

As a further defense against extraneous heat losses (or gains), the plenum chamber, the test section, and the mixing chamber were situated within an insulation enclosure. The enclosure consisted of a plywood box with a 30.5 cm (1 ft) square

cross section whose inner walls were lined with styrofoam sheet insulation. The styrofoam enclosed a space having cross-sectional dimensions of 21.6 x 21.6 cm (8.5 x 8.5 in.). Into this space was poured silica aerogel powder insulation whose thermal conductivity is about eighty-five percent that of air. The test section was suspended from the frame of the plywood box by monofilament nylon lines, and no other supports were employed.

Power supply and instrumentation. Electric power was supplied to the test section via a system which served to stabilize the voltage and to provide the high current and low voltage called for by the low-resistance test section. Test section voltage and current (both read as voltages) were measured by a true rms digital voltmeter (Keithly model 179). This type of meter was selected because of concern that possible departures from a sinusoidal wave form would introduce errors in the readings of other types of voltmeters.

All thermocouple emf's were read with a Fluke 2240B datalogger capable of programmable scanning. It provided a printed output with a smallest digit corresponding to 1 μV. The programming capabilities of the datalogger enabled the lengthy approach of the apparatus to thermal equilibrium to be monitored without human intervention. However, as a matter of course, the final attainment of equilibrium and the collection of data were always monitored and controlled by the experimenter. Both the datalogger and the aforementioned true rms voltmeter were new at the beginning of the research and were, therefore, under their calibration warranties.

The rate of air flow through the apparatus was measured by one of three rotameters, depending on the magnitude of the flow. All rotameters were calibrated against a secondary standard.

Pressure measurement and flow visualization. A separate set of experiments were performed to determine the pressure drop due to the presence of the plenum chamber. For this purpose, the heated test section tube, its attached mixing chamber, and the insulation enclosure were removed from the airflow loop. A stainless steel

tube (84 diameters long), that had been cut from the same length as the test section, was mated to the downstream end-face of the plenum via a plexiglass flange (the fiberglass disk remained with the heated test section). The tube was internally honed for smoothness and was equipped with pressure taps located sufficiently far downstream of the plenum so as to lie in the redeveloped flow regime. There was also a series of taps deployed along the hydrodynamic development tube (upstream of the plenum) which were employed in the determination of the plenum-related pressure drop.

The pressure signals were sensed by a Baratron solid-state capacitance-type pressure meter. The output of the Baratron was read with the aforementioned Keithly digital voltmeter. Pressure differences as small as 10^{-4} mm Hg could be detected by the Baratron. It, too, was new and under its warranty calibration during th duration of the experiments.

The flow visualization study was made prior to the heat transfer and pressure drop experiment. The specific focus of the visualization study was to detect the presence or absence of flow separation in the test section tube just downstream of the inlet cross section.

The visualization apparatus was made entirely of plexiglass and was equipped with dye injection taps both along the cylindrical wall of the plenum and along the upstream portion of the test section tube. Water was supplied to the apparatus from a constant-head tank suspended from the ceiling of the laboratory. The discharge from the apparatus was ducted to a weigh tank for flow metering.

DATA REDUCTION

Heat transfer results. The procedures employed in deducing local heat transfer coefficients and Nusselt numbers will now be described. For the evaluation of the local heat transfer coefficient, the needed inputs are the local heat flux, wall temperature, and bulk temperature. Among these, only the local wall temperature is directly measured, so that the other quantities have to be obtained via data reduction.

The first step in the analysis is to envision the wall of the test section tube as being subdivided into axial segments of length Δx_i. Each such segment serves as a control volume for a heat balance. The axial boundaries of the respective control volumes are positioned midway between the adjacent temperature measurement stations. Thus, if x_{i-1}, x_i, and x_{i+1} denote the axial locations of successive wall temperature measurements, then the axial boundaries of the i^{th} control volume are at $(x_{i-1} + x_i)/2$ and at $(x_{i+1} + x_i)/2$ and, correspondingly, the control volume length $\Delta x_i = (x_{i+1} - x_{i-1})/2$.

The energy transfer to and from a control volume include the following:

(1) an internal heat source due to ohmic dissipation

(2) convective heat transfer from the inner surface of the control volume to the airflow

(3) heat loss from the outer surface of the control volume through the insulation to the ambient air

(4) conduction heat transfer into the downstream face of the control volume from the adjacent portion of the tube wall

(5) conduction heat transfer out of the upstream face of the control volume into the adjacent portion of the wall

Under steady state conditions, these inflows and outflows are in balance. As will now be described, numerical values can be supplied to the heat balance equation for items (1), (3), (4), and (5), enabling the determination of the convective heat flow from the control volume to the fluid (item (2)).

The ohmic dissipation for control volume i was determined by prorating the overall dissipation by the ratio $\Delta x_i/x_L$, where x_L is the length of the test section tube. For the heat loss through the insulation to the ambient, a conduction shape factor was found by setting up a two-dimensional finite difference network that spanned the two types of insulation (silica aerogel and styrofoam) and the surrounding wooden containment structure. A total of 1600 grid points were used to resolve

the complex geometry which included both curved and straight boundaries. The details of this work are presented in {9}. With the shape factor available, the heat loss through the insulation was calculated by multiplying the shape factor with the temperature difference $(T_w(x_i) - T_\infty)$ and by the axial length Δx_i, where $T_w(x_i)$ is the meeasured wall temperature at x_i and T_∞ is the ambient temperature.

The axial conduction along the wall, items (4) and (5), was found by applying a central difference representation of Fourier's law. If A_w represents the cross-sectional area of the wall and k_w denotes the thermal conductivity of stainless steel (regarded as a function of temperature), then items (4) and (5) may be expressed as

$$k_w A_w (T_w(x_{i+1}) - T_w(x_i))/(x_{i+1} - x_i) \tag{1}$$

$$k_w A_w (T_w(x_i) - T_w(x_{i-1}))/(x_i - x_{i-1}) \tag{2}$$

Equations (1) and (2) were evaluated using the measured wall temperatures at stations x_{i-1}, x_i, and x_{i+1}.

The foregoing discussion has demonstrated that all contributions to the energy balance for a typical tube-wall control volume i can be evaluated from the experimental data, aside from the convection term. Therefore, these operations yield the rate of convective heat transfer Q_i from the control volume to the fluid. The thus-determined Q_i for the successive control volumes are employed directly in the evaluation of the heat transfer coefficient and also for the computation of the local bulk temperature, as will now be described.

The axial distribution of the local bulk temperature was also found from a control volume analysis. For this analysis, the control volumes are cylinders of diameter d (equal to the tube diameter) and axial length Δx_i. The axial coordinates of the upstream and downstream faces of these control volumes are the same as those for the control volumes used earlier in the determination of the convective heat transfer rates Q_i.

For control volume i, let T_{in}^i be the bulk temperature of the fluid entering the

control volume at its upstream face and T^i_{out} denote the fluid bulk temperature at the downstream face. Then,

$$T^i_{out} = T^i_{in} + Q_i/\dot{m}c_p \tag{3}$$

Thus, with the already determined Q_i and the measured inlet bulk temperature, equation (3) can be used in a marching fashion to compute the fluid bulk temperature at all the control volume faces. Then, the bulk-temperature $T_b(x_i)$ at any thermocouple measurement station x_i was found by linear interpolation between the faces of the corresponding control volume.

Then, with the information generated from the foregoing computations, the local heat transfer coefficient and Nusselt number at any station i was evaluated from

$$h_i = \frac{Q_i/A_i}{T_w(x_i) - T_b(x_i)} \quad , \quad Nu_i = \frac{h_i d}{k_i} \tag{4}$$

where $A_i = \pi d \Delta x_i$ and k_i is the thermal conductivity of air at $T_b(x_i)$. Although h_i may have the appearance of a "local average" heat transfer coefficient, it is, for the most part, a truly local coefficient. In this regard, it can be verified by carefully re-examining the foregoing data reduction procedure that the only quantity that is actually related to the finite axial length of the control volume is the axial conduction in the wall. Since the net axial conduction is only of significance at the first few measurement stations, it is only there that h_i is a local average. At all other points, h_i is strictly local.

The results will be parameterized by the Reynolds number defined as

$$Re = 4\dot{m}/\mu\pi d \tag{5}$$

where μ is the viscosity corresponding to the mean bulk temperature of the air.

Variable fluid properties played only a minor role (e.g., maximum wall-to-bulk temperature difference about 11°C, 20°F). Nevertheless, for the reporting of fully developed Nusselt numbers, the foregoing definitions of Nu and Re were altered to respectively include k_{fd} and μ_{fd}, which correspond to the mean bulk temperature in

the fully developed regime.

Pressure drop results. The net pressure drop due to the presence of the plenum chamber will be reported as a dimensionless pressure loss coefficient K whose evaluation will now be described. First, it may be recalled that there are pressure taps in the tubes both upstream and downstream of the plenum. These taps are so situated that for both the upstream and downstream regions, the respective p vs x distributions are straight lines. Envision next a graph where the p vs x data for a given run are plotted. Within the accuracy of the measurements, the aforementioned straight lines for the upstream and downstream regions are parallel but not colinear. Rather, there is a vertical separation between them (to be denoted by ΔP_p) which is due entirely to the presence of the plenum.

In terms of ΔP_p, the pressure loss coefficient is defined as

$$K = \Delta P_p / (\tfrac{1}{2}\rho V^2)^* \qquad (6)$$

The denominator of equation (6) is the velocity head corresponding to the density ρ^* of the fluid in the tube at the inlet of the plenum. For the evaluation of K, ΔP_p was determined from least-squares straight lines fitted to the pressure data, and the pressure needed for ρ^* was obtained via extrapolation from the upstream pressure data.

RESULTS AND DISCUSSION

Basic data. To illustrate the nature of the basic data collected during the experiments, Fig. 1 has been prepared. The figure shows wall and bulk temperature distributions for two data runs. The data points for the wall temperature distributions represent direct measurements. For the bulk temperature, only the inlet and exit values were directly measured, and these are identified by blackened data symbols. The other plotted points for the bulk temperature distribution were computed as described in the preceding part of the paper. Smooth curves are drawn through the data points for continuity; in the case of the bulk temperature, the faired curve is virtually indistinguishable from a straight line.

The wall and bulk temperature distributions shown in the lower part of the figure are typical of those for the overwhelming majority of the data runs. They are, in fact, exemplary specimens of what is expected for turbulent heat transfer in a uniformly heated tube. These distributions are exemplary from three standpoints: (1) they are remarkably free of data scatter, (2) the wall and bulk temperature distributions are precisely parallel in the downstream (fully developed) region, and (3) the computed bulk temperature distribution extrapolates almost exactly to the measured value at exit. With regard to the latter characteristic, it may be noted that in the majority of the data runs, overall energy balances closed to within one percent.

The results shown in the upper portion of Fig. 1 are unusual in that the wall temperature distribution exhibits an overshoot before attaining the fully developed straight-line increase. This overshoot was encountered only at the largest L/d (= 10) and for Reynolds numbers of 7,000 and lower. It can be attributed to the transition of the developing boundary layer from laminar to turbulent flow.

To illustrate the nature of the heat transfer coefficients measured here, a set of distribution curves for a given plenum geometry (D/d = 3, L/d = 10) is plotted in Fig. 2 in the form of h vs. x/d. Results are shown for nine distinct Reynolds numbers between 5,200 and 59,200. These results are distinguished by the general absence of scatter and by the true constancy of h in the thermally developed regime.

The distribution curves for Re > 10,000 display the classical shape that is characteristic of turbulent pipe flows, while the curves for Re $\leq$ 7,000 are characterized by a slight undershoot prior to the attainment of the fully developed value. This undershoot is a reflection of the already-discussed wall temperature overshoot in Fig. 1.

An important observation in Fig. 2 is the complete absence of any indication of flow separation adjacent to the tube wall just downstream of the inlet. The characteristic signature signalling the presence of such a separation region is an

h vs. x distribution which rises to a maximum at the point of flow reattachment and decreases thereafter. Clearly, such a pattern is not in evidence in the present results. Furthermore, the flow visualization studies did not reveal any separated regions within the test section tube.

Another basic issue of the research is the role of guard heating/cooling of the electrical bus adjacent to the tube inlet, and this issue is addressed in Fig. 3. The figure contains two panels in which results are respectively presented for a low and a high Reynolds number (Re = 5,000 and 50,000). In each panel there are three curves of Nu/Nu_{fd} vs. x/d, where Nu and Nu_{fd} respectively denote the local and fully developed Nusselt numbers. These curves have been faired through the experimental data, but the data have been omitted from the figure to avoid confusion.

One of the curves (the solid line) corresponds to the case where the guard heater/cooler is adjusted to null out extraneous heat transfer. The other curves correspond to $\pm$ 15 μV imbalances across the differential thermocouples installed on the copper current-carrying spokes. This imbalance is typical of that which would have occurred in the absence of guard heating.

The results speak for themselves--that is, guard heating is strictly necessary at low Reynolds numbers, but, while desirable, it is dispensable at Re = 50,000 or greater.

Plenum-related heat transfer enhancement. Attention will now be turned to the main focus of the research--the effect of plenum length and diameter on the heat transfer characteristics of a tube to which fluid is delivered by the plenum. Results documenting the plenum size effect will be presented in the next six figures, which will now be discussed sequentially.

The effect of plenum length for a fixed plenum diameter D/d = 3 is dealt with in Figs. 4 and 5. These figures encompass five individual graphs which pertain respectively to fixed axial stations x/d = 1, 2, 3, 5, and 8. At each station, Nu/Nu_{fd} is plotted as a function of Reynolds number for three different plenum

lengths characterized by L/d = 1, 5, and 10. In this format, the effect of plenum length on the local heat transfer coefficient is readily identified by comparing the ordinates of the various L/d curves at a given Reynolds number.

From an examination of Figs. 4 and 5, it is seen that the plenum length has a decisive effect on the heat transfer coefficient when x/d is small, but the extent of the effect decreases with increasing downstream distance. At x/d = 1 and at the larger Reynolds numbers, the h value for L/d = 10 is about forty percent greater than that for L/d = 1. The percentage increases are slightly smaller at lower Reynolds numbers. Thus, a relatively long plenum serves as an enhancement device.

At x/d = 2 and 3, heat transfer enhancement due to plenum length persists and is significant, but is smaller than that at x/d = 1. However, at x/d = 5, there is no apparent difference between the results for L/d = 5 and 10, and at this x/d the greatest enhancement in evidence due to the plenum length is about six percent. At x/d = 8, the curves tend to overlap, and while enhancement still persists at the larger Reynolds numbers, it is only a few percent. For still larger x/d (not shown), all three curves collapse to the line $Nu/Nu_{fd} = 1$.

A presentation similar to that of Figs. 4 and 5, but for a fixed plenum diameter D/d = 6, is provided by Figs. 6 and 7. The format of these figures is identical to those of the preceding figures. In actuality, the similarities between the two sets of figures are deeper than mere format. Aside from some minor differences in detail, the qualitative and quantitative behavior already identified for the D/d = 3 case appears to be reproduced for the D/d = 6 plenum.

To explore in greater detail the relationship between the results for the two plenum diameters, Fig. 8 has been prepared. This figure consists of two graphs, the upper of which conveys information for a fixed plenum length L/d = 10 while the lower is for the fixed length L/d = 5. In each graph, Nu/Nu_{fd} is plotted versus Reynolds number for both of the plenum diameters. The data for D/d = 3 are connected by faired curves but those for D/d = 6 are not fitted with curves to avoid

the possible confusion of too many closely positioned lines.

If attention is first given to the longest plenum L/d = 10, it is seen that the data at x/d = 1, 2, and 3 for the larger diameter plenum fall slightly below that for the smaller plenum, but the maximum deviations are only about five percent. At x/d = 5 and 8, the data for the two cases are coincident. Next, turning to the results for the intermediate length plenum L/d = 5 (lower graph), the same relationship between the Nusselt numbers for the two plenum diameters prevails but the deviations are even smaller. A comparison similar to that of Fig. 8 was also made for the shortest plenum L/d = 1 {9}, and only very small diameter-related deviations were observed.

If consideration is now given to the findings of Figs. 4 through 8, it may be concluded that for the ranges investigated, plenum length has a much greater effect on the heat transfer coefficients than does plenum diameter. Indeed, considering the modest effect of plenum diameter, it appears that the results presented here are valid for all plenums with $D/d \geq 3$.

An alternative perspective on the plenum-related heat transfer enhancement is provided by Fig. 9. Here, Nu/Nu_{fd} is plotted versus x/d for three different Reynolds numbers, respectively Re = 6,000, 15,000, and 50,000, in the three panels of the figure. Each panel contains curves for three plenum lengths, L/d = 1, 5, and 10, and the objective of the figure is to show how the entirety of the h vs. x distribution curve is affected by the length of the plenum. The figure is for D/d = 3, but a similar figure for D/d = 6 conveys nearly identical results {9}.

The figure shows that at small x/d, the curves are ordered in a regular way with L/d, with that for the longest plenum being highest. However, the larger the L/d, the more rapidly do the curves drop off, and this causes all curves to ultimately cross. However, in the regions of the crossings, the Nu/Nu_{fd} values do not differ appreciably. The low-Reynolds-number curves (left-hand panel) are separated by as much as ten percent at downstream stations $x/d \sim 15$ owing to the absence or

presence of the undershoot effect.

Before leaving Figs. 4 - 9, a brief comment appears appropriate about another enhancement mechanism, namely, the boundary layer development that gives rise to Nu/Nu_{fd} values well in excess of one in the entrance region. The figures show that entrance-region enhancement is greater at low Reynolds numbers than at high Reynolds numbers, a characteristic which does not appear to be well documented in the literature.

Thermal entrance lengths. The results presented in the preceding section, especially Figs. 2 and 9, suggest that the rapidity of the thermal development is affected by both the plenum geometry and the Reynolds number. To quantize the rate of thermal development, a thermal entrance length x_e has been defined as the distance from the test section inlet at which $Nu/Nu_{fd} = 1.05$. Dimensionless thermal entrance lengths x_e/d based on this definition are listed in Table 1.

It is seen from the table that the overall range of the thermal entrance length extends from ten to seventeen tube diameters. The plenum length appears to play a significant role in that the dependence of x_e/d on Re is affected by L/d. With a short plenum in place (i.e., L/d = 1), the thermal entrance length increases only very slightly with Reynolds number for $Re \geq 20,000$, but is quite sensitive to Reynolds number at lower Re. These characteristics are similar to those expected when the plenum is absent (i.e., hydrodynamically developed flow at the inlet of the heated tube). On the other hand, for the two longer plenums (L/d = 5 and 10), there is an appreciable increase of x_e/d with Reynolds number for $Re \geq 10,000$, while at lower Re the variation of x_e/d is slight. These marked differences in the characteristics of the thermal entrance length are reflective of flow field differences that are caused by the presence of the plenum.

Further inspection of Table 1 shows that the plenum diameter plays a secondary role. In general, the x_e values for the two plenum diameters do not differ by more than one tube diameter.

Literature comparisons. The first of the literature comparisons is for the fully developed Nusselt number Nu_{fd}. Among the available predictive equations for Nu_{fd}, the semi-empirical equation of Petukhov and Popov {10} is widely regarded as the most accurate. That equation is purported to be accurate to $\pm$ 6 percent for Prandtl numbers between 0.5 and 200 and for the Reynolds number range from 10^4 to 5×10^6. To avoid massive data overlap, the present results for D/d = 3 and D/d = 6 have been plotted on separate graphs and respectively compared with the Petukov-Popov equation. The two graphs are identical in all respects, and only that for D/d = 3 is presented here in Fig. 10.

The figure conveys two main messages. The first is that the fully developed Nusselt number is independent of L/d, and this is to be taken together with the aforementioned independence of Nu_{fd} from D/d. This finding confirms the expectation that given sufficient length of run, the specific details of the inlet velocity field will ultimately disappear so that the fully developed regime is truly universal.

The other noteworthy feature of Fig. 10 is the excellent agreement of the present data with the Petukov-Popov equation in the range Re $\geq$ 10,000, with a maximum deviation of five percent. At lower Reynolds numbers, the Petukov-Popov equation departs more and more from the data, which is entirely expected because it is based on a fully turbulent model.

With regard to other comparisons with the literature, it has already been noted that there are no prior systematic studies of the effect of plenum geometry on heat transfer in a tube fed by the plenum. Thus, definitive comparisons of the present results with the literature are precluded. To enable limited comparisons to be made, a special set of experiments was performed in which L/d was set at its minimum possible value (L/d = 1/4) consistent with the thermocouple installation in the plenum and with the avoidance of extraneous conduction between the upstream and downstream faces of the plenum. This arrangement was thought to be a close approximation for the case in which an already hydrodynamically developed flow enters

a heated tube.

The results of those experiments (Re = 10,000 and 50,000, D/d = 6) are presented in Fig. 11 along with analytical predictions of {11} and {12} which correspond to turbulent flow in a uniformly heated tube with an axially unchanging velocity distribution. The predictions of {12} fall well below the data, and this tendency has been noted by others (e.g., {2}). On the other hand, for Re = 50,000, the predictions of {11} are in remarkably good agreement with the data. The agreement at Re = 10,000 is not as good, but the deviation might well be due, at least in part, to the gap associated with L/d = 1/4 ≠ 0. The lower the Reynolds number, the more sensitive is the flow to the presence of such a gap.

The foregoing comparisons may be regarded both as a support of the present experimental technique as well as of the predictions of {10} and {11}.

Plenum-related pressure losses. As defined in equation (6) and discussed in the related text, the net pressure loss ΔP_p due to the presence of the plenum will be reported as a dimensionless loss coefficient K which is the ratio of ΔP_p to the velocity head in the tube at the plenum inlet. The experimentally determined values of K are listed in Table 2.

The most significant message of the table is the tight correlation between the magnitude of K and L/d. As L/d varies from 1 to 5 to 10, K varies, in global terms, from 0.1 to 0.5 to 1. This trend is entirely reasonable in that the two major contributions to K, the abrupt expansion at the plenum inlet and the abrupt contraction at the plenum exit, assert their separate identities more and more as L/d increases. However, even for L/d = 10, the K values listed in the table are less than the sum of the separate expansion and contraction coefficients.

With regard to Reynolds number effects, K varies somewhat irregularly when Re > 12,000. At low Reynolds numbers, there is a general tendency of K to increase as Re decreases, with the greatest sensitivity in evidence for L/d = 1. In general, K is not very sensitive to D/d for the two values of D/d that were investigated.

CONCLUDING REMARKS

A systematic experimental study has been performed to determine the effect of plenum geometry on the turbulent heat transfer characteristics of a tube fed by the plenum. Measurements were also made of the plenum-related pressure drop. The experiments were designed and executed with painstaking care in order to provide a set of results of impeccable quality which can serve both as a guide to design and as a standard against which to compare candidate analytical models.

It was found that at axial stations in the near neighborhood of the tube inlet, the local heat transfer coefficients were higher for longer plenums. Thus, a longer plenum functions as an enhancement device. As an example of the enhancement, it may be noted that at $x/d = 1$, the heat transfer coefficient is forty percent larger at a plenum length $L/d = 10$ than when $L/d = 1$. The extent of the enhancement decreases as x/d increases and can be regarded as negligible for $x/d \geq 8$. The plenum diameter appears to play a minor role with regard to the enhancement, so that the present results may be regarded as being applicable for all $D/d \geq 3$.

Thermal entrance lengths x_e, based on a five percent approach to complete thermal development, encompassed the range from ten to seventeen tube diameters for the investigated operating conditions. Longer plenums brought about a greater sensitivity of x_e to the Reynolds number in the fully turbulent regime but gave rise to a lesser sensitivity to Re in the low-Reynolds-number turbulent regime. The entrance lengths were not found to be sensitive to the plenum diameter.

The fully developed Nusselt numbers Nu_{fd} were independent of both the length and diameter of the plenum chamber. Excellent agreement prevailed between the measured Nu_{fd} values and those predicted by the Petukhov-Popov equation for $Re \geq 10{,}000$, which is the range of applicability of the equation.

The pressure loss coefficient, which compares the plenum-related pressure loss with the velocity head in the tube, increased more or less linearly with the length of the plenum.

As a relevant adjunct to the main focus of the research, a study was performed to examine the role of guard heating/cooling at the electrical bus adjacent to the tube inlet. It was found that such heating/cooling was necessary for accurate Nusselt number results at low Reynolds numbers (Re $\sim$ 5,000) and was desirable, but not strictly necessary at higher Reynolds numbers (Re $\geq$ 50,000).

REFERENCES

1. Boelter, L.M.K., Young, G., and Iverson, H. W., "An Investigation of Aircraft Heaters XXVII--Distribution of Heat Transfer Rate in the Entrance Section of a Circular Tube," NACA TN 1451, 1948.
2. Mills, A. F., "Experimental Investigation of Turbulent Heat Transfer in the Entrance Region of a Circular Conduit," Journal of Mechanical Engineering Science, Vol. 4, 1962, pp. 63-77.
3. Wesley, D. W. and Sparrow, E. M., "Circumferentially Local and Average Turbulent Heat Transfer Coefficients in a Tube Downstream of a Tee," International Journal of Heat and Mass Transfer, Vol. 19, 1976, pp. 1205-1214.
4. Ede, A. J., Hislop, C. I., and Morris, R., "Effect on the Local Heat Transfer Coefficient in a Pipe of an Abrupt Disturbance of the Fluid Flow: Abrupt Convergence and Divergence of Diameter Ratio 2/1," Proceedings of the Institution of Mechanical Engineers, London, Vol. 170, No. 38, 1956, pp. 1113-1126.
5. Ede, A. J., "Effect of an Abrupt Disturbance of the Flow on the Local Heat Transfer Coefficient in a Pipe," HEAT 164, National Engineering Laboratory, East Kilbride, Glasgow, Scotland, 1959.

6. Ede, A. J., Morris, R. and Birch, E. S., "The Effect of Abrupt Changes of Diameter on Heat Transfer in Pipes," NEL Report No. 73, National Engineering Laboratory, East Kilbride, Glasgow, Scotland, 1962.

7. Emerson, W. H., "Heat Transfer in a Duct in Regions of Separated Flow," Proceedings of the Third International Heat Transfer Conference, Vol. 1, 1966, pp. 267-275.

8. Zemanick, P. P. and Dougall, R. S., "Local Heat Transfer Downstream of Abrupt Circular Channel Expansion," ASME Journal of Heat Transfer, Vol. 92, 1970, pp. 53-60.

9. Lau, S. C., "Effect of Plenum Length and Diameter on Turbulent Heat Transfer in a Downstream Tube and on Plenum-Related Pressure Losses," Ph.D. Thesis, Department of Mechanical Engineering, University of Minnesota, Minneapolis, Minnesota, 1980.

10. Petukhov, B. S., "Heat Transfer and Friction in Turbulent Pipe Flow with Variable Physical Properties," in Advances in Heat Transfer, Academic Press, New York, 1970, pp. 503-564.

11. Seigel, R. and Sparrow, E. M., "Comparison of Turbulent Heat Transfer Results for Uniform Wall Heat Flux and Uniform Wall Temperature," ASME Journal of Heat Transfer, Vol. 82, 1960, pp. 152-153.

12. Deissler, R. G., "Analysis of Turbulent Heat Transfer and Flow in the Entrance Regions of Smooth Passages," NACA TN 3016, 1953.

Table 1

Thermal Entrance Lengths, x_e/d

		L/d		
D/d	Re	1	5	10
3	5,000	16.5	11	9.5
	10,000	14	11	10
	20,000	12.5	12.5	12
	30,000	13	14	14
	40,000	13	15	15
	50,000	13.5	16	16
	60,000	13.5	16.5	16.5
6	5,000	17	11	9.5
	10,000	15	11.5	10
	20,000	13	13.5	12
	30,000	13.5	15	13.5
	40,000	14	16	14.5
	50,000	14	16.5	15.5
	60,000	14.5	17	16

Table 2

Pressure Loss Coefficient K

(a) D/d = 3

L/d = 1		L/d = 5		L/d = 10	
Re	K	Re	K	Re	K
5,700 - 6,700	0.211	5,900 6,300	0.722 0.658	5,500 6,200	0.973 0.935
8,100	0.183	6,700	0.628		
12,000	0.166	12,000	0.572	12,000	0.928
20,000	0.105	20,000	0.518	20,000	0.940
28,000	0.084	28,000	0.505	28,000	1.012
45,000	0.070	45,000	0.532	44,000	1.019
61,000	0.073	60,000	0.580	61,000	1.021

(b) D/d = 6

5,700 - 6,200	0.170	5,600 5,900	0.680 0.607	5,500 5,800	0.880 0.831
6,400	0.106	6,800	0.539	6,400	0.782
8,000	0.107	8,000	0.512		
12,000	0.101	12,000	0.460	12,000	0.797
21,000	0.084	21,000	0.423	21,000	0.819
28,000	0.077	28,000	0.420	29,000	0.832
45,000	0.074	45,000	0.430	45,000	0.921
53,000	0.091	59,000	0.461	59,000	0.941
59,000	0.110				

FIGURE CAPTIONS

Fig. 1 Illustrative wall and bulk temperature distributions

Fig. 2 Illustrative axial distributions of the heat transfer coefficient for parametric values of Reynolds number, D/d = 3 and L/d = 10

Fig. 3 Effect of guard heating/cooling on the axial distribution of the Nusselt number

Fig. 4 Effect of plenum length on the Nusselt numbers at x/d = 1 and 2 for D/d = 3

Fig. 5 Effect of plenum length on the Nusselt numbers at x/d = 3, 5, and 8 for D/d = 3

Fig. 6 Effect of plenum length on the Nusselt numbers at x/d = 1 and 2 for D/d = 6

Fig. 7 Effect of plenum length on the Nusselt numbers at x/d = 3, 5, and 8 for D/d = 6

Fig. 8 Effect of plenum diameter on the Nusselt numbers at x/d = 1, 2, 3, 5, and 8 for L/d = 5 and 10

Fig. 9 Effect of plenum length on the axial distributions of the Nusselt number at Re = 6,000, 15,000, and 50,000 for D/d = 3

Fig. 10 Fully developed Nusselt numbers for D/d = 3

Fig. 11 Comparisons of measured Nusselt number distributions for L/d = 0.25 with analytical predictions corresponding to hydrodynamically developed flow in a uniformly heated tube

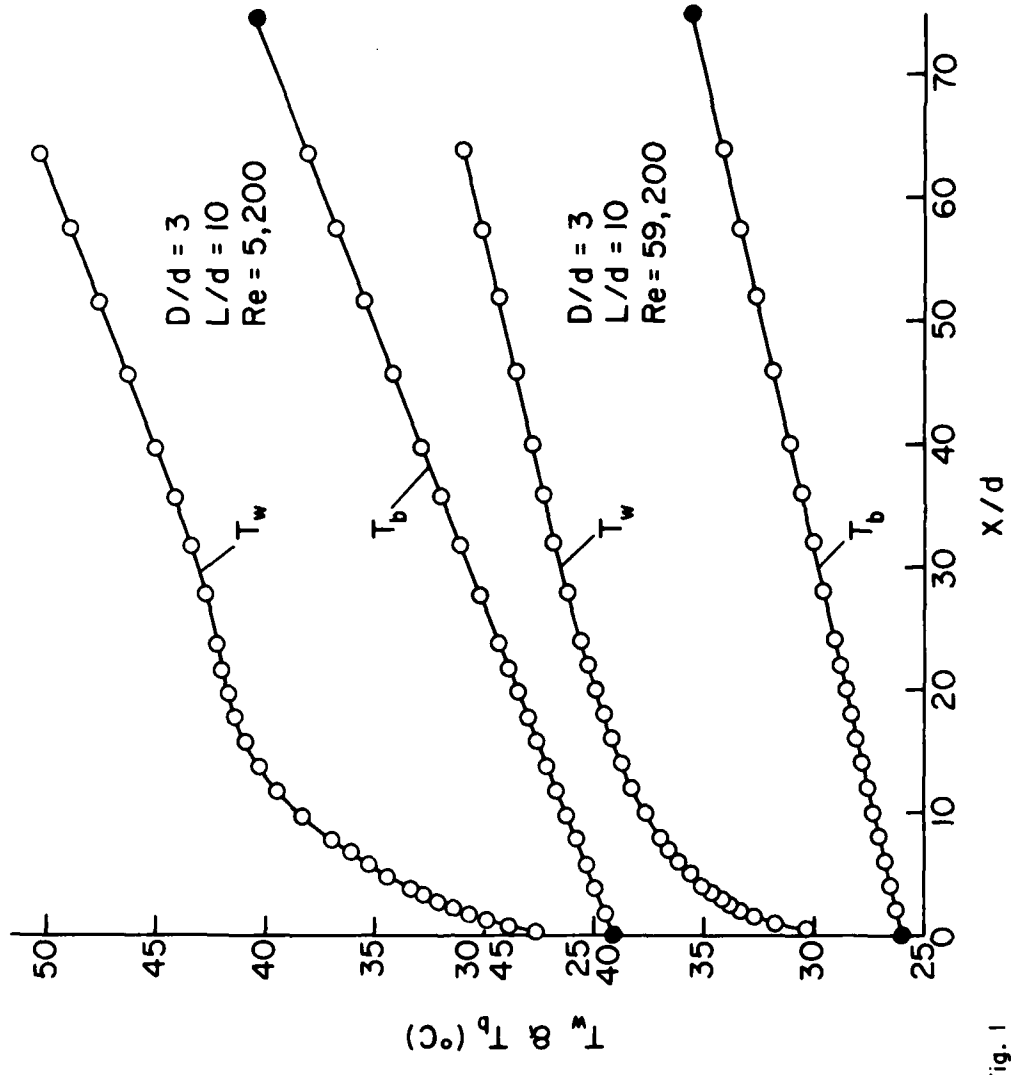
D/d = 3
L/d = 10
Re = 5,200
D/d = 3
L/d = 10
Re = 59,200
T_w
T_b
T_w
T_b
T_w & T_b (°C)
X/d
50
45
40
35
30
25
0
10
20
30
40
50
60
70

Fig. 1

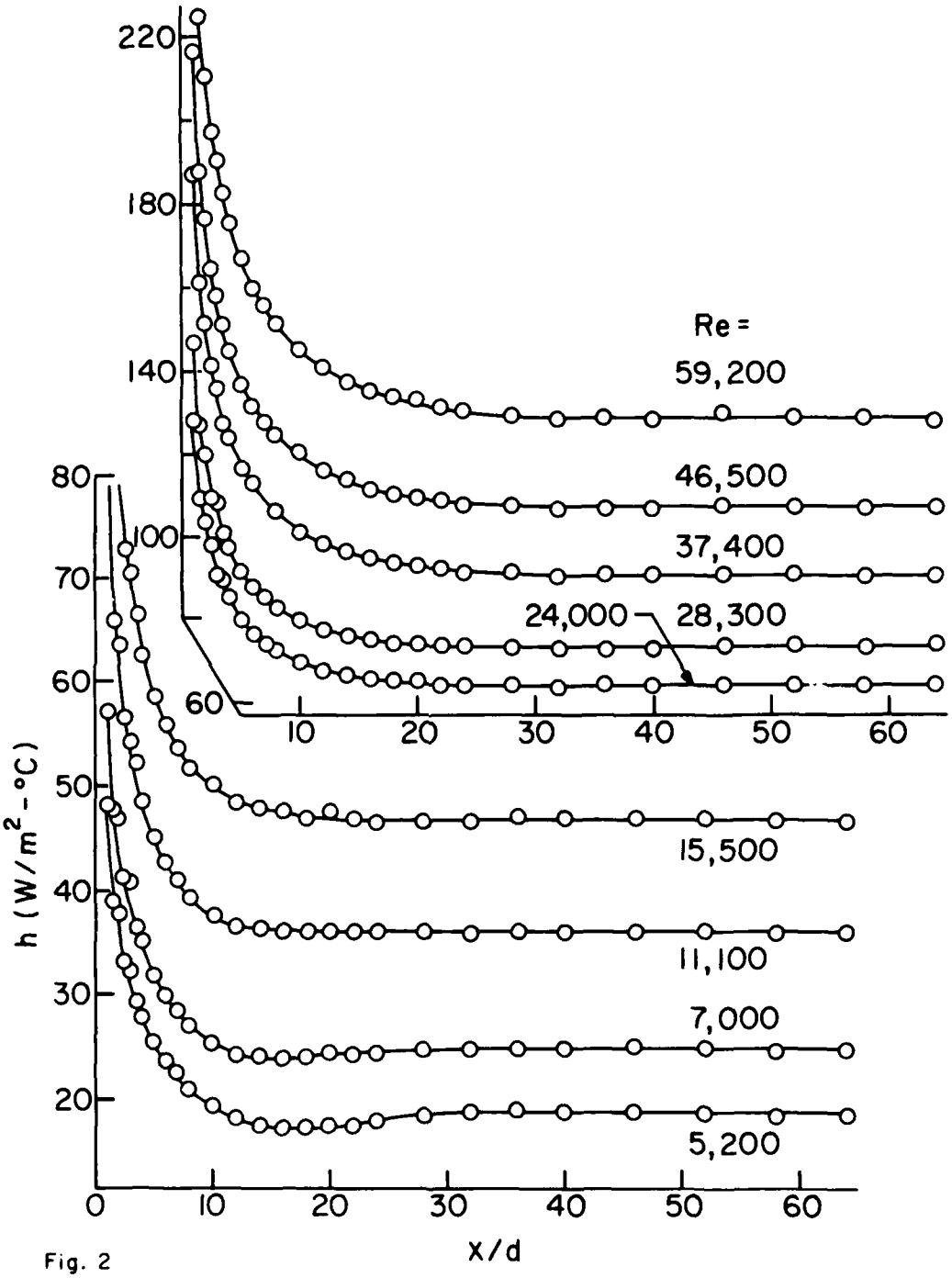
220
180
140
100
80
70
60
50
40
30
20
60
10
20
30
40
50
60
Re =
59,200
46,500
37,400
24,000
28,300
15,500
11,100
7,000
5,200
h (W/m²-°C)
0
10
20
30
40
50
60
X/d

Fig. 2

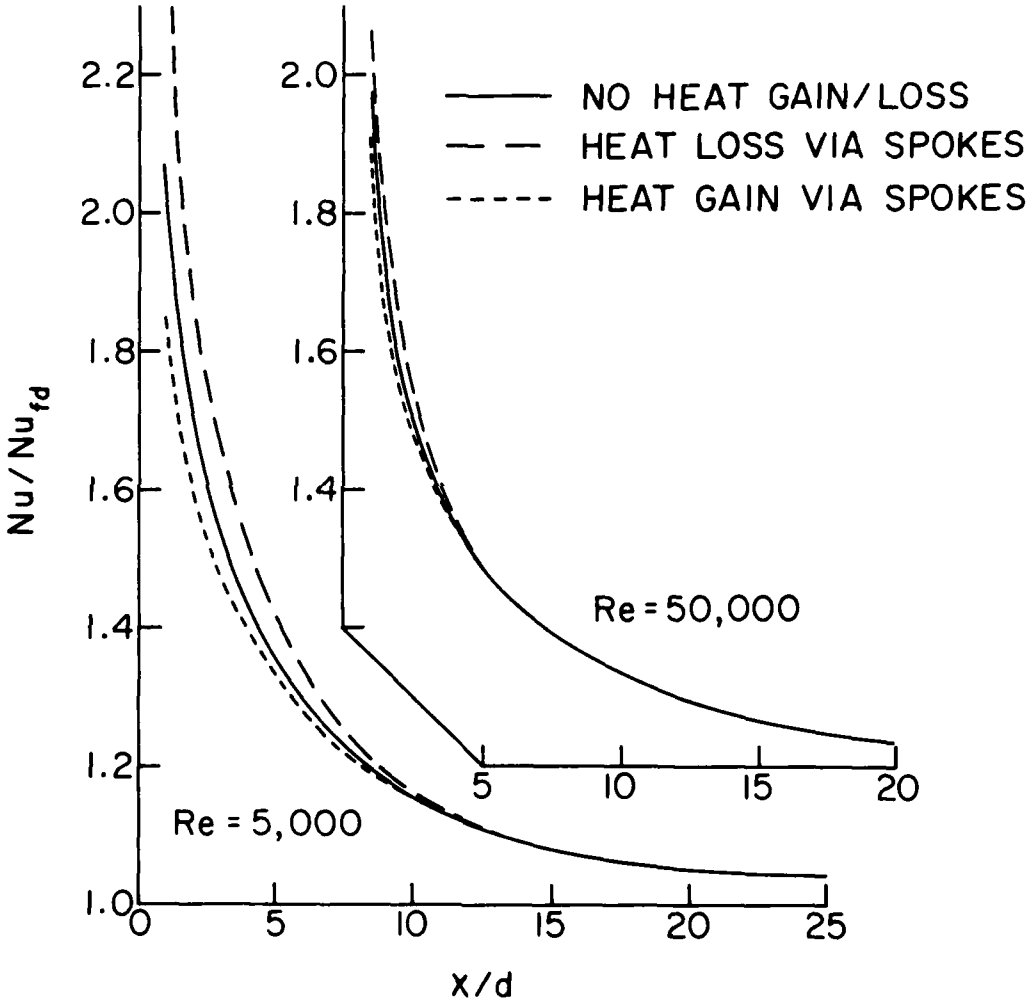
NO HEAT GAIN/LOSS
HEAT LOSS VIA SPOKES
HEAT GAIN VIA SPOKES
Re = 50,000
Re = 5,000
Nu/Nu_fd
X/d
2.2
2.0
1.8
1.6
1.4
1.2
1.0
0
5
10
15
20
25

Fig. 3

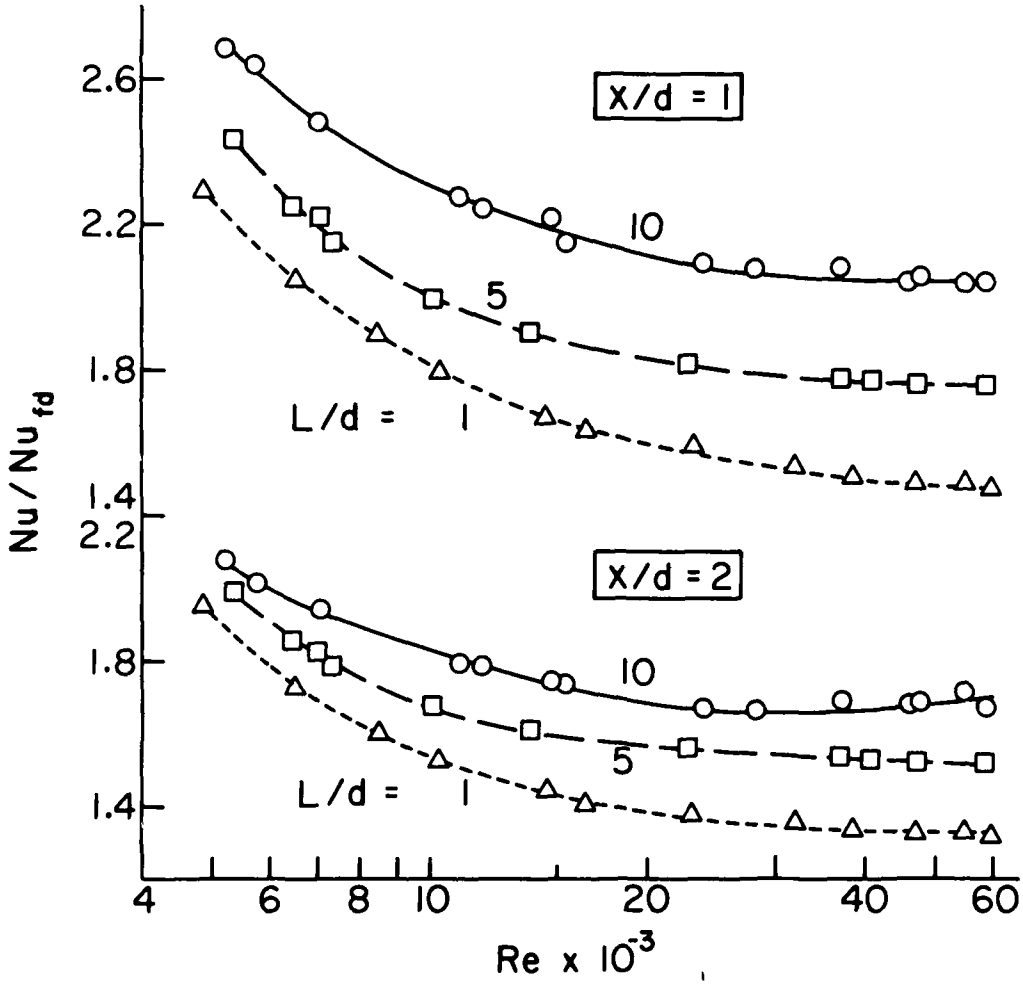
2.6
2.2
1.8
1.4
2.2
1.8
1.4
Nu / Nu fd
X/d = 1
10
5
L/d = 1
X/d = 2
10
5
L/d = 1
4
6
8
10
20
40
60
Re x 10-3

Fig. 4

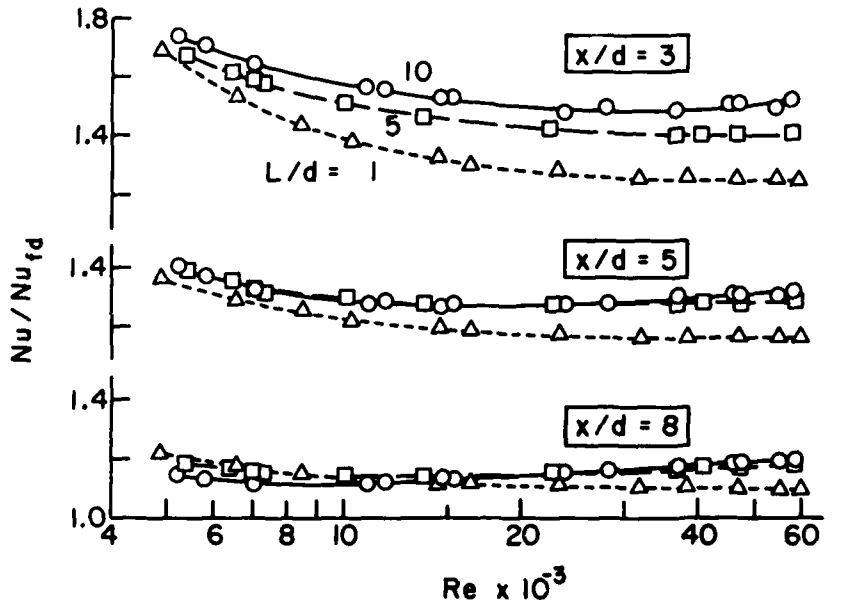

Fig. 5

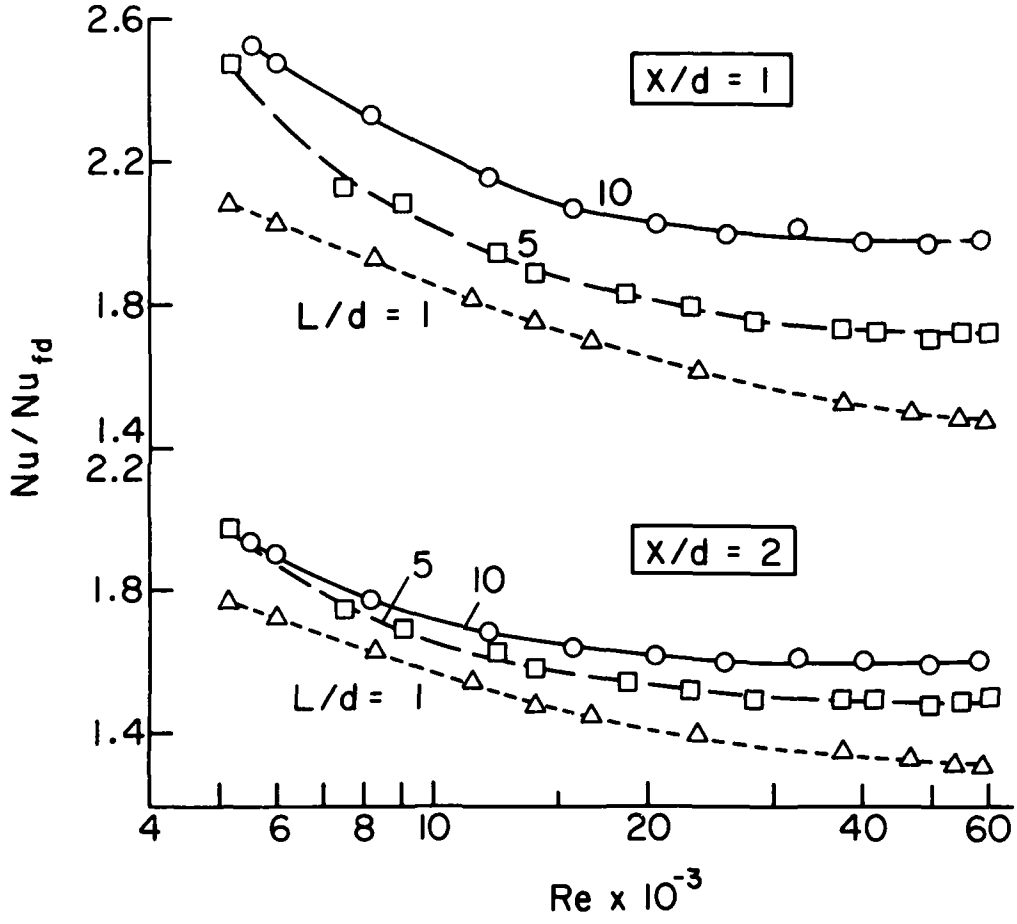
2.6
2.2
1.8
1.4
Nu / Nu fd
X/d = 1
10
5
L/d = 1
2.2
1.8
1.4
X/d = 2
5
10
L/d = 1
4
6
8
10
20
40
60
Re x 10-3

Fig. 6

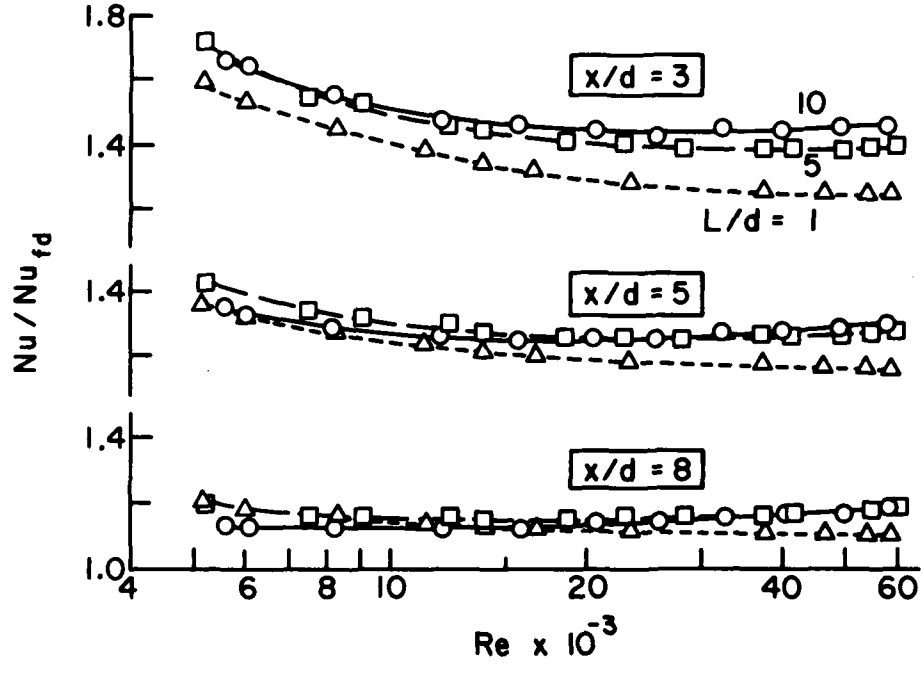

Fig. 7

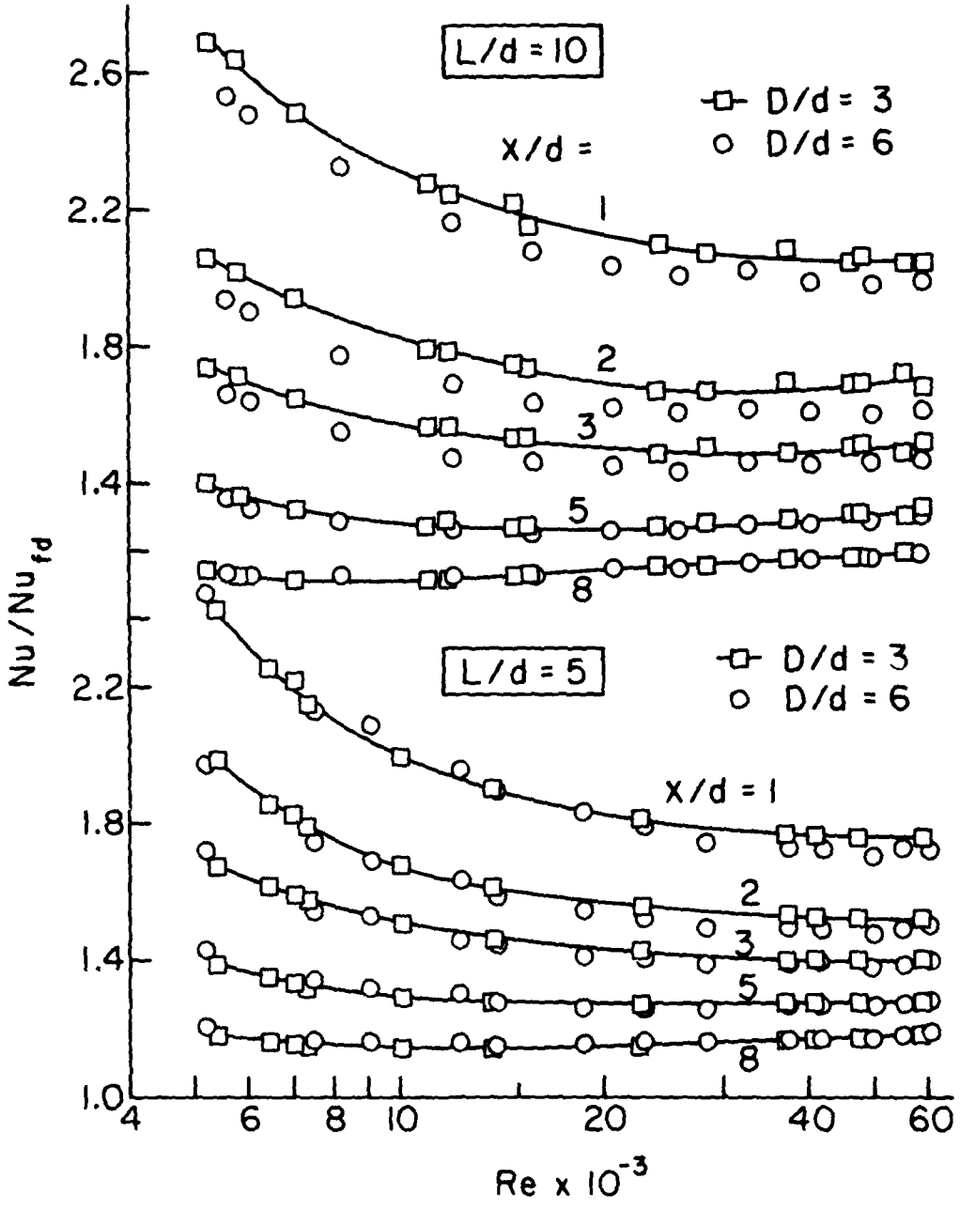
L/d = 10
D/d = 3
D/d = 6
X/d =
1
2
3
5
8
L/d = 5
D/d = 3
D/d = 6
X/d = 1
2
3
5
8
Nu/Nu_fd
2.6
2.2
1.8
1.4
2.2
1.8
1.4
1.0
4
6
8
10
20
40
60
Re x 10^-3

Fig. 8

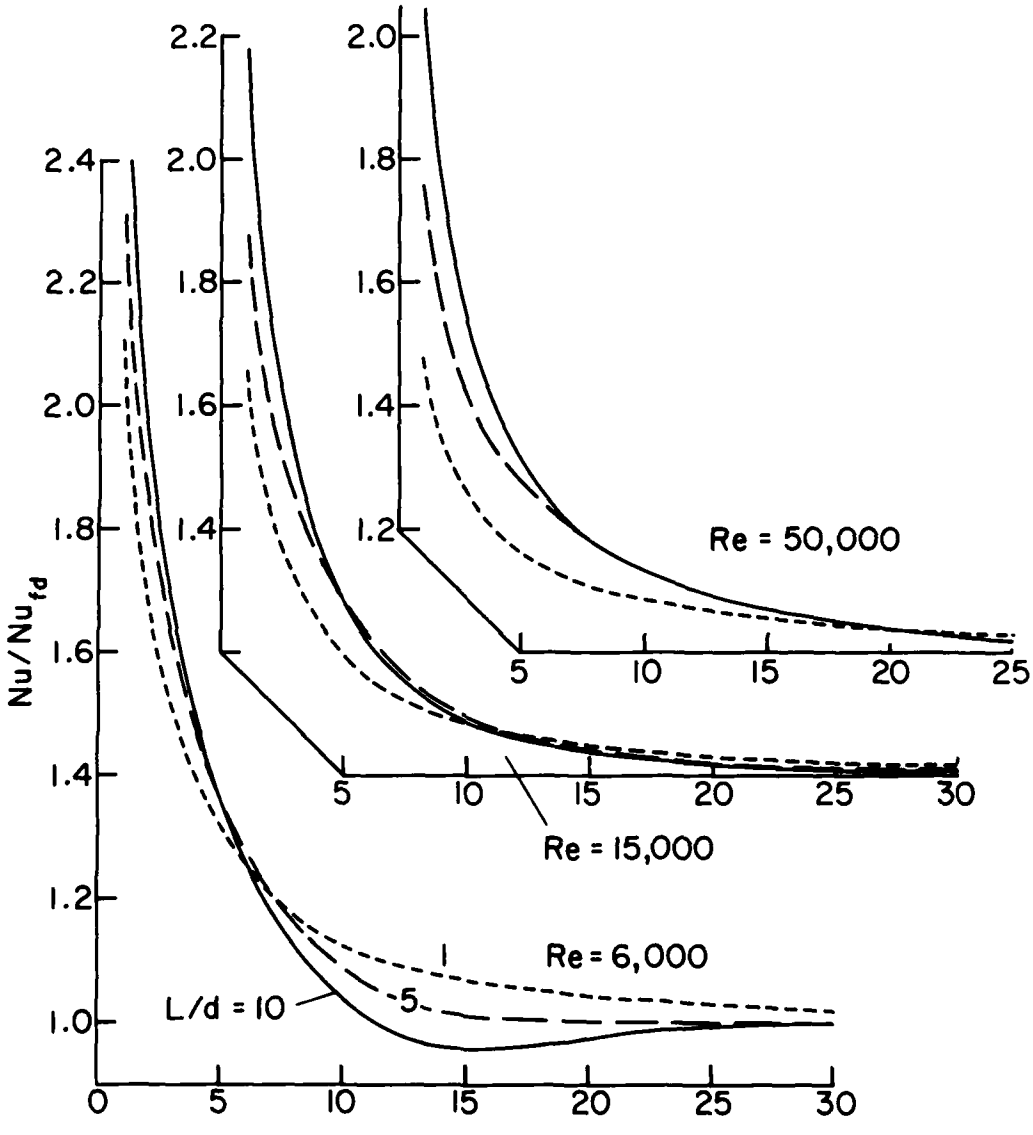

Fig. 9

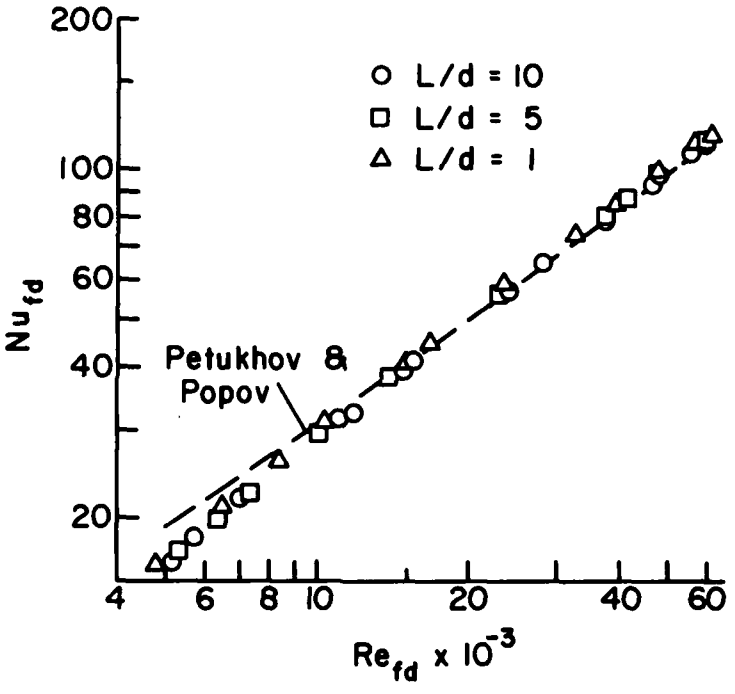
200
100
80
60
40
20
Nu_{fd}
○ L/d = 10
□ L/d = 5
△ L/d = 1
Petukhov &
Popov
4
6
8
10
20
40
60
$Re_{fd} \times 10^{-3}$

Fig. 10

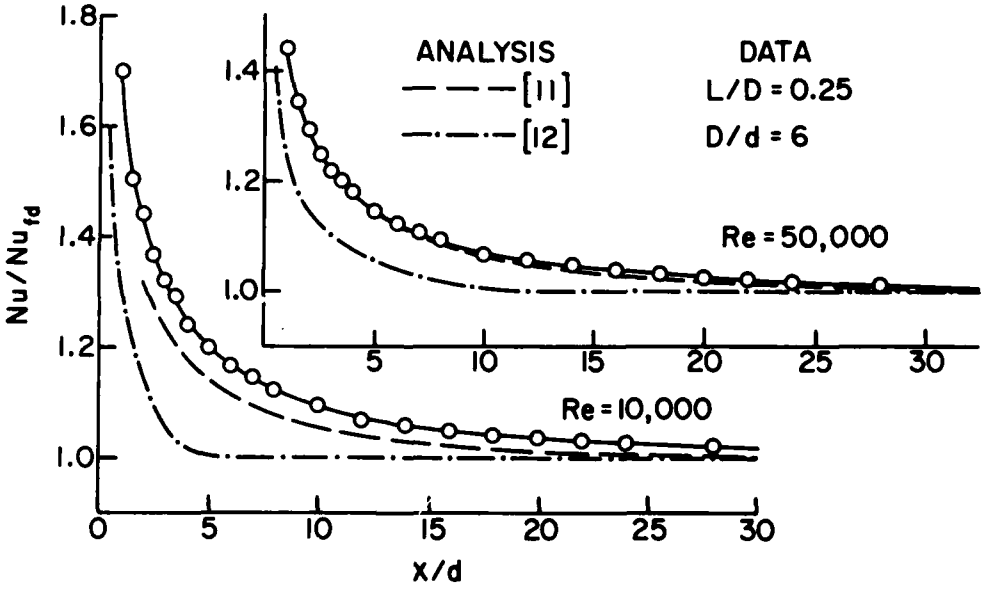
ANALYSIS
[11]
[12]
DATA
L/D = 0.25
D/d = 6
Re = 50,000
Re = 10,000
Nu/Nu_fd
X/d
1.8
1.6
1.4
1.2
1.0
0
5
10
15
20
25
30

Fig. 11

Chapter 2

HEAT TRANSFER IN A TUBE DOWNSTREAM OF A TEE IN WHICH AIRSTREAMS OF DIFFERENT TEMPERATURE ARE MIXED

NOMENCLATURE

D	diameter of test section tube
$\bar{h}_x$	circumferential average heat transfer coefficient at x
$h_x(\theta)$	local heat transfer coefficient at x,θ
k	thermal conductivity
$\dot{m}$	mass flow rate in test section
$\dot{m}_1$	mass flow rate entering side port
$\dot{m}_2$	mass flow rate entering center port
Nu_{fd}	fully developed Nusselt number
$\overline{Nu}_x$	circumferential average Nusselt number at x, $\bar{h}_x D/k$
$Nu_x(\theta)$	local Nusselt number at x, θ, $h_x(\theta)D/k$
Re	test section Reynolds number, $4\dot{m}/\mu\pi D$
T_b	bulk temperature
T_{b1}	bulk temperature of airstream entering side port
T_{b2}	bulk temperature of airstream entering center port
T_w	wall temperature
x	axial coordinate
θ	angular coordinate
μ	viscosity
Φ	bulk temperature imbalance ratio, $\lvert T_{b2} - T_{b1}\rvert/(T_w - T_b)_{fd}$

INTRODUCTION

It was demonstrated experimentally in {1} that the mixing of two air streams in a tee gives rise to enhanced heat transfer in a tube situated downstream of the tee. In those experiments, air was ducted to the center port and one of the side ports of a tee. The discharge from the other side port passed through a uniformly heated tube which served as the test section for heat transfer measurements. In the test setup used in {1}, the temperatures of the two air streams entering the tee were the same. Under such conditions, the heat transfer results in the downstream tube reflect the numerous and complex hydrodynamic processes which are induced by the mixing of the streams.

The present experiments were undertaken as a sequel to those of {1} with the aim of investigating the mixing of air streams of different temperatures. Thus, compared with {1}, the present results will reflect not only mixing-related hydrodynamic processes but also the effects of the thermal imbalance of the component air streams.

THE EXPERIMENTS

The mixing arrangement is pictured schematically in the inset of Fig. 1. As shown there, the air stream entering the side port of the tee has a bulk temperature T_{b1}, while that entering the center port has a bulk temperature T_{b2}. The respective mass flow rates are $\dot{m}_1$ and $\dot{m}_2$, and $\dot{m} = \dot{m}_1 + \dot{m}_2$ is the mass flow rate of the merged flow which passes from the other side port into the uniformly heated test section tube.

Both the $\dot{m}_1$ and $\dot{m}_2$ air streams were supplied from a central compressor. The $\dot{m}_2$ stream was ducted through a 100-diameters-long electrically heated circular tube en route to the center port of the tee. On the other hand, the $\dot{m}_1$ stream passed through an adiabatic-walled tube of similar length which delivered the air to the side port. Thus, the heating of the $\dot{m}_2$ stream coupled with the nonheating of the $\dot{m}_1$ stream gave rise to a difference $|T_{b2} - T_{b1}|$ in the bulk temperatures of the entering

streams*.

To obtain a dimensionless characterization which will reflect whether $|T_{b2} - T_{b1}|$ is large or small compared with a representative temperature difference in the flow in the test section tube, the ratio

$$\Phi = |T_{b2} - T_{b1}|/(T_w - T_b)_{fd} \tag{1}$$

was employed. The quantity $(T_w - T_b)_{fd}$ is the wall-to-bulk temperature difference in the fully developed regime which is attained in the downstream portion of the tube. During the course of the experiments, the Φ ratio was varied from zero to three.

Aside from the bulk temperature imbalance as reflected by Φ, the conduct of the experiments and the data reduction procedure were similar to that of {1}, and {1} may be consulted for details. For a given test section Reynolds number

$$Re = 4\dot{m}/\mu\pi D \tag{2}$$

data runs were carried out for parametric values of the flow mixing ratio $\dot{m}_1/\dot{m}$. The extreme values of $\dot{m}_1/\dot{m}$, namely, $\dot{m}_1/\dot{m} = 0$ and 1, are irrelevant to the present study of temperature imbalance effects since they represent single stream inflows. Data runs corresponding to values of $\dot{m}_1/\dot{m} = 0.25$, 0.50, and 0.75 were made for each Reynolds number.

The original research plan included a parametric study involving several Reynolds numbers. However, with increasing Reynolds number and at higher Φ values, it was not possible to null out radial heat flows in the bus bars used to deliver current to the upstream end of the electrically heated test section. The bus bars were fitted with guard heaters and differential thermocouples, but under the aforementioned conditions the guard heaters were unable to reduce the readings of the differential thermocouples to zero. Satisfactory operation was obtained for the data runs corresponding to a Reynolds number of 20,000, but the Re = 30,000 results contain some uncertainty. Fortunately, all of the trends in evidence for Re = 20,000 also appear

* The absolute value of the difference between T_{b2} and T_{b1} will be used here because the results should be applicable both for $T_{b2} > T_{b1}$ and $T_{b2} < T_{b1}$.

in the results for Re = 30,000. Because of their greater certainty and because they show all the basic trends, only the Re = 20,000 results are presented here. Those for Re = 30,000 may be found in {2}.

Owing to the right-angle intersection of the two streams entering the tee, circumferential variations of the test-section heat transfer coefficients are encountered in addition to axial variations. In view of this, two types of heat transfer coefficients are employed in the presentation of the results. One of these is the circumferential average heat transfer coefficient $\bar{h}_x$ corresponding to an axial station x. If $\bar{q}_x$ is the circumferential average rate of heat transfer per unit area at x and $\bar{T}_{wx}$ is the circumferential average wall temperature, also at x, then

$$\bar{h}_x = \bar{q}_x/(\bar{T}_{wx} - T_{bx}) \tag{3}$$

where T_{bx} is the local bulk temperature of the air. The data reduction methods used in the evaluation of equation (3) may be found in {1} or {2}. The local Nusselt number corresponding to $\bar{h}_x$ is

$$\overline{Nu}_x = \bar{h}_x D/k \tag{4}$$

in which k was evaluated at T_{bx}.

The other heat transfer coefficient used in the presentation of results is the local angular coefficient $h_x(\theta)$, which pertains to an angular position θ at an axial station x. The defining equations for $h_x(\theta)$ and its dimensionless counterpart $Nu_x(\theta)$ are

$$h_x(\theta) = q_x(\theta)/(T_{wx}(\theta) - T_{bx}), \quad Nu_x(\theta) = h_x(\theta)D/k \tag{5}$$

where, again, k corresponds to the local bulk temperature. For the evaluation of equation (5), the local wall temperature $T_{wx}(\theta)$ is determined by direct measurement while $q_x(\theta)$ is obtained from a data reduction procedure which accounts for internal heat generation and circumferential conduction in the tube wall and for heat losses to the surroundings {1, 2}.

RESULTS AND DISCUSSION

The circumferential average heat transfer results for Re = 20,000 are presented in Figs. 1 - 3, respectively for $\dot{m}_1/\dot{m}$ = 0.25, 0.5, and 0.75. In each figure, the Nusselt number ratio $\overline{Nu}_x/Nu_{fd}$ is plotted as a function of the dimensionless axial coordinate x/D, where x is measured from the geometric center of the tee and the heated tube begins at x/D = 0.76. The quantity Nu_{fd} is the fully developed Nusselt number. The data appearing in each figure are parameterized by the inlet bulk-temperature imbalance ratio $|T_{b2} - T_{b1}|/(T_w - T_b)_{fd}$. The limiting case $|T_{b2} - T_{b1}|/(T_w - T_b)_{fd} = 0$, which corresponds to identical temperatures of the two streams entering the tee, serves as a baseline case against which to compare the results for the cases with temperature imbalance.

Examination of the figures shows that the expected trend of $\overline{Nu}_x/Nu_{fd}$ decreasing with x/D is preserved for all of the inlet temperature imbalances investigated here. Aside from a few exceptions at the smaller x/D, there is a trend toward lower values of $\overline{Nu}_x/Nu_{fd}$ as the inlet temperature imbalance increases. Thus, it appears that the effect of temperature imbalance is to decrease the circumferential average Nusselt number. The influence of the imbalance is greatest at small x/D and diminishes as the fully developed region is approached.

Further inspection of the figures suggests that there is an overall trend for the results to be more sensitive to the inlet temperature imbalance as $\dot{m}_1/\dot{m}$ increases. Indeed, aside from the most upstream station, the Nusselt numbers for $\dot{m}_1/\dot{m}$ = 0.25 are nearly independent of the imbalance. Even for $\dot{m}_1/\dot{m}$ = 0.5, there is only a small spread in the data for different $|T_{b2} - T_{b1}|/(T_w - T_b)_{fd}$. The greatest sensitivity of the results to the imbalance is for $\dot{m}_1/\dot{m}$ = 0.75.

To rationalize the aforementioned trend with $\dot{m}_1/\dot{m}$, attention may be called to the fact that the smaller the $\dot{m}_1/\dot{m}$, the larger are the values of $\overline{Nu}_x/Nu_{fd}$. This is entirely reasonable since small $\dot{m}_1/\dot{m}$ signifies a relatively large inflow through the center port of the tee. The fluid entering via the center port experiences a complex

and chaotic turning process (replete with impingement on the wall of the tee) en route to the exit (side) port of the tee. This process generates highly intense turbulence, mixing, and three-dimensional motions, the totality of which contributes to the heat transfer enhancement that is in evidence when $\dot{m}_1/\dot{m}$ is small (i.e., when $\dot{m}_2/\dot{m}$ is large). When $\dot{m}_1/\dot{m}$ is large, the turning process is relatively placid, and the enhancement is small.

These ideas can now be used to explain why a flow with small $\dot{m}_1/\dot{m}$ is less sensitive to the inlet bulk-temperature imbalance than is a flow with large $\dot{m}_1/\dot{m}$. First, it should be noted that if perfect thermal mixing of the $\dot{m}_1$ and $\dot{m}_2$ streams were to occur before the merged flow enters the heated test section tube, then the Nusselt number results would be completely unaffected by the difference between T_{b2} and T_{b1}. It is also reasonable to expect that if no thermal mixing were to occur before the merged flow enters the test section, there would be high sensitivity of the Nusselt number results to the imbalance between T_{b2} and T_{b1}. On the basis of the preceding paragraph, it can be expected that much greater thermal mixing will occur for $\dot{m}_1/\dot{m} = 0.25$ than for $\dot{m}_1/\dot{m} = 0.75$, thereby explaining the trend of the results of Figs. 1 - 3.

There are isolated axial stations in evidence in Figs. 1 - 3 at which the general trends identified in the foregoing paragraphs are not in force. This is especially true at the first axial station in Fig. 1. These deviations may be true reflections of the participating physical phenomena or, alternatively, they may reflect extraneous effects such as bus bar heat losses (or gains). It appears that this issue cannot be conclusively settled with the information at hand.

Attention is now turned to the angular distributions of the local transfer coefficient $h_x(\theta)$. Representative results, corresponding to Re = 20,000 and $\dot{m}_1/\dot{m} = 0.5$, are presented in Fig. 4 (other angular distributions are available in {2}). The figure contains four columns of graphs, with each column conveying data for a specific value of $|T_{b2} - T_{b1}|/(T_w - T_b)_{fd}$. In each graph, the ratio $Nu_x(\theta)/\overline{Nu}_x$ is plotted as a

function of the angular coordinate θ. The $\theta = 0$ position corresponds to the top of the tube as it is pictured in the inset of Fig. 1 (i.e., $\theta = 0$ lies along the centerline of the center port), while $\theta = \pi$ is at the bottom of the tube. Angular distributions are presented at a number of axial stations for which the x/D values are indicated in the graphs.

The main message of the figure relates to the different nature of the angular variations at the first several stations for $|T_{b2} - T_{b1}| = 0$ and $|T_{b2} - T_{b1}| > 0$. For the former, the highest heat transfer coefficients occur at $\theta = 0$ and the lowest at $\theta = \pi$. An opposite relationship is in force for the latter, and the deviation between the bottom and top coefficient values increases as $|T_{b2} - T_{b1}|/(T_w - T_b)_{fd}$ increases. With increasing downstream distance, the angular variations ultimately die away, but residual variations are still present as far downstream as x/D = 36.

REFERENCES

1. Sparrow, E. M. and Kemink, R. G., "The Effect of a Mixing Tee on Turbulent Heat Transfer in a Tube," International Journal of Heat and Mass Transfer, Vol. 22, 1979, pp. 909-917.

2. Cur, N., "Heat Transfer Downstream of a Tee which Mixes Airstreams of Different Temperature," M.S. Thesis, Department of Mechanical Engineering, University of Minnesota, Minneapolis, Minnesota, 1980.

FIGURE CAPTIONS

Fig. 1 Circumferential average Nusselt numbers, Re = 20,000 and $\dot{m}_1/\dot{m} = 0.25$. The inset is a schematic of the mixing arrangement.

Fig. 2 Circumferential average Nusselt numbers, Re = 20,000 and $\dot{m}_1/\dot{m} = 0.5$

Fig. 3 Circumferential average Nusselt numbers, Re = 20,000 and $\dot{m}_1/\dot{m} = 0.75$

Fig. 4 Angular distributions of the local Nusselt number, Re = 20,000 and $\dot{m}_1/\dot{m} = 0.5$

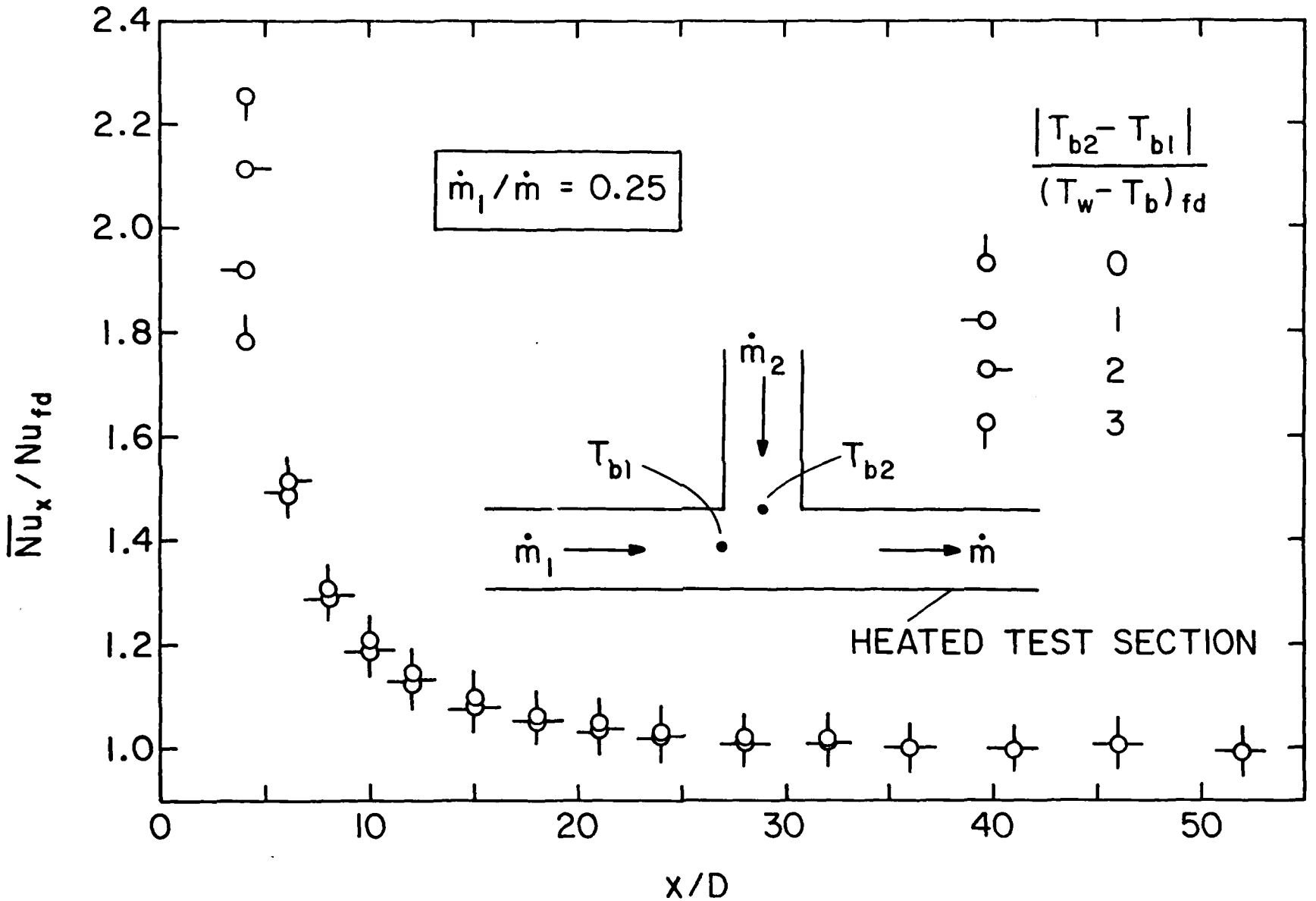
2.4
2.2
2.0
1.8
1.6
1.4
1.2
1.0
0
10
20
30
40
50
X/D
$\overline{Nu}_x / Nu_{fd}$
$\dot{m}_1 / \dot{m} = 0.25$
$\frac{|T_{b2} - T_{b1}|}{(T_w - T_b)_{fd}}$
0
1
2
3
$\dot{m}_2$
T_{b1}
T_{b2}
$\dot{m}_1$
$\dot{m}$
HEATED TEST SECTION

Fig. 1

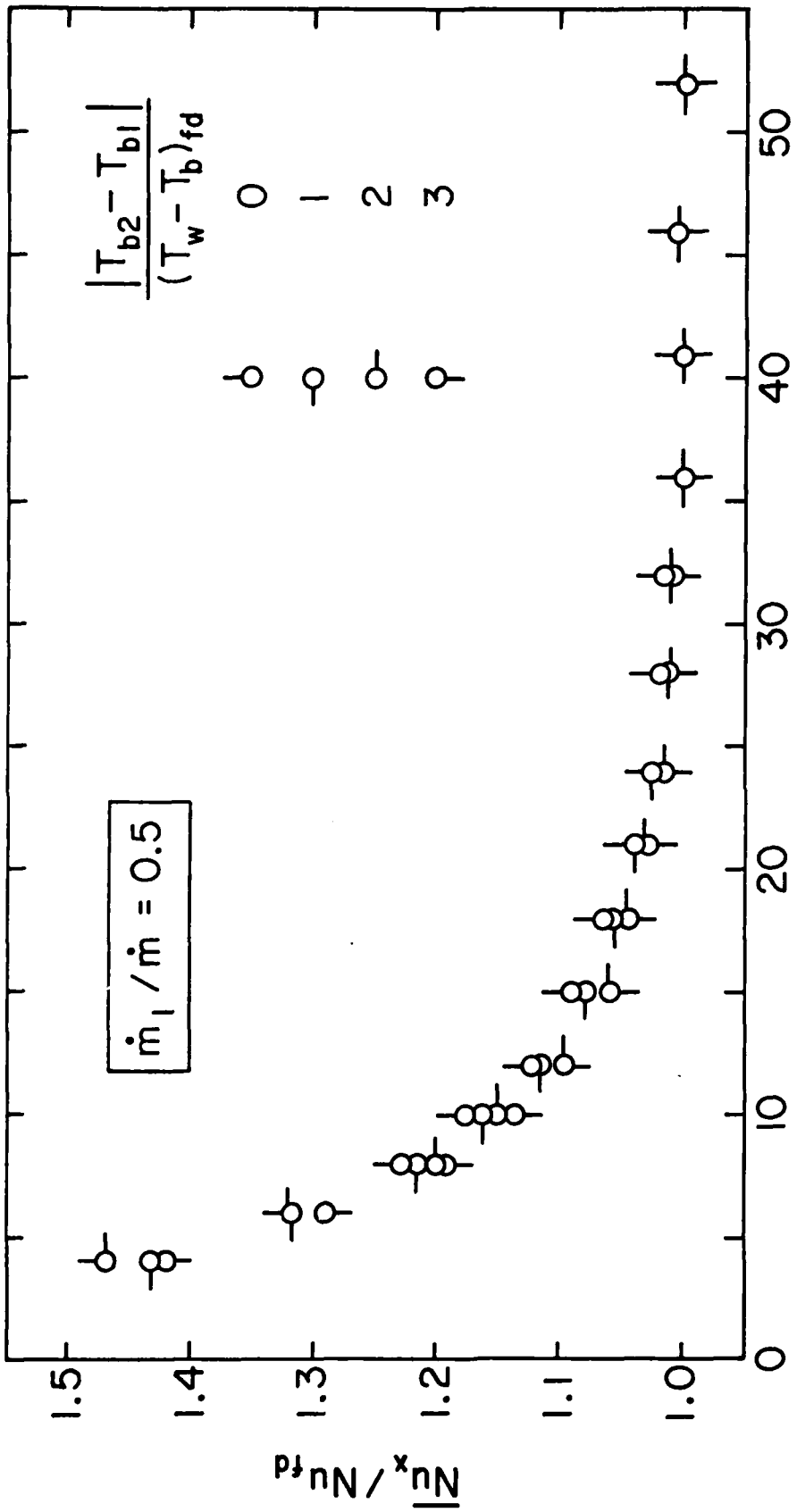
$\frac{|T_{b2}-T_{b1}|}{(T_w-T_b)_{fd}}$
0
1
2
3
$\dot{m}_1/\dot{m} = 0.5$
$\overline{Nu}_x/Nu_{fd}$
X/D
1.0
1.1
1.2
1.3
1.4
1.5
0
10
20
30
40
50

Fig. 2

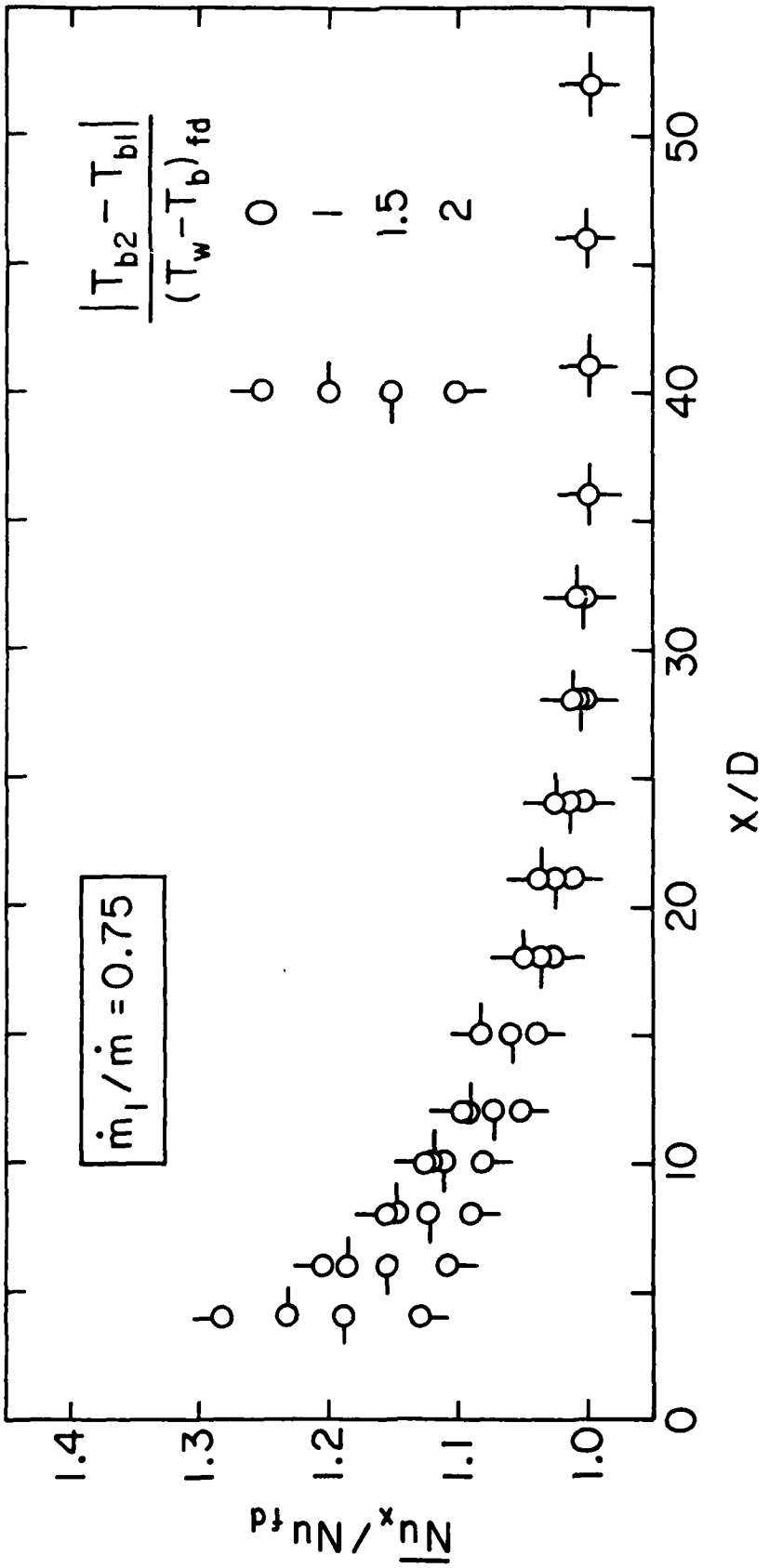
$\dot{m}_1/\dot{m} = 0.75$
$\left|\frac{T_{b2} - T_{b1}}{(T_w - T_b)_{fd}}\right|$
0
1
1.5
2
$\overline{Nu}_x/Nu_{fd}$
1.0
1.1
1.2
1.3
1.4
X/D
0
10
20
30
40
50

Fig. 3

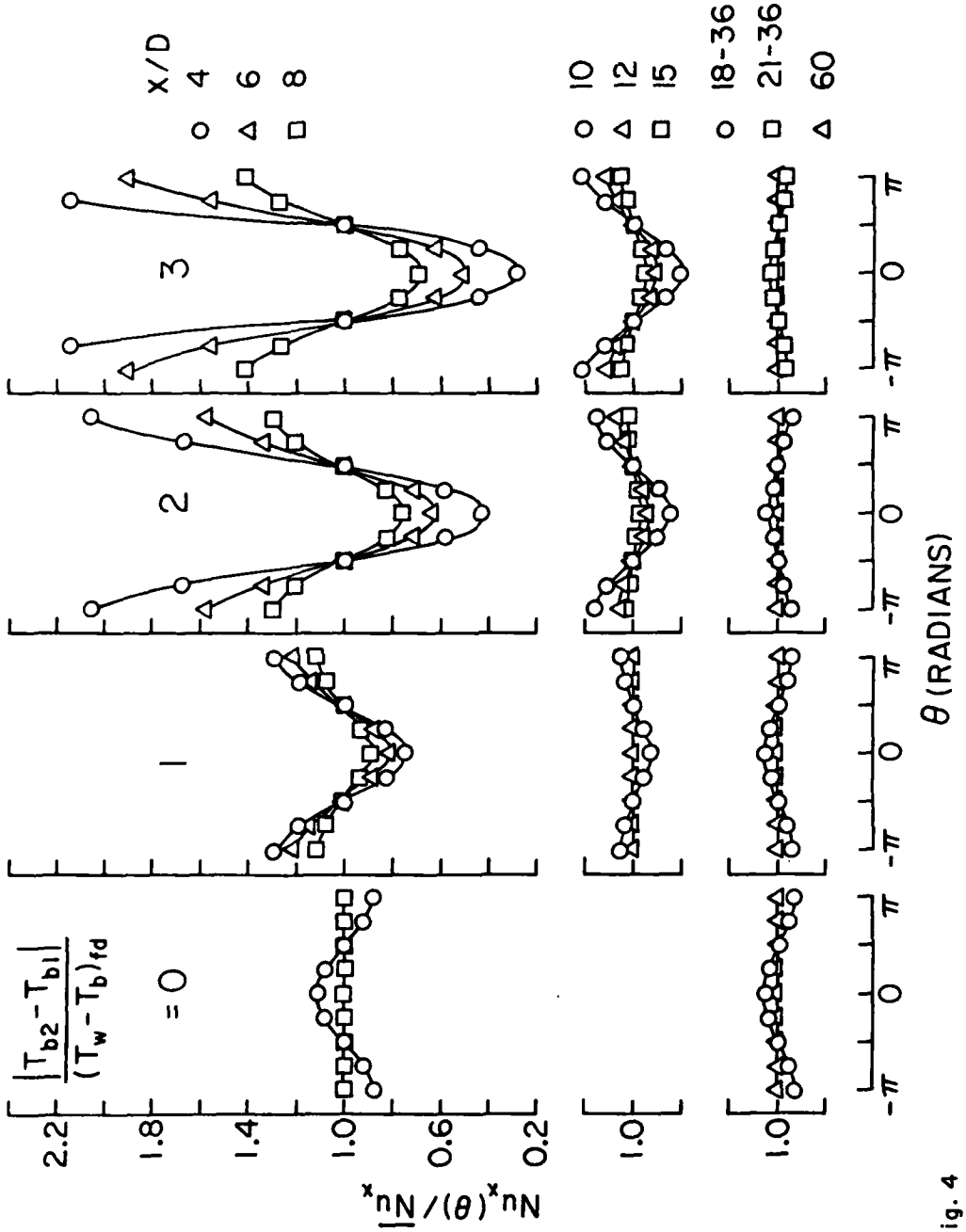
x/D
4
6
8
10
12
15
18-36
21-36
60
$\frac{|T_{b2}-T_{b1}|}{(T_w-T_b)_{fd}}$ = 0
1
2
3
$Nu_x(\theta)/\overline{Nu}_x$
2.2
1.8
1.4
1.0
0.6
0.2
-π
0
π
θ (RADIANS)

Fig. 4

Chapter 3

PRESSURE DROP CHARACTERISTICS FOR A SHROUDED LONGITUDINAL-FIN ARRAY WITH TIP CLEARANCE

INTRODUCTION

The design of energy-efficient heat exchange devices requires a knowledge of pressure drop (and/or pumping power) characteristics as well as of heat transfer characteristics. Pressure drop information is especially relevant in connection with enhanced heat transfer devices, since the heat transfer enhancement frequently gives rise to higher pressure losses. Among enhancement techniques, fins are, perhaps, the most prevalent and, therefore, their pressure drop characteristics are of practical relevance.

In this report, pressure drop experiments are described for airflow through an array of longitudinal fins attached to one of the principal walls of a flat rectangular duct. The other principal wall of the duct can be regarded as a shroud. In the absence of such a shroud, air would escape from the interfin spaces into the surroundings beyond the tips of the fins.

If the fin tips are in intimate contact with the shroud, then any pair of adjacent fins, together with the fin base surface and the shroud, forms a subchannel that is separate from the other similarly constituted subchannels. Each subchannel is, itself, a rectangular duct, and the pressure drop characteristics of rectangular ducts are sufficiently well studied so as not to require further elaboration.

If, on the other hand, a clearance gap is present between the tips of the fins and the shroud, there will be longitudinal flow through the gap as well as through the interfin spaces. The extent to which the flow subdivides itself between these parallel paths depends on the relative magnitude of the resistances encountered along the respective paths. In turn, the relative resistances depend on such

geometrical parameters as the size of the clearance gap, the interfin spacing, and the height of the fins.

The research reported here is concerned with the fully developed pressure drop characteristics (i.e., friction factors) of an array of longitudinal fins in the presence of a clearance gap. The experimental apparatus was designed with a high degree of flexibility so that the key geometrical parameters could be varied without a major rebuilding of the system. All told, nine different geometrical configurations were investigated with the same apparatus, encompassing variations of interfin spacing, fin height, and fin-shroud clearance gap. For each configuration, the Reynolds number was varied over the full range permitted by the air supply and the instrumentation. Auxiliary experiments were carried out for rectangular ducts of various aspect ratios in order to confirm the experimental technique. Fully developed friction factors are presented for all cases.

A search of the literature failed to reveal any experimental work on the fin arrangement investigated here. The most closely related configuration for which experimental friction factors are reported is the longitudinally internally finned circular tube, for which {1} is a representative reference. Analytical results for the present fin arrangement have been reported in {2}, but they are for laminar flow, while the experimental results obtained here are for turbulent and transitional flow.

THE EXPERIMENTS

A schematic cross-sectional view of the test section is shown in the upper part of Fig. 1. As seen there, the base plate, the upper wall, and the two side walls are made of heavy structural members (respectively 1.270-cm thick aluminum plate and 1.905-cm thick cold-rolled steel bars). On the base plate rest eleven spacer bars distributed across the span of the duct. Each bar is 0.635 cm thick and is made of cold-rolled steel. The spacer bars serve to support and position the fins, as can be seen from the enlarged view in the lower portion of Fig. 1. Each fin is held between the adjacent pair of spacer bars, with the lower part of the fin situated

sandwich-style between the bars and the upper part jutting into the flow passage. Thus, the flow passage consists of the interfin space above the bars and the clearance gap between the fin tips and the upper wall.

The fins were fabricated from 0.0762-cm thick galvanized steel sheet selected specifically because of its surface smoothness. They were first cut to the approximate final height by a shear. The cut edges were finished to right angles with the aid of a large surface grinder, with a resulting tolerance of $\pm$ 0.00127 cm on the fin height being maintained over the entire longitudinal extent of each fin.

The overall height H of the flow passage was maintained at 2.54 cm for all of the data runs; in addition, a fixed thickness t = 0.0762 cm was employed for all of the fins. The interfin spacing S and the fin height h were varied parametrically. Three interfin spacings were investigated, respectively characterized by S/H = 1/4, 1/2, and 1. For each fixed S/H, the fin height h/H was varied from 3/8 to 5/8 to 7/8, with corresponding values of C/H = 5/8, 3/8, and 1/8. The length of the test section in the flow direction is 121.9 cm.

The diagram in the upper part of Fig. 1 portrays the duct cross section with the widest spacer bars (i.e., S = 2.54 cm) in place. When the smaller spacers are installed, either S = 1.27 cm or 0.635 cm, the overall width of the flow cross section (equal to 11S + (10)(0.0762) cm) diminishes. This narrowing of the cross section was accommodated by the rightward repositioning of the left-hand wall of the test section. The installation or removal of the spacers and fins was accomplished by removal of the top wall of the test section.

For the measurement of the axial pressure distribution, twenty-one taps were distributed along the length of the test section. The taps were installed in the upper wall of the duct, along the centerline of the central subchannel (thus, a different set of taps was used for each of the three interfin spacings). In addition, to check on the uniformity of the flow distribution among the various subchannels, auxiliary taps were installed along the centerline of the next-to-the-outermost

channel adjacent to each sidewall. The pressure signals were conveyed via plastic tubing to a selector switch and thence to a Baratron solid-state capacitance-type pressure meter. Either of two pressure sensing heads were used depending on the flow rate. The heads could resolve pressure differences of 10^{-4} and 10^{-5} mm Hg respectively. The output of the Baratron was read with a digital voltmeter.

Air was drawn into the inlet of the test section from the laboratory room. After passing through the test section, the air discharged into a large plenum chamber, from which it was ducted to a rotameter and a control valve. One of three rotameters was used for flow metering depending on the flow rate.

RESULTS AND DISCUSSION

Fully developed flow, as evidenced by the linear decrease of the pressure along the duct, was established after a short hydrodynamic development length. The linear region typically encompassed ten or more pressure taps. Figure 2 shows the axial pressure distribution for a representative data run.

A least-squares straight-line fit was employed to determine the pressure gradient (-dp/dx) for each case. Then, the fully developed friction factor was evaluated from its definition

$$f = (-dp/dx)D_h/\tfrac{1}{2}\rho\bar{V}^2 \tag{1}$$

The hydraulic diameter D_h appearing in equation (1) corresponds to a subchannel bounded by the upper and lower walls of the flow passage and by the vertical symmetry lines passing through the half thickness of each fin. Thus, with A and P respectively designating the cross sectional area and the wetted perimeter,

$$D_h = 4A/P, \quad A = SH + 2(t/2)C \tag{2}$$

$$P = S + 2h + 2(t/2) + S + 2(t/2) \tag{3}$$

The mean velocity appearing in equation (1) was evaluated by prorating the measured mass flow uniformly among the eleven subchannels. The friction factors will be plotted as a function of the Reynolds number Re

$$Re = \rho\bar{V}D/\mu, \quad \rho\bar{V} = \dot{m}/A \tag{4}$$

where $\dot{m}$ is the subchannel mass flow.

The first set of results to be reported are those for the rectangular ducts which correspond to operation of the test section without the spacer bars and fins in place. These ducts will be designated by their aspect ratios 2.44, 4.64, and 9.04. The rectangular-duct friction factors are plotted as a function of the Reynolds number in the upper graph of Fig. 3. Also plotted there is the Prandtl equation

$$f^{-1/2} = 2\log(Ref^{1/2}) - 0.8 \tag{5}$$

which is the best established circular-tube friction factor correlation. It is frequently applied to noncircular ducts by substituting the hydraulic diameter D_h in place of the tube diameter.

Examination of the figure shows that the data for the three aspect ratios are in generally good agreement with each other. Furthermore, the trend of the data follows that of the Prandtl equation, with a mean deviation of the data from the Prandtl line of about four percent. Such a deviation is entirely acceptable, since it is well established in the literature that the hydraulic diameter does not precisely adapt circular-tube friction factors to rectangular ducts {3}. In general, the comparison shown in the upper part of Fig. 3 lends support to the experimental technique.

The friction factor results for the longitudinal fin arrays are presented in Fig. 4, with the lower, middle, and upper graphs corresponding respectively to fixed interfin spacings S/H = 1/4, 1/2, and 1. In each graph, the data for the various fin heights h/H and clearance gaps C/H are identified by different symbols. Curves have been faired through the data to provide continuity.

From an examination of Fig. 4, it is seen that in each graph (that is, at a fixed interfin spacing S/H), the data for the various fin heights and clearance gaps fall together, so that the friction factors are independent of h/H or C/H. This finding indicates that the use of the hydraulic diameter is effective in eliminating

the tip-to-shroud clearance as an independent parameter in the friction factor--Reynolds number relationship. The fact that the f,Re correlation is independent of the clearance gap is an important design simplification.

Further inspection of Fig. 4 suggests that there are differences in the slopes of the f,Re distributions for the various interfin spacings S/H. To address this issue more directly, the faired curves from the three graphs of Fig. 4 have been brought together in the lower portion of Fig. 3, where the Prandtl equation is also plotted. From this comparison, it is seen that the spread among the experimental results is no greater than ten percent. At the high Reynolds number end of the range, however, there appears to be a tendency for the friction factors for the S/H = 1/2 and 1 spacings to decrease more slowly than do the f values for the S/H = 1/4 spacing and from the Prandtl equation.

The fact that there is a spread of the experimental results with S/H indicates that the use of the hydraulic diameter is not fully able to eliminate the effects of interfin spacing. On the other hand, the relatively slower decrease of the larger-spacing friction factors at the higher Reynolds numbers is suggestive of possible fluid flow complexities. In this connection, it may be noted that a slowly decreasing friction factor with Reynolds number has been encountered in duct flows where there are significant inertial losses (e.g., roughness). It may be conjectured that in the present flow configuration, inertial-type losses may be induced by secondary flows (i.e., corkscrew-like flows). Such flows are known to exist in rectangular ducts under turbulent conditions. It is to be expected that the more vigorous the secondary flow, the greater the inertial losses. Thus, it would appear that the secondary flows are more constrained when the interfin spacing is small and are more vigorous for larger interfin spacings.

REFERENCES

1. Carnavos, T. C., "Heat Transfer Performance of Internally Finned Tubes in Turbulent Flow," in Advances in Enhanced Heat Transfer, American Society of Mechanical Engineers, New York, 1979, pp. 61-67.

2. Sparrow, E. M., Baliga, B. R., and Patankar, S. V., "Forced Convection Heat Transfer from a Shrouded Fin Array With and Without Tip Clearance," ASME Journal of Heat Transfer, Vol. 100, 1978, pp. 572-579.

3. Jones, O. C., Jr., "An Improvement in the Calculation of Turbulent Friction in Rectangular Ducts," ASME Journal of Fluids Engineering, Vol. 98, 1976, pp. 173-181.

FIGURE CAPTIONS

Fig. 1 Schematic cross-sectional view of the test section (upper diagram) and detail of a subchannel (lower diagram)

Fig. 2 Representative axial pressure distribution; the data are for S/H = 1/4, h/H = 7/8, and volume flow = 74 scfm

Fig. 3 Upper graph: Rectangular-duct friction factors; lower graph: comparison of friction factor results for various longitudinally finned ducts

Fig. 4 Friction factor results for longitudinally finned ducts

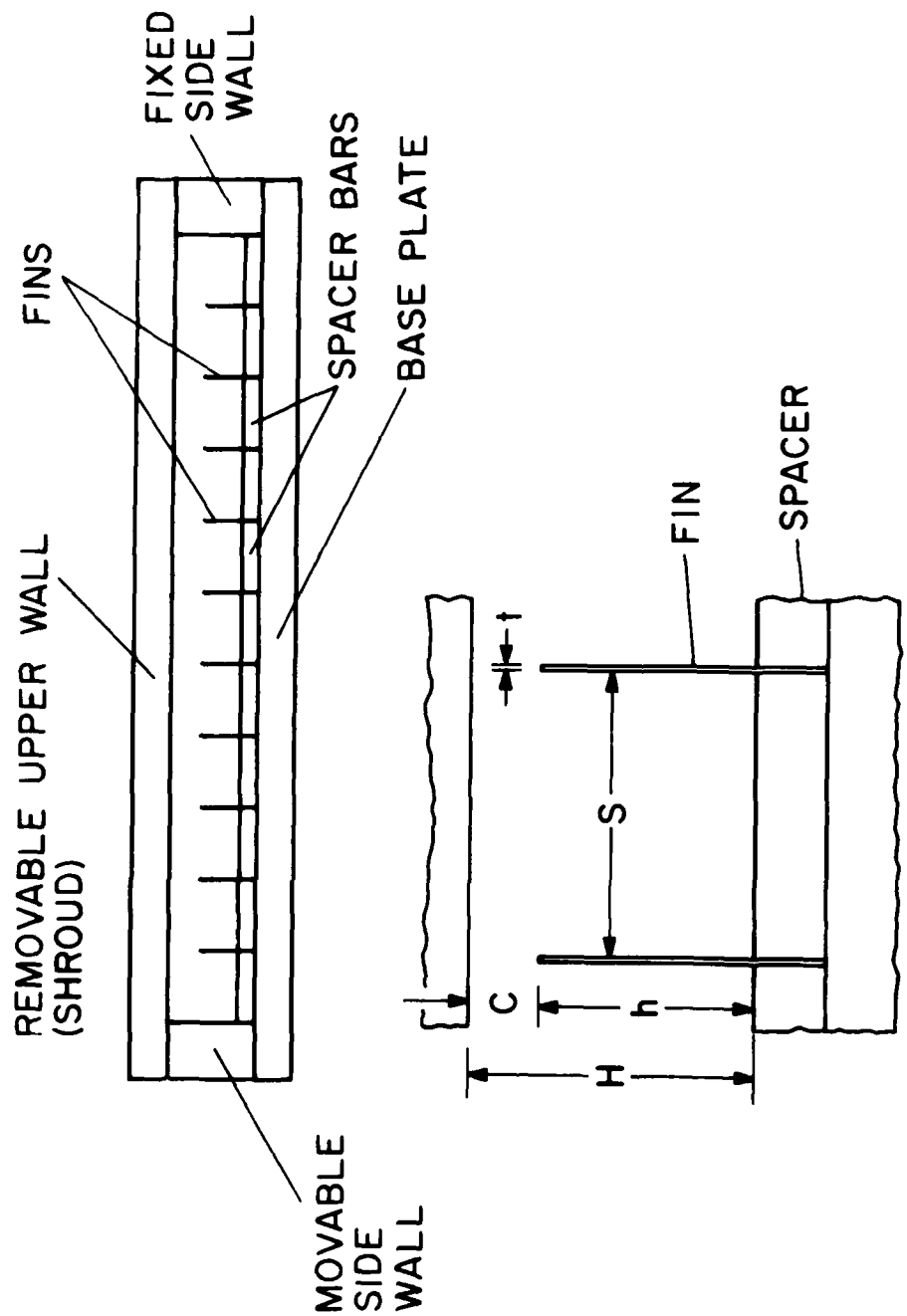
FIXED SIDE WALL
FINS
SPACER BARS
BASE PLATE
REMOVABLE UPPER WALL (SHROUD)
MOVABLE SIDE WALL
FIN
SPACER
t
S
C
h
H

Fig. 1

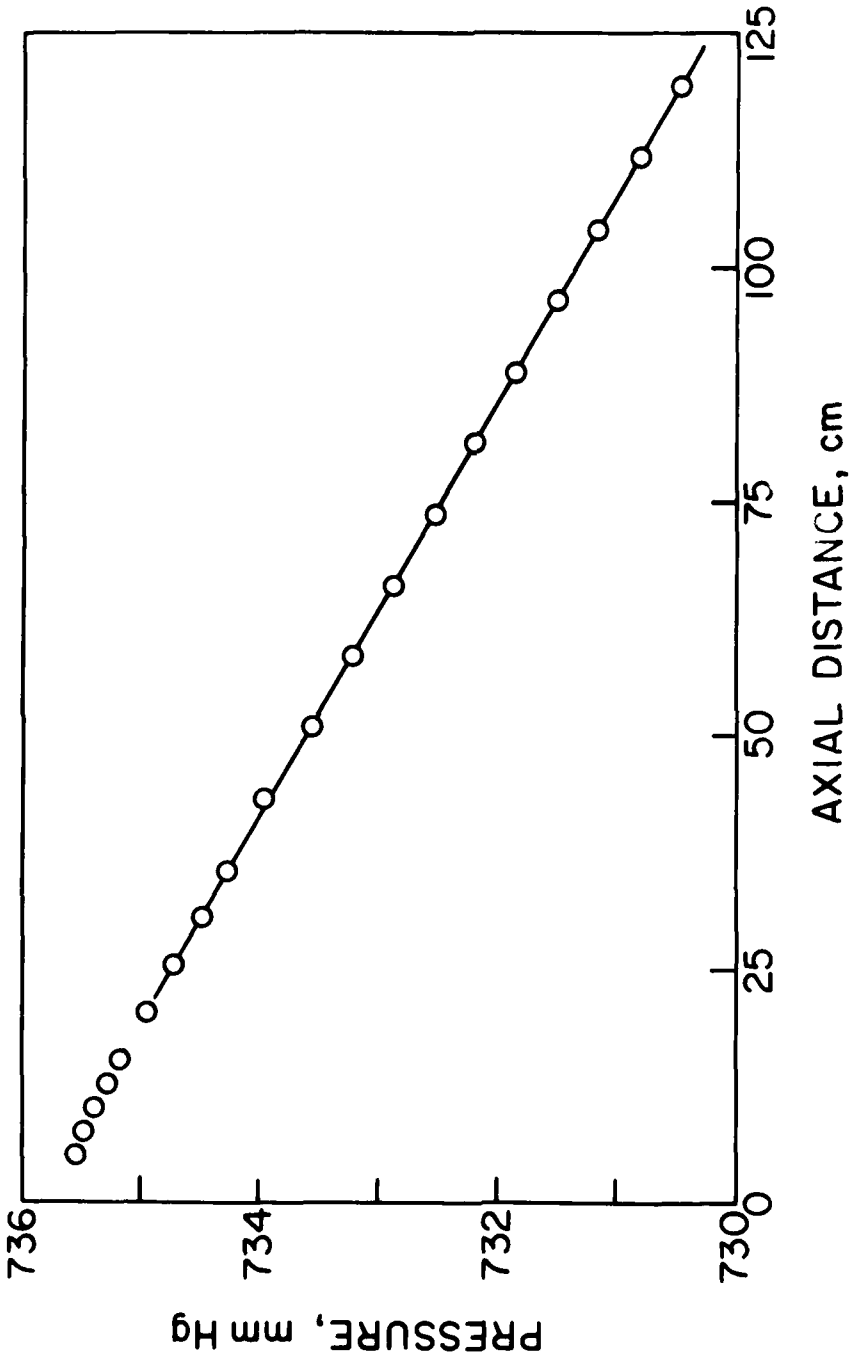
PRESSURE, mm Hg
736
734
732
730
0
25
50
75
100
125
AXIAL DISTANCE, cm

Fig. 2

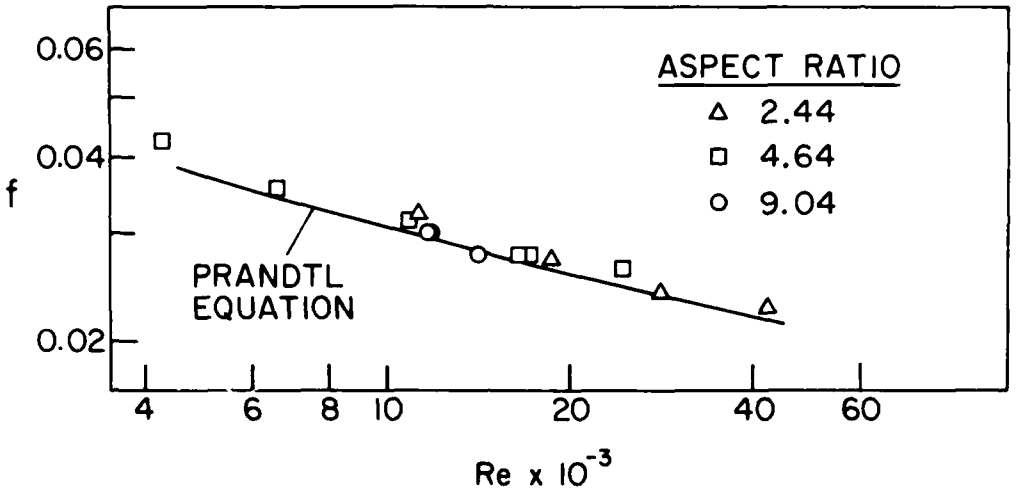
0.06
0.04
0.02
f
ASPECT RATIO
2.44
4.64
9.04
PRANDTL
EQUATION
4
6
8
10
20
40
60
Re x 10^-3

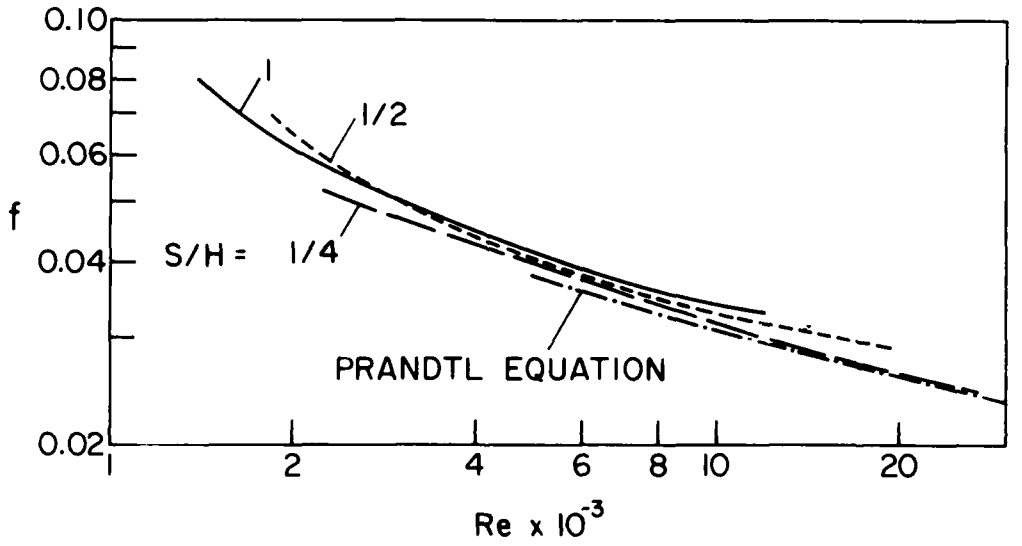
0.10
0.08
0.06
0.04
0.02
f
1
1/2
S/H = 1/4
PRANDTL EQUATION
1
2
4
6
8
10
20
Re x 10^-3

Fig. 3

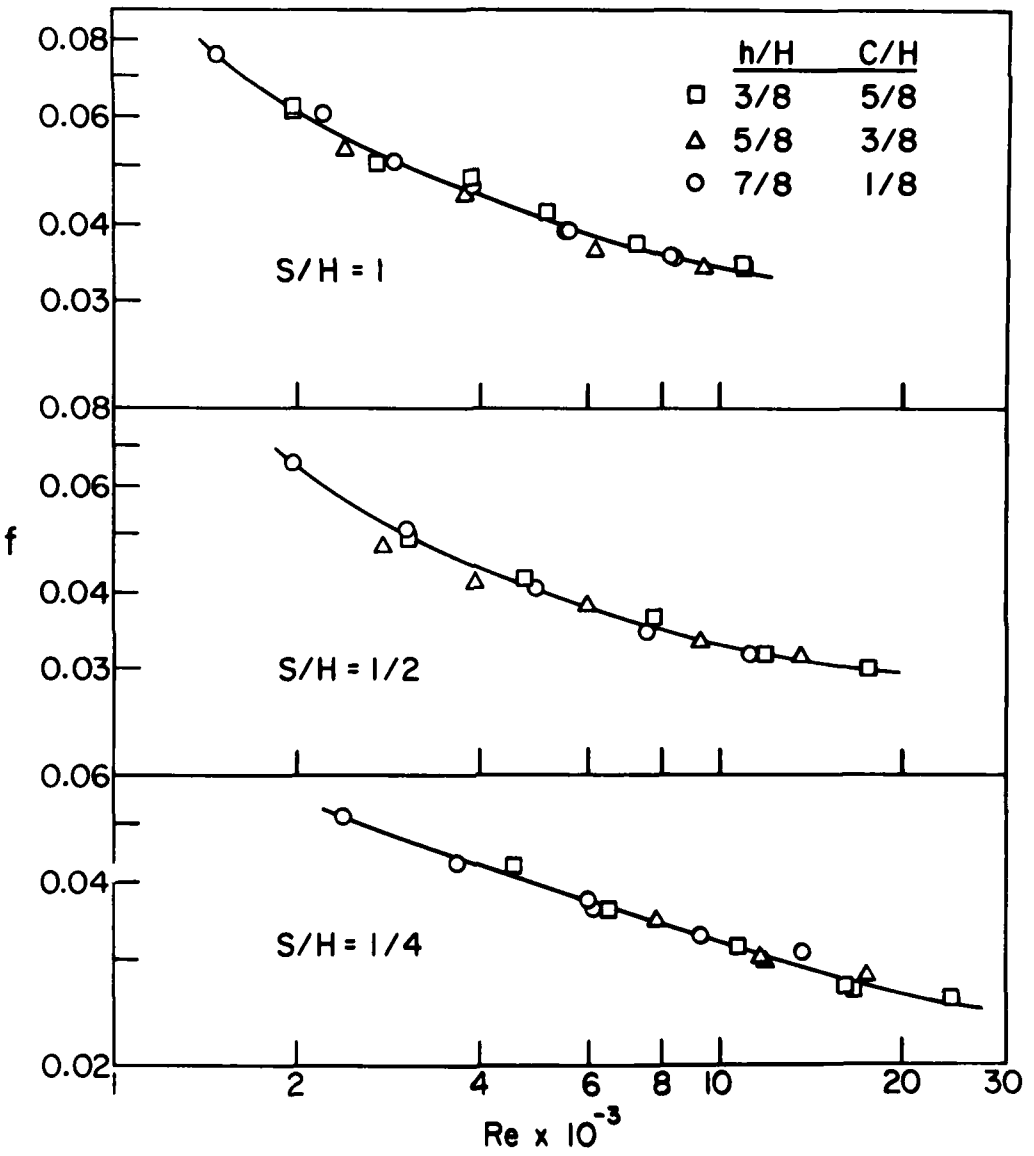
h/H C/H
3/8 5/8
5/8 3/8
7/8 1/8
S/H = 1
S/H = 1/2
S/H = 1/4
f
0.08
0.06
0.04
0.03
0.02
1
2
4
6
8
10
20
30
Re x 10^-3

Fig. 4

Chapter 4

DEVELOPMENT OF A TURBULENCE MODEL FOR RECTANGULAR PASSAGES

NOMENCLATURE

A	cross-sectional area
A^+	damping constant, equation (26)
c_p	specific heat
C	tip clearance, Fig. 6
D_h	hydraulic diameter
D_x, D_y	damping factors, equation (23)
f	friction factor, $-(dp/dz)D_h/(\frac{1}{2}\rho\bar{w}^2)$
h	heat transfer coefficient
H	geometrical dimension, Figs. 1 and 6
k	thermal conductivity
k_t	turbulent conductivity
k^+	dimensionless turbulent conductivity, k_t/k
ℓ	mixing length
ℓ_x, ℓ_y	mixing lengths in the x and y directions
L_x, L_y	the undamped mixing lengths
m	a constant, equation (22)
Nu	Nusselt number, hD_h/k
p	pressure
P_h	heat transfer perimeter
Pr	Prandtl number
Pr_t	turbulent Prandtl number

q	heat flux
Q	total heat input per unit axial length
Re	Reynolds number, $\rho\bar{w}D_h/\mu$
S	geometrical dimension, Figs. 1 and 6
T	temperature
T_b	bulk temperature, equation (7)
T_w	wall temperature
w	velocity in the z direction
W	dimensionless velocity, equation (4)
$\bar{w},\bar{W}$	mean values of w,W
x,y	cross-sectional coordinates
X,Y	dimensionless coordinates, equation (3)
x^+,y^+	dimensionless distances, equation (28)
z	streamwise coordinate
α	thermal diffusivity, $k/\rho c_p$
θ	dimensionless temperature, equations (9), (13), (14)
λ	bulk-temperature parameter, equation (15)
μ	viscosity
μ_t	turbulent viscosity
μ^+	dimensionless turbulent viscosity, μ_t/μ
ρ	density
τ_w	wall shear stress
ϕ	dimensionless temperature, θ/λ

INTRODUCTION

Rectangular ducts and other rectangular flow passages are commonly encountered in engineering practice. Streamwise corners and fin arrays often have rectangular geometry. The prediction of flow and heat transfer in such passages is needed for their design. The purpose of this chapter is to report the development of a turbulence model to predict the friction and heat transfer in passages with rectangular geometry.

Although advanced turbulence models requiring the solution of a number of differential equations have been developed, their use in ducts with a number of interacting walls becomes quite expensive in terms of the required computer time and storage. In this chapter, a simple mixing-length model is developed; it is computationally inexpensive to use and yet gives results that are satisfactory for engineering design.

In the development of the model, considerable attention is given to rectangular ducts and parallel-plate channels. It is shown that the model predicts both friction factor and heat transfer with satisfactory agreement with experimental data. Towards the end of the chapter, the application of the model to a shrouded fin array is described. The predictions are compared with the experimental results that were presented in Chapter 3. This comparison is only partially satisfactory; further work in this area is in progress.

Deissler {1} and Deissler and Taylor {2} made some early attempts to predict the turbulent flow in rectangular ducts. Subsequently, their proposals were shown to produce substantial departure from experimental data. Buleev {3} proposed a generalized mixing-length hypothesis for arbitrarily shaped ducts. It was, however, soon recognized that any turbulence model based on an isotropic turbulent viscosity would not predict the secondary flows that are known to exist in the fully developed region of rectangular ducts. Even the well-known k-ε model, which has been quite successful in predicting many complex flows, would be unable to display the secondary

flows.

Research workers, therefore, have given attention to special models designed to predict the secondary motion. Launder and Ying {4} identified the secondary-flow generating terms in the vorticity-transport equation and modeled them by reference to the Reynolds stress closure of Hanjalic and Launder {5}. Gessner and Emery {6} and Gessner and Po {7} have also employed a simplified version of the Hanjalic-Launder model to predict secondary flows.

Although these efforts are significant in advancing the capabilities of turbulence models, the resulting prediction schemes have become computationally expensive. After all, the secondary motion exerts only a small influence on overall quantities such as the friction factor or the heat transfer coefficient. For design purposes, a convenient simple model is highly desirable. One such model was developed by Patankar, Ivanovic and Sparrow {8} for flow in internally finned tubes. In the present chapter, a similar model is developed for flow in rectangular passages. The model is of the mixing-length variety and does not predict the secondary flows in the duct cross section. Its main purpose is the prediction of overall quantities for flow and heat transfer.

MATHEMATICAL FORMULATION

The geometry of the cross section of a rectangular duct is shown in Fig. 1. When the aspect ratio S/H approaches infinity, the duct becomes a parallel-plate channel. Only the fully developed flow and heat transfer will be considered. Also, as explained earlier, the secondary flows in the duct cross section will be assumed to be absent.

Governing differential equations. The velocity w in the z direction is governed by the differential equation

$$\partial/\partial x((\mu + \mu_t)\partial w/\partial x) + \partial/\partial y((\mu + \mu_t)\partial w/\partial y) = dp/dz \qquad (1)$$

where the flow field has been assumed to be fully developed. The pressure p is then dependent only on the axial coordinate z; the gradient dp/dz thus drives the

axial flow. The velocity components u and v (in the x and y directions) are absent, while the component w does not depend on the streamwise coordinate z. The symbols μ and μ_t denote the laminar and turbulent viscosities respectively. The function of a turbulence model is to provide an expression for the turbulent viscosity μ_t.

The energy equation for the fully developed duct flow can be written as

$$\rho c_p w(\partial T/\partial z) = \partial/\partial x((k + k_t)\partial T/\partial x) + \partial/\partial y((k + k_t)\partial T/\partial y \qquad (2)$$

Here k and k_t are the laminar and turbulent conductivities respectively. Thermally fully developed condition is achieved only for certain boundary conditions. Equation (2) is to be appropriately manipulated for each specific boundary condition. This will be illustrated while casting the differential equations in dimensionless form.

Dimensionless form of the velocity equation. Equation (1) can be transformed into a convenient form by introducing the dimensionless variables

$$X = x/H, \quad Y = y/H \qquad (3)$$

$$W = -(\mu w)/(H^2 dp/dz) \qquad (4)$$

$$\mu^+ = \mu_t/\mu \qquad (5)$$

The differential equation governing the dimensionless velocity W is

$$\partial/\partial X((1 + \mu^+)\partial W/\partial X) + \partial/\partial Y((1 + \mu^+)\partial W/\partial Y) + 1 = 0 \qquad (6)$$

Dimensionless forms of the energy equation. The energy equation requires different treatment for different boundary conditions. Three commonly encountered thermal boundary conditions will now be discussed.

(1) Uniform heat flux over certain perimeter. Let $\bar{q}$ be the uniform heat flux supplied over a perimeter P_h, with the remainder of the wall surface being adiabatic. The thermally developed condition for this case is characterized by all the temperatures rising linearly in the z direction. The gradient $\partial T/\partial z$ is then equal to dT_b/dz, the bulk temperature T_b being defined by

$$T_b = \int TwdA/\int wdA \qquad (7)$$

where the area integrals are to be taken over the duct cross section. From an

overall heat balance, it can be concluded that

$$\rho c_p \bar{w} A(dT_b/dz) = qP_h \tag{8}$$

where A is the cross-sectional area of the duct and $\bar{w}$ is the mean velocity. A dimensionless temperature θ can now be introduced as

$$\theta = (T - T_b)/(qP_h/k) \tag{9}$$

Further, a dimensionless turbulent conductivity will be defined as

$$k^+ = k_t/k \tag{10}$$

These relations lead to the following dimensionless form of the energy equation

$$(H/S)(W/\bar{W}) = \partial/\partial X((1 + k^+)\partial\theta/\partial X) + \partial/\partial Y((1 + k^+)\partial\theta/\partial Y) \tag{11}$$

(2) Uniform heat flow per unit axial length. If the wall material has a high thermal conductivity, there will be circumferentially uniform wall temperature. Further, if the total heat input per unit length in the z direction is kept constant at Q, the wall temperature T_w (and all the local fluid temperatures) will rise linearly in the z direction. The overall heat balance can then be written as

$$\rho c_p \bar{w} A(dT_b/dz) = Q \tag{12}$$

If the dimensionless temperature θ is defined by

$$\theta = (T - T_w)/(Q/k) \tag{13}$$

equation (11) continues to represent the dimensionless form of the energy equation.

(3) Uniform wall temperature. If the temperature of all walls remains at a constant value T_w, a different kind of thermally developed condition is achieved. In this condition, the fluid temperature gradually approaches the wall temperature, and the heat transfer rate exponentially decays to zero. The appropriate dimensionless temperature θ is defined as

$$\theta = (T - T_w)/(T_b - T_w) \tag{14}$$

It can be noted that θ depends only on x and y, and not on z. The rate of change of the bulk temperature T_b is such that the parameter λ defined by

$$\lambda = (dT_b/d(z/H))(H\bar{w}/\alpha)/(T_b - T_w) \tag{15}$$

becomes a constant. Here the quantity α is the thermal diffusivity $k/\rho c_p$. With these definitions, the dimensionless form of the energy equation can be written as

$$\lambda\theta(W/\bar{W}) = \partial/\partial X((1 + k^+)\partial\theta/\partial X) + \partial/\partial Y((1 + k^+)\partial\theta/\partial Y) \tag{16}$$

For computational convenience, a related variable ϕ is introduced

$$\phi = \theta/\lambda \tag{17}$$

The energy equation is now given by

$$\lambda\phi(W/\bar{W}) = \partial/\partial X((1 + k^+)\partial\phi/\partial X) + \partial/\partial Y((1 + k^+)\partial\phi/\partial Y) \tag{18}$$

The constant λ is obtained by rewriting equation (7) as

$$\lambda = \int dA/\int (W/\bar{W})\phi dA \tag{19}$$

where the integrals are to be taken over the whole cross section of the duct.

The quantity μ_t in equation (1) and k_t in equation (2) are to be expressed in terms of the properties of the flow. This is done via a turbulence model, which is discussed next.

Turbulence model. A version of the mixing-length hypothesis is employed here. The development of the model is based on some of the ideas used by Patankar, Ivanovic, adn Sparrow [8] for flow through internally finned tubes.

The turbulent viscosity μ_t is first expressed as

$$\mu_t = \rho\ell^2((\partial w/\partial x)^2 + (\partial w/\partial y)^2)^{1/2} \tag{20}$$

where ρ is the density, and ℓ is the mixing length. The calculation of the mixing length, which forms the major part of the model, will be discussed shortly. The turbulent conductivity k_t is related to μ_t via

$$k_t = c_p(\mu_t/Pr_t) \tag{21}$$

where Pr_t is the turbulent Prandtl number. Pr_t is usually given the constant value 0.9, which is also employed here. Incidentally, all the calculations presented here are for air, for which the laminar Prandtl number was set at 0.7.

With reference to Fig. 1, the mixing length at P(x,y) is considered to be the

resultant of two contributions: a mixing length ℓ_x influenced by the two vertical walls, and a mixing length ℓ_y influenced by the two horizontal walls. The combination of the two lengths should be such that, when P lies very close to one of the walls, the mixing length ℓ should be wholly governed by the distance from that wall. It is, therefore, proposed that the resultant mixing length ℓ be calculated from

$$\ell = (\ell_x^{-m} + \ell_y^{-m})^{-1/m} \tag{22}$$

where m is a constant. The choice of the value of m is later made by reference to experimental data.

It appears that a suitable expression for the mixing length distribution between two parallel plates has not been proposed in the literature. Examination of the experimental data for parallel-plate channels revealed that the corresponding mixing length distribution was almost identical to what Nikuradse {9} found in circular pipes. Thus, a Nikuradse-type distribution was chosen for ℓ_x and ℓ_y.

Very close to a wall, the Nikuradse length scale must further be damped by a van Driest damping factor. Thus,

$$\ell_x = D_x L_x \quad , \quad \ell_y = D_y L_y \tag{23}$$

where D_x and D_y are the damping factors and L_x and L_y are the Nikuradse length scales. The expressions for L_x and L_y are given by

$$L_x/(S/2) = 0.14 - 0.08(1 - x/(S/2))^2 - 0.06(1 - x/(S/2))^4 \tag{24}$$

$$L_y/(H/2) = 0.14 - 0.08(1 - y/(H/2))^2 - 0.06(1 - y/(H/2))^4 \tag{25}$$

The damping factors D_x and D_y for the lower left-hand quadrant in Fig. 1 (i.e., for $0 \leq x \leq S/2$ and $0 \leq y \leq H/2$) can be calculated from

$$D_x = 1 - \exp(-x^+/A^+) \tag{26}$$

$$D_y = 1 - \exp(-y^+/A^+) \tag{27}$$

where the constant A^+ equals 26. The dimensionless distances x^+ and y^+ are calculated from

$$x^+ = x(\tau_w \rho)^{1/2}/\mu \quad , \quad y^+ = y(\tau_w \rho)^{1/2}/\mu \tag{28}$$

Here τ_w is the value of the local shear stress on the corresponding wall. The expressions for the damping factors in other quadrants can be written in a symmetrical manner.

Equations (20) - (28) completely specify the calculation of μ_t and k_t. The value of m introduced in equation (22), however, remains to be determined. For this purpose, computations were performed with a range of values of m for the flow and heat transfer in a square duct. The resulting friction factor and Nusselt number are plotted in Fig. 2. It can be seen that, for $m > 5$, the predictions are more or less indpendent of m. Further, as will be shown later, the predictions for $m > 5$ agree well with experimental data. Here the value $m = 20$ has been chosen for all subsequent work, but any value in excess of 5 should produce almost identical results.

Computational details. The equations for the velocity w and the temperature T were solved by a finite difference method. The actual details of the method can be found in {10}. The velocity equation was solved first and the resulting velocity field was used as an input to the temperature equation. Due to the dependence of μ_t on the velocity field, the velocity equation was solved by iteration. During any iteration, μ_t was evaluated from the velocity field produced by the previous iteration. The energy equation does not require iterative solution except for the case of uniform wall temperature. For this case, λ is obtained by substituting into equation (19) the ϕ values produced by the previous iteration and, with this value of λ , equation (18) is solved to yield a new field of ϕ.

For most of the computations, about 1500 grid points were used. The accuracy of numerical solution was verified by repeating some of the computations with more grid points. A nonuniform grid was used so that a higher density of grid points could be provided near the walls. This is especially important in a turbulent flow, in which a correct calculation of the laminar sublayer and the buffer region is crucial for the prediction of wall shear and heat flux. In the present computations, a uniformly fine grid was provided from the wall to a location corresponding to x^+ or

y^+ of 15. Beyond this point, the grid spacing was gradually increased towards the center of the duct. The adequacy of the grid was tested by changing the distribution of grid points and noting that this did not noticeably alter the solution.

When the heat transfer problem was solved with the different thermal boundary conditions described earlier, the resulting Nusselt numbers were almost equal. This confirms the well-known finding that, unlike in a laminar flow, the heat transfer coefficients in a turbulent flow are insensitive to the actual thermal boundary condition employed.

RESULTS

To determine the satisfactoriness of the model, the computed results were compared with available experimental data. These comparisons will now be presented.

Flow and heat transfer between parallel plates. A limiting case of the rectangular duct is the parallel-plate channel. Since the mixing-length model appears not to have been applied to the parallel-plate situation, the present computations are the first test of the model for this geometry. Figure 3 shows the predictions for the friction factor f and the Nusselt number Nu for a range of the Reynolds number. The friction factor results are compared with the experimental data of Barrow {1}, Hussain and Reynolds {12}, and Byrne et al {13}. For heat transfer, the only available data seem to be those of Barrow {1}, which are compared in Fig. 3 with the predictions for the Nusselt number. Figure 3 indicates that the implications of the turbulence model are in good agreement with the experimental data.

Friction factor for rectangular ducts. Predictions of the friction factor f for rectangular ducts of aspect ratios 1, 5, and 10 are shown in Fig. 4. These are compared with the experimental data of Hartnett et al {14}. Within the scatter of the data, the predictions can be judged to be very satisfactory.

Heat transfer in rectangular ducts. As explained before, the heat transfer computations can be performed for a variety of boundary conditions. The predicted values of the Nusselt number, however, are not very sensitive to the type of the

boundary condition employed. It is, therefore, sufficient to present the results for any one boundary condition. Figure 5 shows the predictions for the Nusselt number for flow in rectangular ducts of aspect ratios 1, 5, and 10. The thermal boundary condition is that of uniform heat flux through two opposite walls (with the two other walls adiabatic). The predictions are compared in Fig. 5 with the experimental data of Novotny et al {15} for the same boundary condition. The agreement can be seen to be quite good.

Friction factor for a shrouded fin array. The turbulence model, which has by now been shown to be satisfactory for rectangular ducts, is next applied to the fully developed flow in a shrouded fin array. This physical situation and the corresponding experimental results have been described in Chapter 3. The geometry of the fin array is schematically shown in the inset of Fig. 6. The mixing length distribution for the region between the fins was calculated in the same manner as for a rectangular duct. The mixing length in the clearance region between the shroud and fin tips was obtained from the formula for a parallel-plate channel.

Figure 6 shows the friction factor results for a fin spacing corresponding to $S/H = 0.25$ and for three values of the clearance ratio C/H. Predictions are compared with the experimental data presented in Chapter 3. The agreement is only partially satisfactory. Especially, the case of $C/H = 0.625$ is rather poorly predicted. It should be noted that, as C/H is increased to 1, the situation approaches a parallel-plate channel, for which good agreement has been demonstrated. The cause of discrepancy for intermediate values of C/H is currently under investigation.

CONCLUDING REMARKS

A simple mixing length model has been developed for flow in rectangular passages. The model is computationally efficient, and therefore, can be conveniently employed in design calculations. The predictions of the model for the friction factor and the Nusselt number in rectangular ducts and parallel-plate channels have been shown to agree well with experimental data over a range of the Reynolds number.

The model has also been applied to the flow in a shrouded fin array. Further work in this area is in progress.

REFERENCES

1. Deissler, R. G., "Turbulent heat transfer and friction in the entrance region of smooth passages," Trans. ASME, 77, p. 1221, 1955.
2. Deissler, R. G. and Taylor, M. F., "Analysis of turbulent flow and heat transfer in non-circular passages," NASA Tech. Rep. R-31, 1959.
3. Buleev, N. I., "Theoretical model of the mechanism of turbulent exchange in fluid flow," AERE Translation 957, 1963.
4. Launder, B. E. and Ying, W. M., "Prediction of flow and heat transfer in ducts of square cross section," Proc. Inst. Mech. Engrs., 187, 1973.
5. Hanjalic, K. and Launder, B. E., "A Reynolds stress model of turbulence and its application to thin shear flows," J. Fluid Mech., 52, p. 609, 1972.
6. Gessner, F. B. and Emery, A. F., "A Reynolds stress model for turbulent corner flows - Part I: Development of the model," J. Fluids Eng. 98, p. 261, 1976.
7. Gessner, F. B. and Po, J. K., "A Reynolds stress model for turbulent corner flows - Part II: Comparison between theory and experiment," J. Fluids Eng., 98, p. 269, 1976.
8. Patankar, S. V., Ivanovic, M., and Sparrow, E.M., "Analysis of turbulent flow and heat transfer in internally finned tubes and annuli," J. Heat Transfer, 101, p. 29, 1979.
9. Nikuradse, J., "Untersuchungen über die Geschwindigkeits in turbulenten Stromungen," ForschHft. Ver. dt. Ing, p. 281, 1926.
10. Patankar, S. V., "Numerical Heat Transfer and Fluid Flow," McGraw-Hill--Hemisphere, 1980.
11. Barrow, H., "An analytical and experimental study of turbulent gas flow between two smooth parallel walls with unequal heat fluxes," Int. J. Heat Mass Transfer, 5, p. 469, 1962.

12. Hussain, A.K.M.F. and Reynolds, W. C., "Measurements in fully developed turbulent channel flow," J. Fluids Eng., 97, p. 568, 1975.

13. Byrne, J., Hatton, A. P., and Mariott, P. G., "Turbulent flow and heat transfer in the entrance region of a parallel wall passage," Proc. Inst. Mech. Engrs., 184, p. 697, 1968-70.

14. Hartnett, J. P., Koh, J.C.Y., and McComas, S. T., "A comparison of predicted and measured friction factors for turbulent flow through rectangular ducts," J. Heat Transfer, 84, p. 82, 1962.

15. Novotny, J. L., McComas, S. T., Sparrow, E. M., and Eckert, E.R.G., "Heat transfer for turbulent flow in rectangular ducts with two heated and two unheated walls," AIChE J., 1964.

FIGURE CAPTIONS

Fig. 1 Cross section of a rectangular duct

Fig. 2 Prediction of the friction factor and the Nusselt number for various values of m

Fig. 3 Prediction of friction and heat transfer in parallel-plate channel

Fig. 4 Friction factors for rectangular ducts

Fig. 5 Nusselt numbers for rectangular ducts

Fig. 6 Prediction of the friction factor for a shrouded fin array

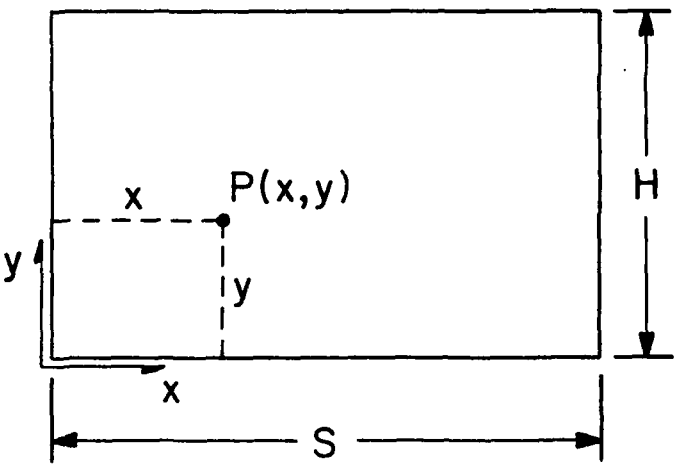

Fig. 1

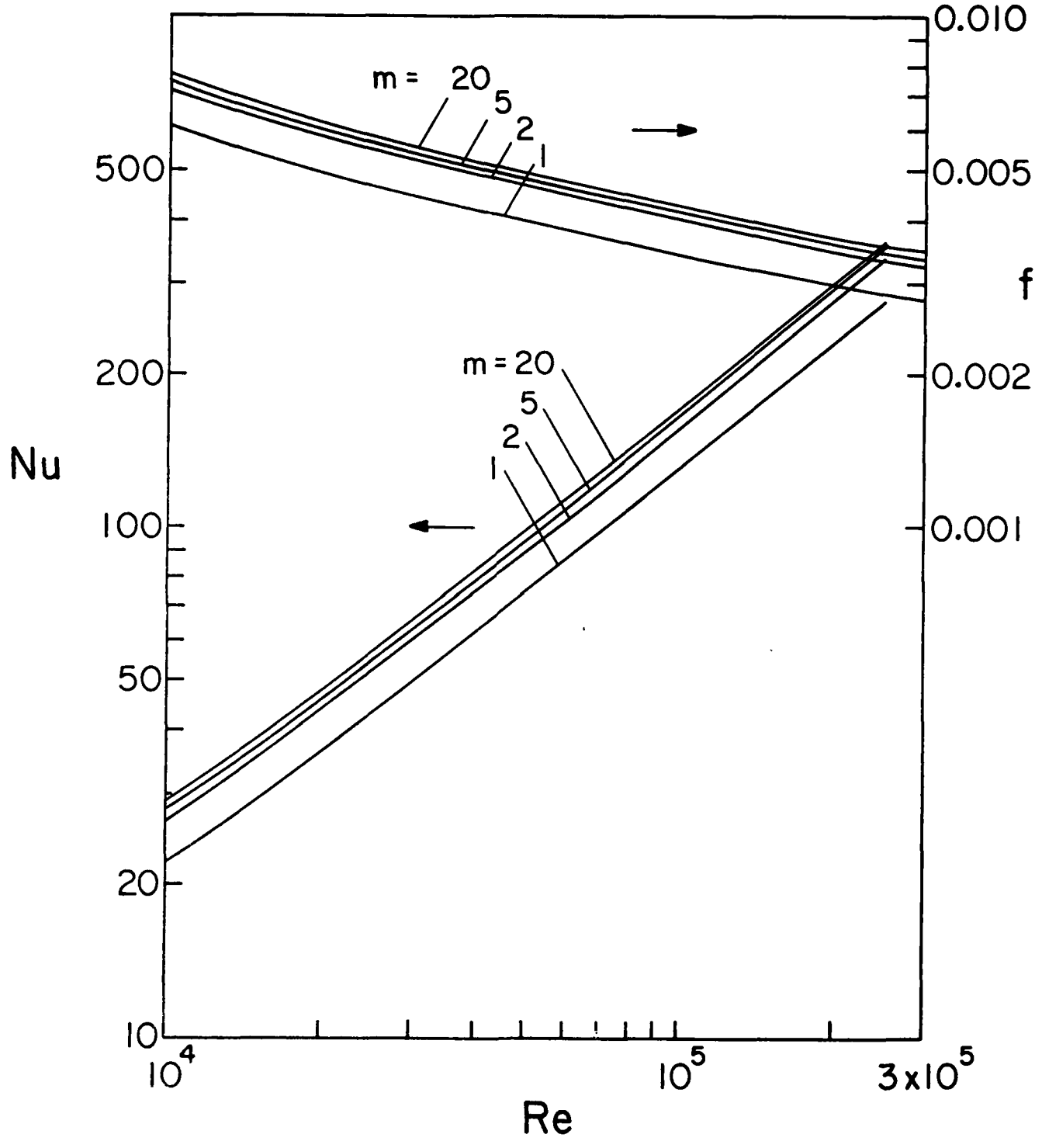
0.010
m = 20
5
2
1
500
0.005
f
200
m = 20
5
2
1
0.002
Nu
100
0.001
50
20
10
10^4
10^5
3×10^5
Re

Fig. 2

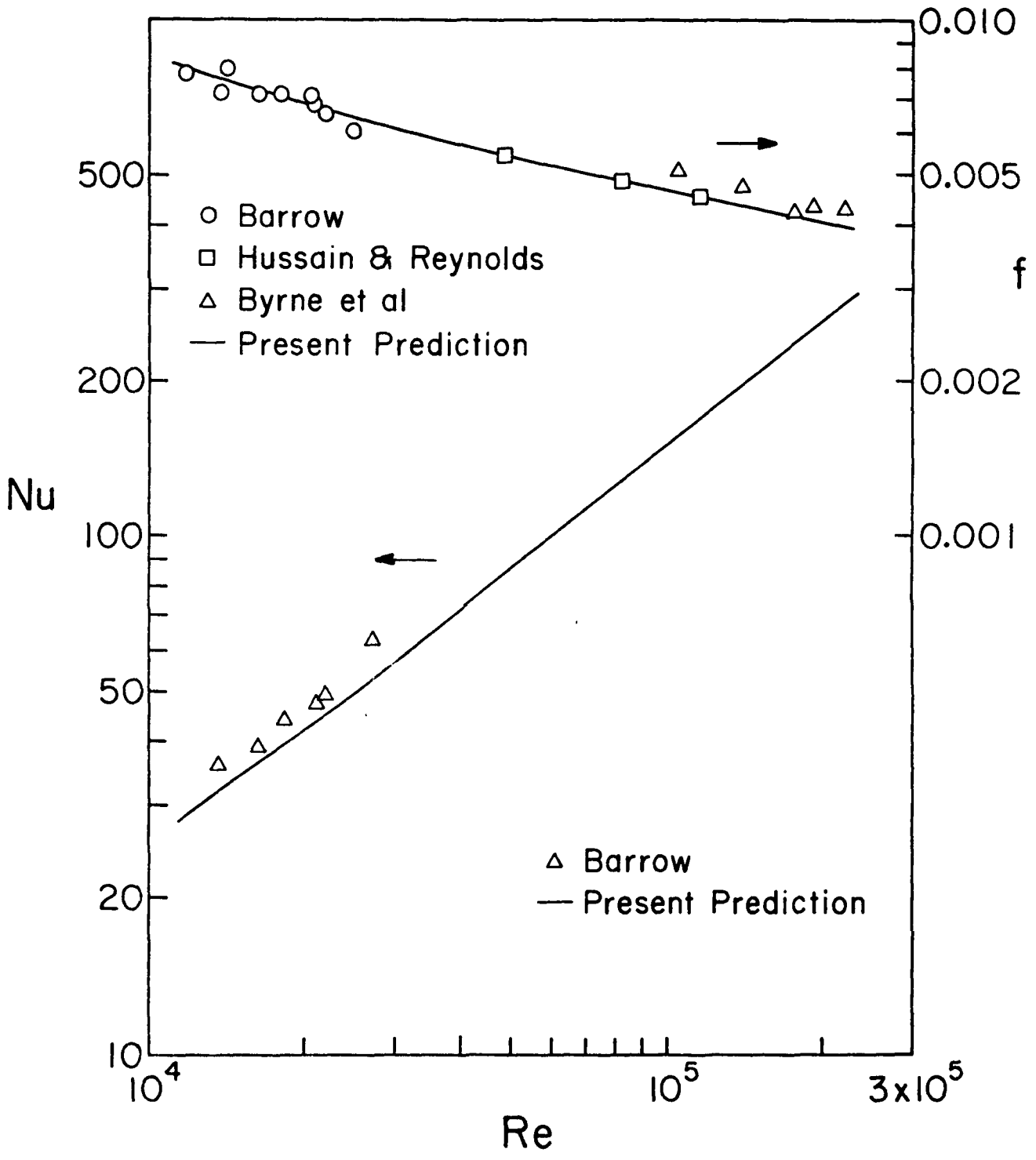
0.010
0.005
0.002
0.001
500
200
100
50
20
10
Nu
f
Barrow
Hussain & Reynolds
Byrne et al
Present Prediction
Barrow
Present Prediction
10^4
10^5
$3x10^5$
Re

Fig. 3

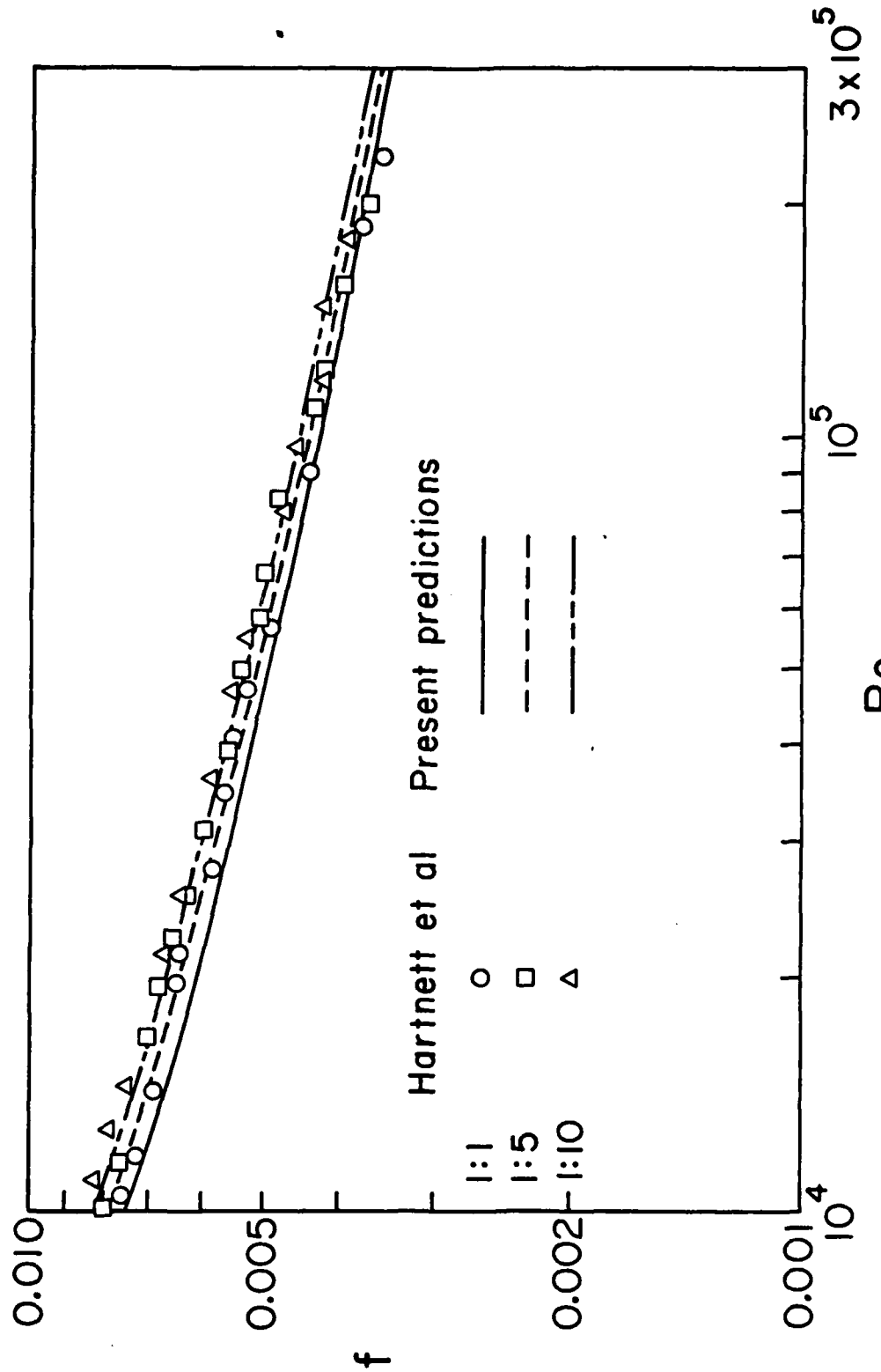
0.010
0.005
0.002
0.001
f
10^4
10^5
3×10^5
Re
Hartnett et al
Present predictions
1:1
1:5
1:10

Fig. 4

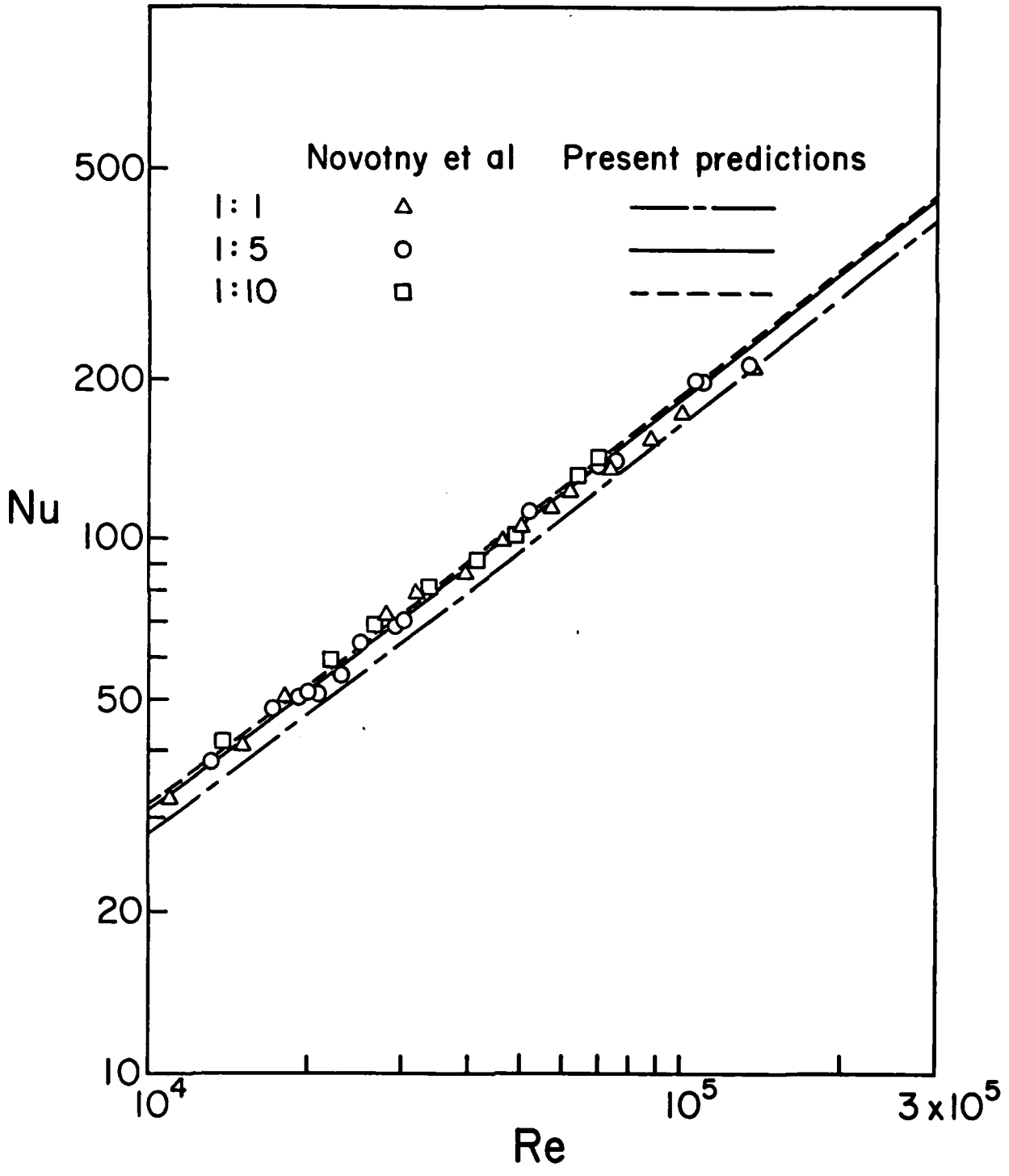
Novotny et al
Present predictions
1:1
1:5
1:10
500
200
100
50
20
10
Nu
10^4
10^5
3×10^5
Re

Fig. 5

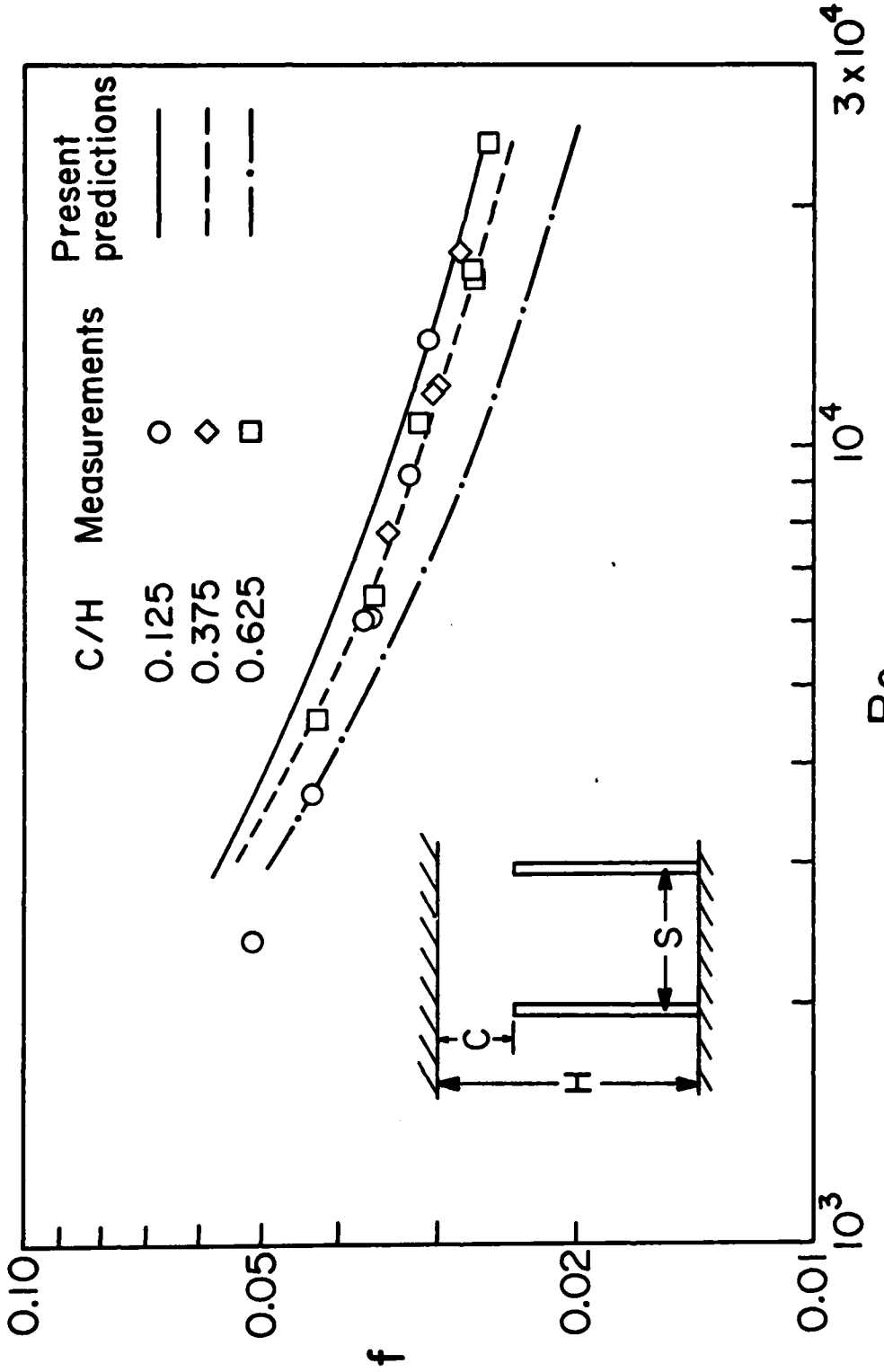
Present predictions
Measurements
C/H
0.125
0.375
0.625
0.10
0.05
0.02
0.01
f
10^3
10^4
3×10^4
Re
C
H
S

Fig. 6

Chapter 5

TURBULENT HEAT TRANSFER AND FLUID FLOW IN AN UNSYMMETRICALLY HEATED TRIANGULAR DUCT

ABSTRACT

Experiments were performed to determine entrance-region and fully developed heat transfer characteristics for turbulent airflow in an unsymmetrically heated equilateral triangular duct; friction factors were also measured. Two of the walls were heated while the third was not directly heated. The resulting thermal boundary conditions consisted of uniform heating per unit axial length and circumferentially uniform temperature on the heated walls. Special techniques were employed to minimize extraneous heat losses, and numerical finite-difference solutions played an important role in both the design of the apparatus and in the data reduction. The thermal entrance lengths required to attain thermally developed conditions were found to increase markedly with the Reynolds number and were generally greater than those for conventional pipe flows--a behavior which can be attributed to the unsymmetric heating. The fully developed Nusselt numbers were compared with circular tube correlations from the literature, from which it was shown that the hydraulic diameter is not fully sufficient to rationalize the circular and noncircular duct results. However, excellent Nusselt number predictions were obtained by employing the Petukhov-Popov correlation in conjunction with the measured friction factors for the triangular duct. This approach may have general applicability for predicting noncircular duct heat transfer. The friction factor results also affirmed the inadequacies of the hydraulic diameter but supported a general noncircular duct correlation available in the literature.

NOMENCLATURE

f	friction factor, equation (4)
h	local circumferential-average heat transfer coefficient
$\hat{h}$	heat transfer coefficient for convection at lower wall
D_h	hydraulic diameter
k	thermal conductivity of air
k_p	thermal conductivity of plexiglass
$\dot{m}$	mass flow rate
Nu	Nusselt number, hD_h/k
P	wetted perimeter of flow cross section
P_q	wetted perimeter of heated walls
Pr	Prandtl number
p	static pressure
Q'	local rate of heat transfer per unit length from heated walls to fluid
Q'_t	total rate of heat transfer per unit length from all walls to fluid
Re	Reynolds number
T	temperature
T_b	bulk temperature
$\hat{T}_b$	bulk temperature for convection at lower wall
T_{bi}	bulk temperature at inlet
T_w	wall temperature
$\bar{u}$	mean velocity
x	axial coordinate
x_{ent}	entrance length
μ	viscosity
ν	kinematic viscosity
ρ	density

INTRODUCTION

Complex duct flows are widely encountered in heat exchange devices and in related piping systems due to the possible presence of noncircular cross sections, blockages, changes of direction, and variations of the flow area. These flows are difficult to analyze, and incisive mathematical models of physical processes (e.g., turbulence) are needed to deal with such situations. The models are necessarily approximate, and experimental data are required for their verification.

A rational approach to the verification of an analytical model is to apply it to a succession of cases such that each case contains only one new ingredient of physical complexity. For instance, if turbulent flow in a circular tube is taken as a base case, then an appropriate first stage of complexity is the presence of secondary flows superposed on the streamwise mainflow. Since secondary motions activate circumferential turbulent transport, experimental results for duct flows which involve secondary motions provide a means for testing turbulence models which incorporate such transport.

The present research is focused on the turbulent heat transfer and fluid flow characteristics for airflow in an unsymmetrically heated triangular duct. Secondary motions are known to exist in triangular duct flows, and the unsymmetrical heating opens the way for the secondary motions to serve as a vehicle for heat transfer. The experiments were carried out with a view toward providing data of impeccable quality which can serve as a standard against which the results of mathematical modeling can be compared. In addition, the applicability of circular tube correlations {1} to noncircular ducts was examined. The analytical-computational model of {2} for turbulent airflow in triangular ducts was tested by comparisons with the data.

The experiments were performed utilizing a sharp-cornered equilateral triangular duct, two walls of which were heated, while the third wall was not directly heated. The geometrical configuration and the heating arrangement were designed to yield a standard thermal boundary condition--uniform heat input per unit axial

length and circumferentially uniform temperature on the heated walls. In the design of the apparatus, numerical finite-difference solutions were employed to aid in the selection of wall thicknesses, in the positioning of heating wire, and in the placement of thermocouples. Once the experimental data had been obtained, finite-difference solutions enabled evaluation of the heat leakage from the directly heated walls of the duct to the unheated wall; heat losses to the environment were also determined by finite differences.

Heat-transfer-related measurements were made which yielded both entrance region and fully developed heat transfer coefficients, as well as thermal entrance lengths. Pressure distributions were also measured, both for isothermal and nonisothermal conditions, from which friction factors were deduced. The experiments encompassed the Reynolds number range from 4000 to 60,000. In the low Reynolds number range, auxiliary data runs were made to explore the possible presence of natural convection effects. Air was the working fluid in all cases.

The relevant literature on turbulent heat transfer in triangular ducts will now be briefly reviewed. In an early investigation of equilateral ducts {3}, average heat transfer coefficients for the duct as a whole were measured at high heating rates such that circumferential temperature variations of up to 55°C (100°F) were encountered. Later, in {4}, measurements of heat transfer and friction characteristics were made in a narrow isosceles duct having an apex angle of 11.46 degrees. Although the duct was 116 hydraulic diameters in length, thermally developed conditions were generally not attained. Somewhat more recently, experiments were performed in a rounded-corner equilateral triangular duct with a corner radius of curvature equal to fifteen percent of the duct hydraulic diameter {5}. Intense heating rates were employed in those experiments, which resulted in a decrease of the Reynolds number from entrance to exit of as much as fifty percent. The foregoing citations encompass the available experimental literature on heat transfer.

The most complete study of turbulent fluid flow phenomena in equilateral

triangular ducts is that of {2}, which included both experiments and analytical-numerical predictions (based on the Buleev mixing length and turbulence kinetic energy model). The numerical solutions were extended to predict heat transfer coefficients, but without experimental confirmation.

THE EXPERIMENTS

The experiments were performed in an open-loop airflow circuit which took air from a building-wide system and ultimately discharged it to the atmosphere. Along its path of flow, the air first encountered a succession of control and regulator valves and a filter, after which it was metered by one of two calibrated sharped-edge orifices which were respectively employed for high and low flow rates. It was then ducted to a plenum chamber fitted with baffles and a flow straightener--the plenum served as a transition from the circular tubing of the upstream piping system to the downstream triangular cross section.

The air exiting the plenum passed into an unheated equilateral triangular duct (made of plexiglass) which served as a hydrodynamic development section. The development section mated with the electrically heated test section. Both sections were of identical internal dimensions; side of triangle = 3.97 cm (1.56 in.), hydraulic diameter = 2.29 cm (0.902 in.). The respective axial lengths of the development and test sections were 53 and 106 hydraulic diameters. After passing through the test section, the air was thermally mixed in a specially designed mixing chamber, from which it was ducted to an outside exhaust.

The key components of the experimental apparatus will now be described. The description will highlight the novel measures that were employed to thermally isolate the heated test section in order to minimize possible extraneous heat losses or gains; another focus is the role of computer modeling as an adjunct to the apparatus design. Details of the apparatus and its design, beyond those that are given here, may be found in {6}.

Heated test section. The triangular duct which served as the test section consisted of two relatively thick metallic walls and a thinner wall of a lesser conducting material. A cross sectional view showing the duct wall configuration is presented in Fig. 1. The metallic walls were of aluminum, with a thickness of 0.952 cm (0.375 in.). The choice of aluminum of this thickness, taken together with the adopted heating method, was made with a view toward obtaining axially uniform heating and circumferentially uniform temperature on the two heated walls.

Heating was accomplished by means of electrical resistance wire embedded in longitudinal grooves machined in the outer face of each aluminum wall (see Fig. 1). Numerical finite-difference solutions of a model of this heating arrangement were employed to demonstrate that for the chosen wall material, wall thickness and heater-groove spacing, and for expected values of the heat transfer coefficient, uniform temperature is attained on the face of the wall that is in contact with the airflow. A generalized version of the analytical model is available in {7} along with representative results.

The third wall of the duct (i.e., the lower wall as pictured in Fig. 1) was made of plexiglass--chosen because of its moderately low thermal conductivity, light weight, surface smoothness, and availability in many sizes. The design objective for this wall was to approximate, as closely as possible, a zero heat flux surface. In practice, heat conduction across the surfaces of contact between the lower wall and the heated walls operates to oppose this objective. Both the size of the contact surface and thickness (0.318 cm, 0.125 in.) of the plexiglass wall were chosen as small as possible relative to mechanical constraints such as strength, wall flatness, and avoidance of leaks. To guide the trade-off between these mechanical constraints and the aforementioned heat transfer objective, the effects of both contact size and wall thickness on the heat flow via the plexiglass into the fluid were examined by means of finite-difference solutions dealed in Chapter 4 of {6}. The quantitative extent of this indirect heating of the fluid

will be presented in the Results section of the paper.

To facilitate the assembly of the duct, bevels were painstakingly cut into the edges of the aluminum walls as indicated in Fig. 1. The bevels extended along the entire 244-cm (8-ft.) length of the duct. The two aluminum walls were held together along their upper extremities by screws and nuts positioned at 10-cm (4-in.) intervals (the recesses for the screws and nuts are indicated by dashed lines in Fig. 1). Fastening of the aluminum side walls to the plexiglass bottom wall was accomplished by nylon screws positioned at the same interval--nylon being chosen to minimize heat conduction. To ensure a leak-free seal, silicone rubber was packed into the V-shaped grooves at the intersections of the walls.

Thermocouples were installed at fourteen axial stations along the test section. The use of the relatively thick-walled aluminum provided the options of surface mounting (on the rear face) or of embedding the thermocouples within the wall. The latter has the apparent advantage of placing the point of measurement closer to the inner surface of the wall, where the temperature value is desired, but also may cause a disturbance of the temperature field in the wall. Rear-face mounting also has both advantages and disadvantages. To resolve the issue, computational models were made for both situations (Chapter 4 of {6}), taking account of conduction in the wall, in the thermocouple leads, and in the insulation around the duct. These computations showed that wall embedding gives rise to a slightly more accurate temperature measurement and argued strongly for the use of iron-constantan wire rather than copper-constantan wire.

The thermocouples in the heated walls were positioned in drill holes which penetrated to within 0.19 cm (0.075 in.) of the inner surface. Prior to the insertion of the thermocouples, the holes were filled with a paste of copper-oxide cement, which subsequently hardened around the inserted thermocouples (copper-oxide cement is a moderately good heat conductor and an excellent electrical insulator). Three to five thermocouples were circumferentially distributed in the

AD-A094 575 MINNESOTA UNIV MINNEAPOLIS DEPT OF MECHANICAL ENGIN--ETC F/G 20/4
EXPERIMENTAL AND COMPUTATIONAL STUDIES OF HEAT TRANSFER IN COMP--ETC(U)
JAN 81 E M SPARROW, S V PATANKAR N00014-79-C-0621

UNCLASSIFIED NL

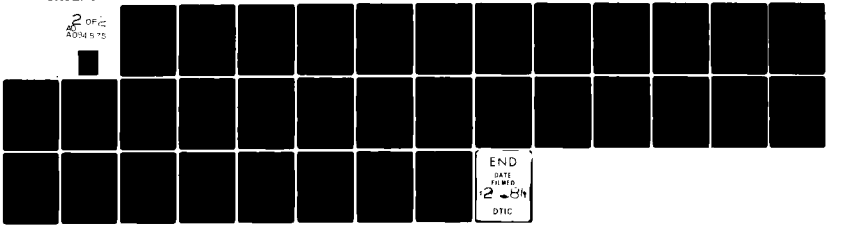

aluminum walls at each instrumented axial station. The coordinates of these stations will be evident from the data to be presented later.

At these same stations, a row of thermocouples was positioned along the spanwise centerline of the lower (plexiglass) wall. Owing to the thinness of this wall, external surface mounting of the thermocouples was the only viable option. Good thermal contact between the thermocouple junctions and the wall was ensured by the use of copper oxide cement, whereas tape and expoxy were employed for strength and positive positioning.

For the determination of the axial pressure distribution along the duct, seven taps were installed in a row in one of the aluminum walls at a streamwise interval of ten hydraulic diameters. The tap in a given cross section was located at the circumferential midpoint of its host wall.

The instrumentation for the temperature and pressure readings will be described shortly.

Prior to the final assembly of the test section, the inner surface of the aluminum walls was hand polished to a high degree of smoothness. Special precautions were taken to eliminate burrs or other irregularities adjacent to the pressure tap holes.

Hydrodynamic development section; mixing box. As was noted earlier, the heated test section was preceded by a 53-diameters-long unheated hydrodynamic development section. The development section was an equilateral triangular duct with inner dimensions identical to those of the test section. It was assembled from three pieces of plexiglass, two of which were bevelled in a manner identical to that for the aluminum walls of the test section. The assembly procedures were the same as for the test section, and the final assembled cross section is, with the exception of the heater wire grooves, well portrayed by Fig. 1.

The two side walls of the development section were 1.25 cm in thickness (1/2 in.), whereas the lower wall was 0.318-cm (0.125-in.) thick. It may be noted

that the latter dimension is identical to the thickness of the plexiglass lower wall of the test section. In fact, to facilitate the assembly of the system, the test-section lower wall was designed to extend upstream, and thus to serve as the downstream end of the lower wall of the development section.

To monitor upstream thermal events, three thermocouples were installed in the wall of the development section (respectively 1, 10, and 20 diameters upstream of the test section). Two additional thermocouples, respectively 10 and 20 diameters from the test section, were passed through the plexiglass wall into the airflow. These thermocouples, whose readings were always identical, yielded the inlet bulk temperature for the test section.

A mixing box was positioned at the downstream end of the test section for the determination of the exit bulk temperature. In view of the asymmetric heating of the airflow, the conventional three- or four-disk mixing box, with either centrally or peripherally positioned throughflow holes in the consecutive disks, is not sufficient for the mixing task. Instead, a special mixing box was designed to promote large scale transverse and circumferential motions (complete drawings are available in [6]). Thermocouple traverses immediately downstream of the mixing box indicated temperature uniformity to within 1 or 2 μV. For the actual temperature measurement of the mixed airflow, two thermocouples were employed, each installed in a six-legged star-shaped copper structure that spanned the cross section of the mixing box at its downstream end.

Minimization of extraneous heat losses. The special measures employed to minimize extraneous heat losses will now be described. The need for extra care in the present experiments stems from the use of a thick-walled heated duct. Direct face-to-face contact of the upstream and downstream edges of the duct with the walls of the development section and of the mixing box would provide active conduction paths for heat loss and, therefore, the cross sections of those paths must be minimized. We will deal here with the adopted measures for curbing heat losses

from the heated test section to the hydrodynamic development section, to the mixing box, and to the surroundings.

Consider first the mating between the aluminum walls of the test section and the corresponding plexiglass walls of the hydrodynamic development section. As shown in Fig. 2, full-face contact was avoided in favor of contact between a thin lamina A, which extends downstream from the plexiglass wall, and the aluminum wall. To prepare for this arrangement, a lap-like recess, 1.27-cm (0.5-in.) long and with a depth of approximately 0.046 cm (0.018 in.), was machined at the downstream end of the plexiglass wall. Then, a 2.54-cm (1-in.)-long phenolic lamina A was cemented into the recess, and the resulting surface was finished smooth. The forward edge of the phenolic extended 1.27 cm (0.5 in.) beyond the plexiglass, and it was this edge that contacted the aluminum.

To avoid leaks at the contact, a thin (0.005 cm, 0.002 in.) pressure-sensitive tape B was pressed in place as shown in Fig. 2. The main defense against leaks was made on the outer face of the walls. Here, a thicker plastic sheet C bridged between the two walls, with an air-tight seal being achieved with silicone rubber D. To hold the just-described arrangement in place, a pair of narrow isolated plexiglass struts (not shown in the figure) bridged the gap just under the plastic sheet C.

Direct contact between the two aluminum walls and their upstream plexiglass counterparts was avoided by the aforementioned arrangement. With regard to the lower, not-directly-heated, wall of the test section (i.e., the plexiglass wall), it extends continuously upstream into the hydrodynamic development section. To minimize conduction along this wall, a spanwise cut was made from the outside surface which reduced the wall thickness to half the original value of 0.318 cm (0.125 in.). This cut was made at the cross section at which the heating was initiated.

Attention will now be turned to the measures used to minimize extraneous heat

transfer between the downstream end of the test section and the mixing box. One of these measures was to reduce the conduction cross section of the aluminum walls by making a spanwise cut in each wall just upstream of the mixing box. The wall thickness at the location of the cut was 0.1 cm (0.040 in.) rather than the original thickness of 0.953 cm (0.375 in.). In addition, a spanwise cut was made in the lower (plexiglass) wall which locally reduced its thickness by a factor of two. Also, on the face of the mixing box which mated with the test section, numerous crater-like holes were drilled to reduce the cross section for heat conduction.

The measures for minimizing heat losses from the duct to the environment will now be discussed. To avoid heat conduction through structural supports, the entire assembly consisting of the hydrodynamic development section, the test section, and the mixing box was suspended by 0.043-cm (0.017-in.) diameter nylon line at five axial stations. The nylon line was carefully monitored for stretch and sag, and none was encountered after an initial break-in period.

The aforementioned assembly was positioned within an insulated chamber of cross sectional dimensions 25 x 25 cm (10 in. x 10 in.). The chamber walls were of styrofoam, leaving a hollow cavity 10 x 15 cm (4 x 6 in.) for the apparatus. Silica aerogel powder insulation, which has a thermal conductivity less than that of air, was poured into the cavity around the apparatus.

The other parts of the piping system were lagged with fiberglass insulation.

Other instrumentation. All thermocouples were made from 30-gage, calibrated iron and constantan wire. After installation of the thermocouples, they were led out of the insulation enclosure in a single bundle which terminated in a thermocouple junction box which contained connectors and switches. The box also contained aluminum bars and insulation to promote temperature uniformity. Thermocouple emfs were read with a Hewlett-Packard 3465A digital multimeter with a smallest digit of 1 μV.

For the test section pressure distribution, the pressure signals were sensed

by a Baratron solid-state capacitance-type meter capable of being read to as low as 10^{-3} torr. The Baratron provided a digital output which was read by the aforementioned HP multimeter.

The test section power input was regulated to ensure constancy and was read by a specially calibrated electrodynamometer wattmeter with a full-scale accuracy of 0.25 percent.

DATA REDUCTION

The main objective of the data reduction procedure was to yield axially local heat transfer coefficients for the heated walls of the triangular duct, both in the thermal entrance region and in the thermally developed region. The coefficients to be determined will represent circumferential average values at each axial station. Friction factors will also be deduced from the measured pressure distributions.

The local circumferential-average heat transfer coefficient for the heated walls is defined here as

$$h = (Q'/P_q)/(T_w - T_b) \qquad (1)$$

where Q' is the rate of convective heat transfer per unit axial length from the heated walls to the fluid, and P_q is the wetted perimeter of the heated walls. The temperatures T_w and T_b respectively represent the values for the heated wall and the bulk. It is worthy of note that all of the wall-embedded thermocouples (i.e, in the aluminum walls) at any axial station gave temperature readings within $0.02^{\circ}C$ of each other. Therefore, the heated walls may be regarded as being circumferentially uniform in temperature. All quantities in equation (1) pertain to a given axial station x.

In equation (1), only T_w is directly measured, whereas Q' and T_b are obtained from the data reduction procedure (P_q is equal to 7.92 cm (3.12 in.)). The starting point in the determination of Q' is the electric power dissipated in the resistance wire situated in the longitudinal grooves on the rear faces of the aluminum

walls*. Two corrections were applied to the power dissipation per unit length in order to obtain Q'. One of these is for the heat loss from the duct outer surfaces to the environment via conduction through the insulation. The other is for the heat which flows by conduction from the heated walls into the plexiglass wall (i.e., the lower wall) and then passes into the airstream by convection at that wall. The latter heat flow is, in fact, not a heat loss; rather it causes a rearrangement of the surface locations at which heat enters the airstream.

The determination of these two corrections involved a lengthy computation which is described in detail in (6) and will be discussed here only in broad terms. For the heat loss through the insulation, a two-dimensional, finite-difference conduction network was set up to accommodate the irregular solution domain encompassing the outer walls of the triangular duct and the somewhat irregular rectangular boundaries of the two zones of insulation (silica aerogel and styrofoam). The temperature inputs needed for these finite-difference solutions included the surface temperatures of the aluminum and plexiglass walls and the temperature of the air in the surroundings. Of these, the temperatures of the aluminum and of the surroundings were known from direct measurement, but the plexiglass surface temperature varies with spanwise position and only the mid-span value is available from measurement. The needed spanwise temperature distribution was obtained from the calculated temperature field in the plexiglass wall, the determination of which will now be described.

As already noted, heat is conducted into the plexiglass wall through its surfaces of contact with the heated aluminum walls and then flows by convection into the airstream. A fine-grid, two-dimensional finite-difference conduction network was superposed on the plexiglass wall to facilitate determination of the temperature distribution and the convective heat transfer. This computation was

*The wattmeter reading was corrected to take account of ohmic dissipation in small segments of heating wire that lay outside the grooves. Also, thermocouple lead losses, which were $\sim$ 0.1 percent, were prorated uniformly along the duct.

elevated from the routine by a philosophical issue related to the convective boundary condition.

To explore this issue, let y denote the direction normal to the inner surface of the plexiglass wall. Then, at that surface

$$-k_p(\partial T/\partial y) = \hat{h}(T - \hat{T}_b) \qquad (2)$$

where k_p is the thermal conductivity of the plexiglass. The quantities $\hat{h}$ and $\hat{T}_b$ respectively represent the heat transfer coefficient and bulk temperature that are relevant to the convective heat transfer at the plexiglass surface. A careful study of the problem reveals that either $\hat{h}$ or $\hat{T}_b$ must be provided as input and, with that, the solution will yield the other of the two via an iterative procedure which makes use of the measured temperature at the mid-span point on the rear face of the wall. The solution also makes use of the measured temperature of the aluminum walls, which is assumed to prevail at the interface with the plexiglass wall.

Both options were explored. In one, $\hat{h}$ was taken equal to the average heat transfer coefficient at the heated walls of the duct, while $\hat{T}_b$ was treated as an unknown. In the other, $\hat{T}_b$ was set equal to the bulk temperature for the cross section as a whole and $\hat{h}$ was the unknown. There was little practical effect of using one option versus the other, as reflected in the fact that the extreme difference in the resulting heat transfer coefficients for the heated walls was only three percent.

For the authors, the first option is more satisfying on physical grounds and, therefore, it has been used for the final data-reduction computations. We do not believe that the bulk temperature T_b, which is primarily set by the heat transfer rates at the aluminum walls, has very much influence on the rate of convective heat transfer at the plexiglass wall*; in a real sense, T_b is quite remote from the

*The calculated convective heat transfer rate at the plexiglass wall ranged from three to ten percent of the total convective input to the air over the Reynolds number range from 59,000 to 4000 (see Table V, p. 136 of {6}).

plexiglass wall. Furthermore, considering the similarity of the flow pattern adjacent to all three walls, it is not unreasonable to use the same h at the plexiglass wall as at the other walls.

The numerical solutions for the plexiglass wall yield the rate at which heat passes out of the heated walls at the surfaces of contact with the plexiglass. This, in turn, completes the determination of Q' for equation (1). These computations were performed at each instrumented axial station. The foregoing description was intended to sketch the broad outlines of the computation procedure, but not to reproduce the details given in {6}.

The bulk temperature appearing in equation (1) was computed by a step-by-step marching procedure that moved downstream along the duct, making use of the net heat transfer to the airstream at each station.

The effects of axial heat conduction in the aluminum walls were also examined. It was found that within the accuracy of the temperature instrumentation, significant effects of axial conduction could not be identified except at the most upstream stations at low Reynolds numbers. Owing to the uncertainty of the axial conduction corrections (i.e., large changes in $\partial^2 T/\partial x^2$ in response to small temperature uncertainties), the questionable data points will be omitted from the forthcoming presentation of results (see uncertainty analysis in Chapter 5 of {6}).

Once the local heat transfer coefficient had been determined from equation (1), the local Nusselt number was evaluated from

$$Nu = hD_h/k \tag{3}$$

where D_h is the hydraulic diameter of the duct (2.29 cm, 0.902 in.) and k is the thermal conductivity of the airstream at the local bulk temperature.

The measured axial pressure distributions yielded, in each case, a straight line on a p vs. x diagram, the slope of which was determined from a least-squares fit. This information was recast in dimensionless form via the friction factor

$$f = (-dp/dx)D_h/\tfrac{1}{2}\rho\bar{u}^2 \qquad (4)$$

where $\rho\bar{u}^2$ was evaluated at the midpoint of the axial length over which p was measured.

The heat transfer and friction factor results are parameterized by the Reynolds number Re defined as

$$Re = \bar{u}D_h/\nu = 4\dot{m}/\mu P \qquad (5)$$

in which $\dot{m}$ is the mass flow rate and P is the perimeter of the walls which bound the flow cross section. For the actual evaluation of Re, the rightmost term of equation (5) was used, with μ at the local bulk temperature.

In general, property variations did not play a major role in the results. The maximum wall-to-bulk temperature difference was about $10^{\circ}C$ ($18^{\circ}F$), and the maximum bulk temperature rise from inlet to exit was of the same general magnitude.

RESULTS AND DISCUSSION

The main focus of the presentation that follows will be the heat transfer results. Friction factors will also be presented, and they will be employed in correlating the fully developed heat transfer coefficients. To avoid interrupting the smooth flow of the heat transfer presentation, initial attention will be directed to the friction factor results.

Friction factors. The friction factor results are plotted as a function of the Reynolds number in Fig. 3, where the open circles represent the isothermal data and the blackened circles correspond to the heat transfer runs. These two sets of data are nearly coincident and show the trend of f decreasing with Re that is typical of flow in smooth ducts.

Three literature correlations are shown in the figure in order to provide a comparison with the present results. The two uppermost curves respectfully represent the Blasius and Prandtl circular tube correlations, which were applied here by employing the hydraulic diameter as the characteristic dimension. The comparison

shows that the hydraulic diameter concept is not sufficient to rationalize the difference between the tube and triangular duct geometries, leaving an accuracy gap for f of 10 to 15 percent. The lower curve represents a general noncircular duct friction factor correlation {8} which was specialized to the present configuration. In the range of Re > 7000, the present data agree with the correlation within two percent, on the average, thereby affirming its validity for the equilateral triangular duct. Since the correlation was developed for fully turbulent flow, the larger deviations at lower Reynolds numbers are not unexpected.

The square data symbols, which represent experimental results from {2}, lie slightly above the present data. Finite difference solutions were also performed in {2} for the Reynolds number range between 40,000 and 300,000. For Reynolds numbers between 40,000 and 60,000, the predicted friction factors are about two percent lower than those given by the correlation of {8}, which means almost exact agreement between the predictions and the present data. This agreement lends support to the computational model used in {2}.

Temperature distributions. Heat transfer data runs were made for eight Reynolds numbers between 4000 and 59,000. The measured axial temperature distributions display an interesting evolution in shape as a function of the Reynolds number, which is fully documented in {6}. Here, it will be sufficient to show results for two Reynolds numbers, one high and one low (59,130 and 6740), in order to illustrate the trends, and Figs. 4 and 5 have been prepared for this purpose.

In these figures, the temperature is made dimensionless in the form

$$(T - T_{bi})/(Q'_t/k) \qquad (6)$$

In this expression, T_{bi} is the inlet bulk temperature and k is the thermal conductivity of the air at the mean bulk temperature. The quantity Q'_t is the total rate of heat transfer to the air per unit axial length, encompassing contributions from the directly heated walls and from the indirectly heated lower wall. Since T_{bi},

Q'_t, and k are fixed constants for each data run, the axial variation of the dimensionless group of equation (6) is a true reflection of the axial temperature variation.

In each figure, there are three sets of data points. The uppermost set depicts the temperature variation along the heated walls (as noted earlier, the temperature of the heated walls is circumferentially uniform). The other two sets, both of which are in the lower part of the figure, respectively depict the calculated values of the bulk temperature and the measured temperatures along the midspan of the rear face of the lower wall.

Attention may first be turned to the high Reynolds number results, Fig. 5. The temperature distribution on the heated wall displays a classical pattern that reflects the uniform heating condition--namely, an initial rapid rise that evolves into an ascending straight line which parallels the temperature rise of the bulk. The bulk temperature itself departs only very slightly from a straight line, the departures being due to slight variations in the heat losses along the duct. The region in which there is parallelism between the heated-wall and bulk temperatures grows larger as the Reynolds number decreases.

Figure 5 also shows that the midspan temperatures on the lower wall fall below the bulk temperature at the higher Reynolds numbers, and this relationship continues to prevail for all Re > 10,000. There is a tendency for the two distributions to become parallel at the most downstream stations. That the temperature of the lower wall is relatively low at these Reynolds numbers is indicative of the low rate at which heat is conducted into the lower wall from the directly heated walls. This low rate of conduction is the result of the relatively efficient convective heat transfer from the directly heated walls to the airstream, which makes the conduction leakage path to the plexiglass relatively unattractive.

The fact that the rear-face midspan temperature of the lower wall falls below the corresponding bulk temperature should not be taken as an indication that heat

is being transferred from the airstream to the wall. In the lower part of the flow cross section, there is a zone of relatively low-temperature air (i.e., temperatures lower than the bulk temperature). It is the temperatures of the air in that zone, rather than the bulk temperature, which controls the magnitude and direction of the convective heat transfer at the lower wall.

The temperature distributions for Re = 6740 (Fig. 4) are quite different from those for Re = 59,130 which were just discussed. These differences evolve progressively with decreasing Reynolds number, as is evidenced in the successive figures presented in {6}. The main characteristics of the low Reynolds number distributions are: (a) parallelism between the heated-wall and bulk temperature distributions that is in force along most of the length of the duct, (b) temperatures on the lower wall that exceed the bulk temperature, and (c) a droop of the heated-wall temperature distribution near the downstream end of the duct.

The first of these characteristics implies a very short thermal development length, and we will return to this matter shortly when the Nusselt number results are presented. The second and third characteristics indicate the strenthened role of heat conduction which results from the less efficient convective heat transfer at the directly heated walls when the Reynolds number is low. Thus, the droop in the heated-wall temperatures at the downstream end of the duct is due to extraneous conduction to the mixing box. Furthermore, conduction from the heated walls into the lower wall is responsible for the elevation of the latter's temperature above the bulk.

Nusselt numbers and thermal entrance lengths. Circumferential-average Nusselt numbers for the heated walls have been determined at a succession of axial stations by employing the data reduction procedures described earlier. These results are presented in Fig. 6, where the Nusselt number is plotted against the dimensionless axial coordinate x/D_h (x = 0 corresponds to the beginning of the heated test section). The figure displays axial distributions for eight Reynolds numbers in the range from

4070 to 59,130. Supplementary data runs for the two lowest Reynolds numbers and for Re ≈ 29,000 yielded results so close to those in the figure that they could not be plotted separately.

Examination of the figure shows the expected trend whereby higher Nusselt numbers correspond to higher Reynolds numbers. Also, the curves for the higher Reynolds numbers display the classic developmental pattern characterized by relatively high heat transfer coefficients near the inlet which decrease smoothly throughout the thermal entrance region and ultimately attain an axially unchanging fully developed value. It is, however, interesting to note that at these Reynolds numbers, the entrance length, as measured in terms of the hydraulic diameter, is rather long; in fact, fully developed conditions are just barely achieved. As the Reynolds number decreases, the length of the entrance region decreases markedly. (Note that at the two lowest Reynolds numbers, data affected by axial conduction have not been presented).

For a quantitative characterization, the thermal entrance length may be defined as the axial location at which the heat transfer coefficient approaches to within five percent of its fully developed value. Entrance lengths corresponding to this definition are presented in Fig. 7, where the marked increase with Reynolds number is clearly evident. To obtain perspective about these results, the relevant literature may be examined. For triangular-duct heat transfer, no entrance lengths were determined in {3} (only average coefficients were measured), while in {5} the large property-related Reynolds number variations along the duct make the definition of an entrance length quite uncertain. In {4}, for a small apex-angle triagular duct, very large entrance lengths were encountered.

Also relevant are the experiments of {9} involving turbulent airflow in a circular tube heated on only half of its circumference. There, it was found that the thermal entrance lengths were considerably greater than those for a circumferentially uniformly heated tube; furthermore, the entrance lengths increased markedly with

Reynolds number, as in the present experiments.

From the foregoing, it can be concluded that nonuniform heating increases the length of the thermal entrance region. The noncircular geometry of the duct cross section may also be a contributing factor.

Fully developed Nusselt numbers. It is relevant to compare the fully developed Nusselt numbers to literature information and to seek the best possible correlation. From the literature, we take the venerable Dittus-Boelter correlation and the newer Petukhov-Popov correlation {1}, respectively

$$Nu = 0.023Re^{0.8}Pr^{0.4} \tag{7}$$

and

$$Nu = (f/8)RePr/(1.07 + 12.7(Pr^{2/3} - 1)(f/8)^{1/2}) \tag{8}$$

where

$$f = (1.82 \log_{10}Re - 1.64)^{-2} \tag{9}$$

Both of these correlations were developed for circular tubes and are specified to be applicable for Re > 10,000.

Equations (7) - (9) have been evaluated using the hydraulic-diameter Reynolds number and are compared with the present data in Fig. 8. For Re > 10,000, the Dittus-Boelter equation overpredicts the data by about thirty percent, while the Petukhov-Popov equation is about fifteen percent above the data*. Although this comparison adds further confirmation of the superiority of the Petukhov-Popov correlation relative to that of Dittus-Boelter, it also demonstrates that the hydraulic diameter does not provide an adequate rationalization of the non-circular geometry.

In considering the causes of less-than-successful performance of the literature correlations, specifically Petukhov-Popov, note may be taken of Fig. 3 which indicates that the circular-tube friction factor results deviate from those of the equilateral triangular duct, even when the hydraulic diameter is employed. This suggests the use of the measured triangular-duct friction factors as input to the

*The Sleicher-Rouse correlation {10} is within about one-half percent of Petukhov-Popov.

Petukhov-Popov equation (8), replacing the circular-tube friction factor equation (9). When this is done, a duct-specific Petukhov-Popov prediction is obtained, as shown in Fig. 9 along with the experimental data. For Re > 10,000, the duct-specific prediction agrees with the data in the 1 - 5 percent range. This level of agreement is actually better than that achieved when the Petukhov-Popov correlation is compared with circular tube data.

Although a fully certain recommendation cannot be made at this time, it appears reasonable, when employing the Petukhov-Popov correlation for a non-circular duct, to input the friction factors for that duct, provided that they are available.

As an alternative correlation of the present data, a power-law fit yields

$$Nu = 0.019Re^{0.781} \tag{10}$$

to an accuracy of about four percent.

The present data will now be compared with the results of the turbulent-flow finite-difference solutions of {2}. For these solutions, the thermal boundary condition was circumferentially uniform temperature (on all three walls) and axially uniform heat input. Numerical results are reported only for Re > 40,000. Comparison with the present data for the two highest Reynolds numbers yields agreement within four percent (the prediction being high). This excellent level of agreement lends support to the analytical model and its numerical implementation.

Natural convection effects. Out of concern for possible natural convection effects, supplementary data runs were made for each of the two lowest Reynolds numbers such that the Grashof number was varied by a factor of two, from 6×10^3 to 1.3×10^4. The Grashof number variation had no detectable effect on the Nusselt number {6}, and it was thus concluded that natural convection effects were negligible.

CONCLUDING REMARKS

The experiments reported here were designed with unusual care and attention to detail in order to provide research results of such quality as to serve as a

standard against which analysis can be compared. Special techniques were employed to minimize extraneous heat conduction. Numerical finite-difference solutions played an important role in both the design of the apparatus and in the data reduction.

The friction factor data underscored the fact that the hydraulic diameter is not completely successful in bringing circular tube correlations into agreement with noncircular duct results. The data did, however, support the predictions of a general noncircular duct correlation {8} as well as those from numerical solutions of a modeled turbulent flow {2}.

Nusselt numbers were determined both in the thermal entrance region and in the fully developed region of the duct. The length of the entrance region increased markedly with Reynolds number. Entrance lengths, based on a five percent approach to fully developed conditions, ranged from 18 to 40 hydraulic diameters over the Reynolds number range from 6700 to 57,000. These lengths are greater than those for conventional duct flows (for air) and are believed to reflect the unsymmetric heating.

The experimentally determined fully developed Nusselt numbers were compared with both the Dittus-Boelter and Petukhov-Popov circular tube correlations (applicable for $Re > 10,000$), with the hydraulic diameter replacing the tube diameter. Although the latter correlation yielded better agreement with the data than did the former, it was still about fifteen percent high. When the measured friction factors were used as input to the Petukhov-Popov equation, agreement between prediction and experiment to better than five percent was attained. This finding suggests that for a noncircular duct, the Petukhov-Popov equation be evaluated with the friction factor specific to that duct. The present data also support the Nusselt number predictions of {2} obtained via finite-difference solutions of a modeled turbulent flow.

REFERENCES

1. Petukhov, B. S., "Heat Transfer and Friction in Turbulent Pipe Flow with Variable Physical Properties," Advances in Heat Transfer, Vol. 6, Academic Press, 1970, pp. 503-564.

2. Aly, A.M.M., Trupp, A. C. and Gerrard, A. D., "Measurements and Prediction of Fully Developed Turbulent Flow in an Equilateral Triangular Duct," Journal of Fluid Mechanics, Vol. 85, 1978, pp. 139-149.

3. Lowdermilk, W. H., Weiland, W. F., and Livingood, J.N.B., "Measurement of Heat Transfer and Friction Coefficients for Flow of Air in Non-Circular Ducts at High Surface Temperatures," NACA RM E53J07, 1954.

4. Eckert, E.R.G. and Irvine, T. F., "Pressure Drop and Heat Transfer in a Duct with Triangular Cross Section," ASME Journal of Heat Transfer, Vol. 82, 1960, pp. 125-138.

5. Campbell, D. A. and Perkins, H. C., "Variable Property Turbulent Heat and Mass Transfer for Air in a Vertical Rounded Corner Triangular Duct," International Journal of Heat and Mass Transfer, Vol. 11, 1968, pp. 1003-1012.

6. Altemani, C.A.C., "Turbulent Heat Transfer and Fluid Flow Characteristics for Air Flow in an Unsymmetrically Heated Triangular Duct," Ph.D. Thesis, Department of Mechanical Engineering, University of Minnesota, Minneapolis, Minnesota, 1980.

7. Sparrow, E. M. and Altemani, C.A.C., "On Attaining Isothermal Convectively Cooled Surfaces with Rear-Side, Discrete Groove-Embedded Heaters," Numerical Heat Transfer, Vol. 2, 1979, pp. 129-136.

8. Malak, J., Hejna, J., and Schmid, J., "Pressure Losses and Heat Transfer in Non-Circular Channels with Hydraulically Smooth Walls," International Journal of Heat and Mass Transfer, Vol. 18, 1975, pp. 139-149.

9. Knowles, G. R. and Sparrow, E. M., "Local and Average Heat Transfer Characteristics for Turbulent Airflow in an Asymmetrically Heated Tube," ASME Journal of Heat Transfer, Vol. 101, 1979, pp. 635-641.

10. Sleicher, C. A. and Rouse, M. W., "A Convenient Correlation for Heat Transfer to Constant and Variable Property Fluids in Turbulent Pipe Flow," International Journal of Heat and Mass Transfer, Vol. 18, 1975, pp. 677-683.

FIGURE CAPTIONS

Fig. 1 Cross section of the heated test section

Fig. 2 Arrangement for minimizing heat conduction at the upstream end of the test section

Fig. 3 Friction factor results

Fig. 4 Axial temperature distributions, Re = 6740

Fig. 5 Axial temperature distributions, Re = 59, 130

Fig. 6 Axial distributions of the Nusselt number

Fig. 7 Thermal entrance lengths based on a five percent approach of Nu to its fully developed value

Fig. 8 Fully developed Nusselt numbers and comparisons with literature correlations

Fig. 9 Comparison of measured fully developed Nusselt numbers with the Petukhov-Popov correlation evaluated with the measured friction factors as input

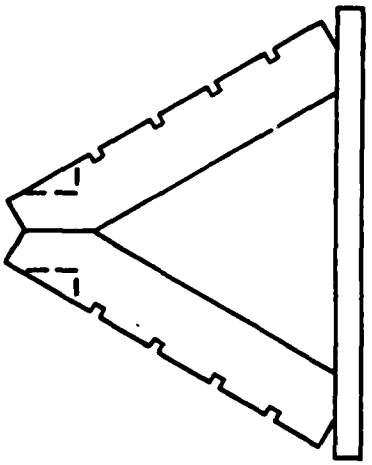

Fig. 1

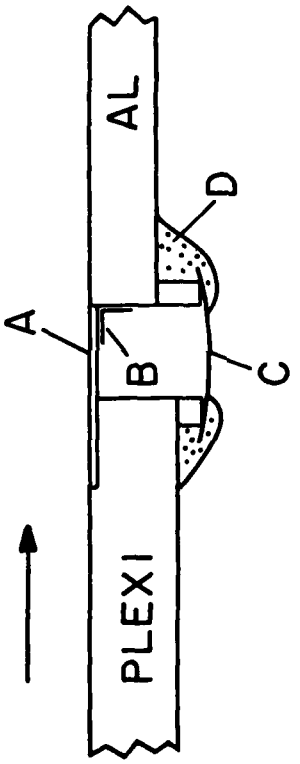

Fig. 2

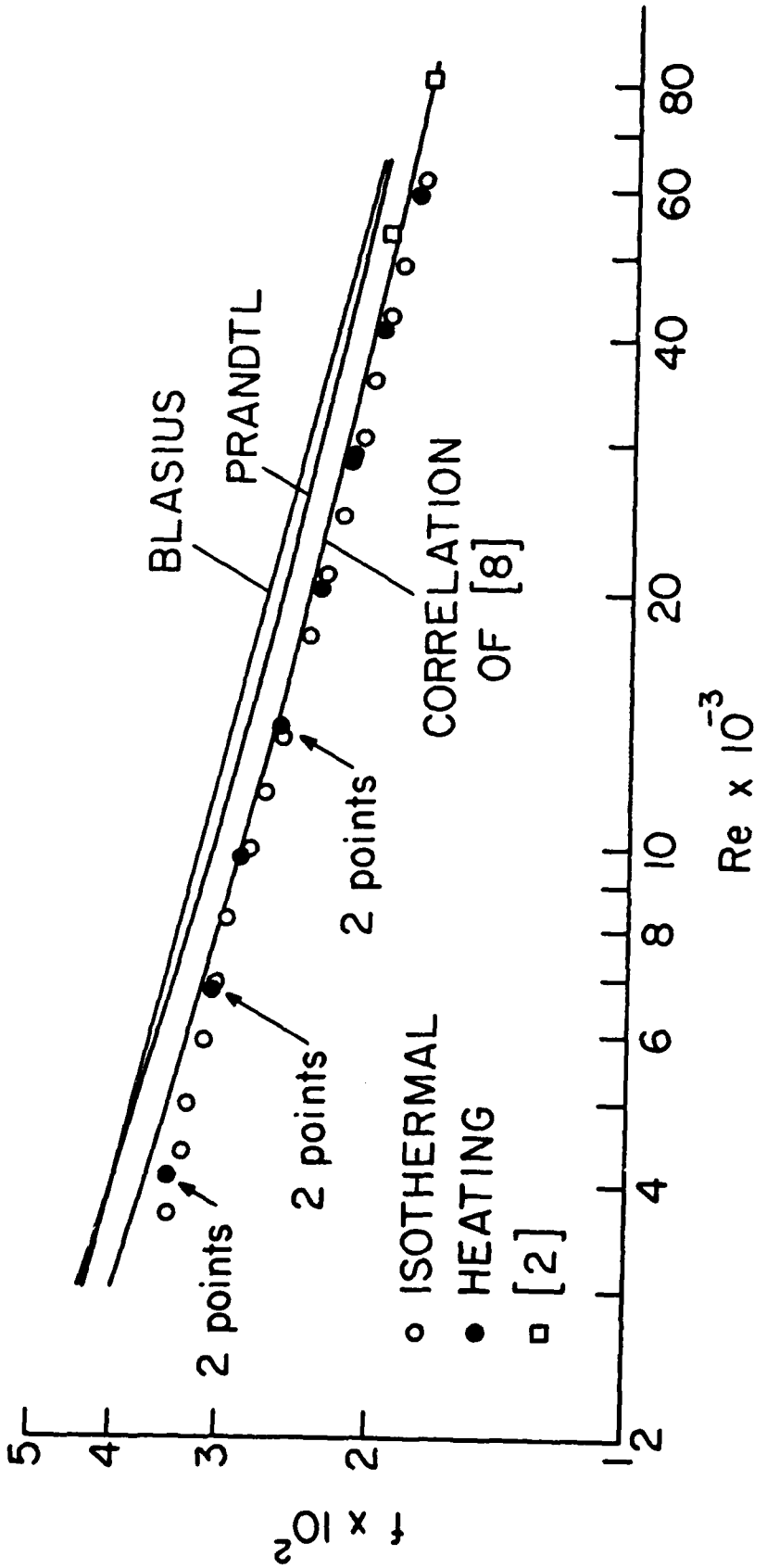
BLASIUS
PRANDTL
CORRELATION OF [8]
2 points
2 points
2 points
o ISOTHERMAL
● HEATING
□ [2]
f x 10²
Re x 10⁻³
1
2
3
4
5
2
4
6
8
10
20
40
60
80

Fig. 3

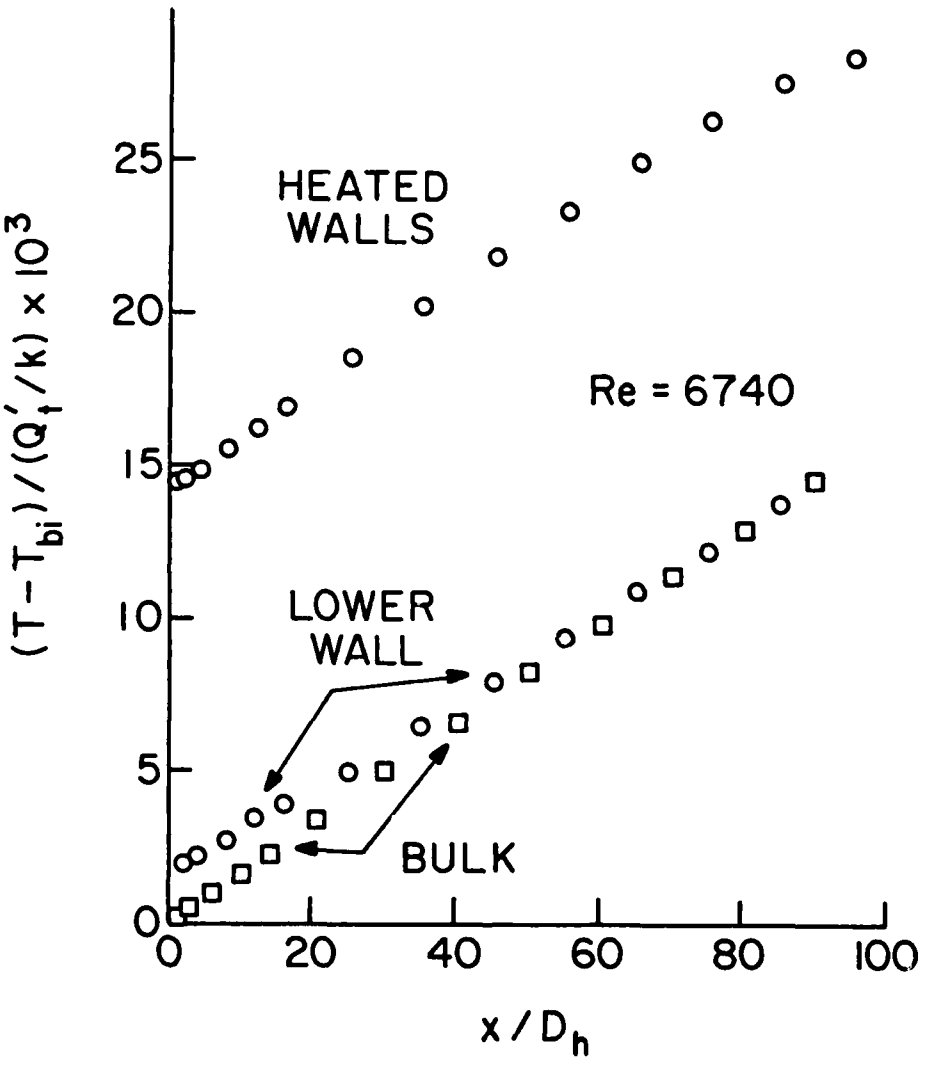
HEATED
WALLS
Re = 6740
LOWER
WALL
BULK
$(T-T_{bi})/(Q_t'/k) \times 10^3$
x/D_h
0
5
10
15
20
25
0
20
40
60
80
100

Fig. 4

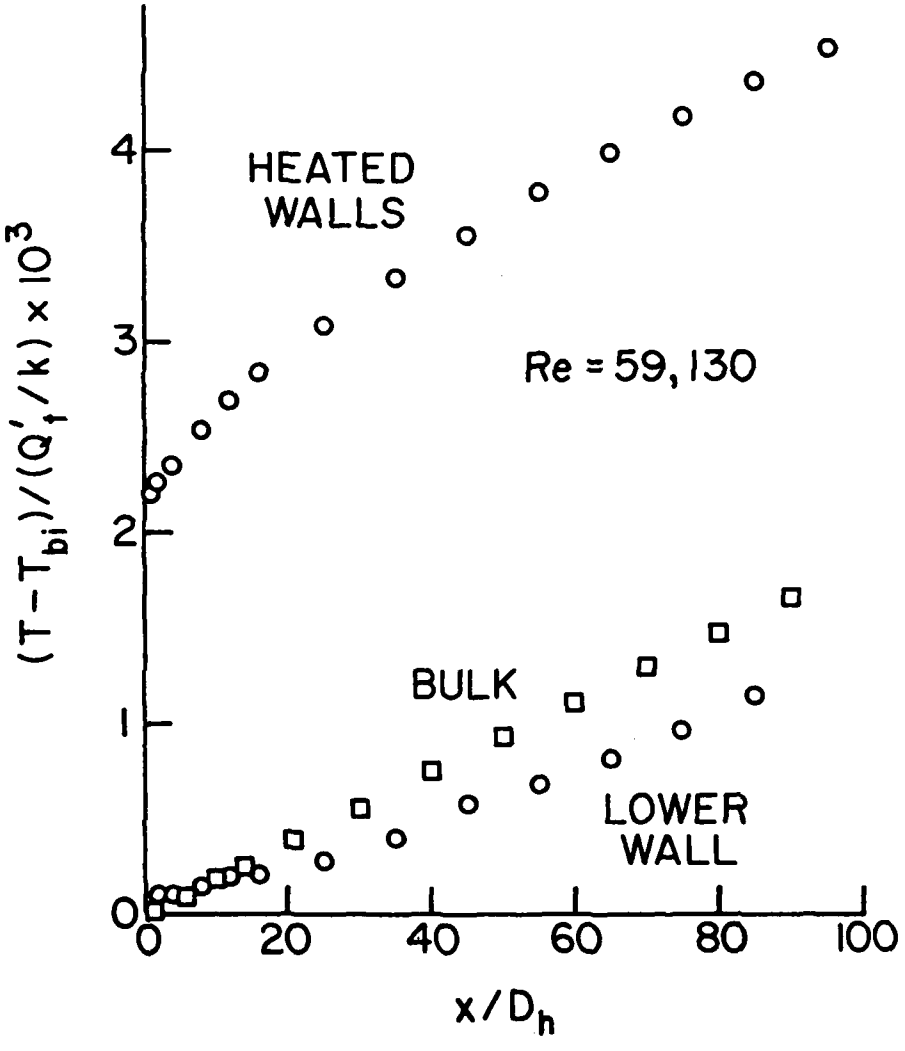
HEATED
WALLS
Re = 59,130
BULK
LOWER
WALL
$(T-T_{bi})/(Q'_t/k) \times 10^3$
x/D_h
0
1
2
3
4
0
20
40
60
80
100

Fig. 5

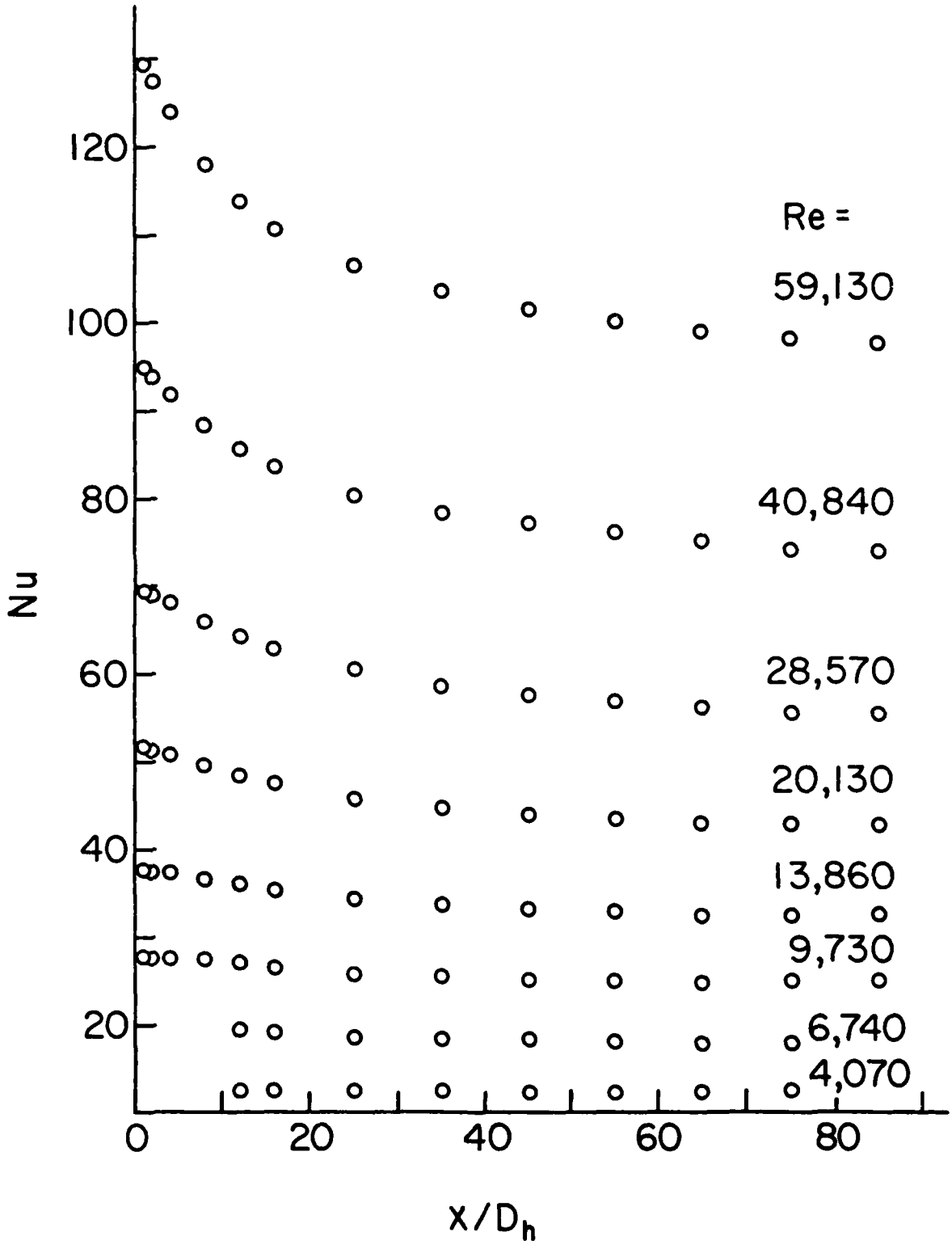
Nu
120
100
80
60
40
20
0
20
40
60
80
X/Dh
Re =
59,130
40,840
28,570
20,130
13,860
9,730
6,740
4,070

Fig. 6

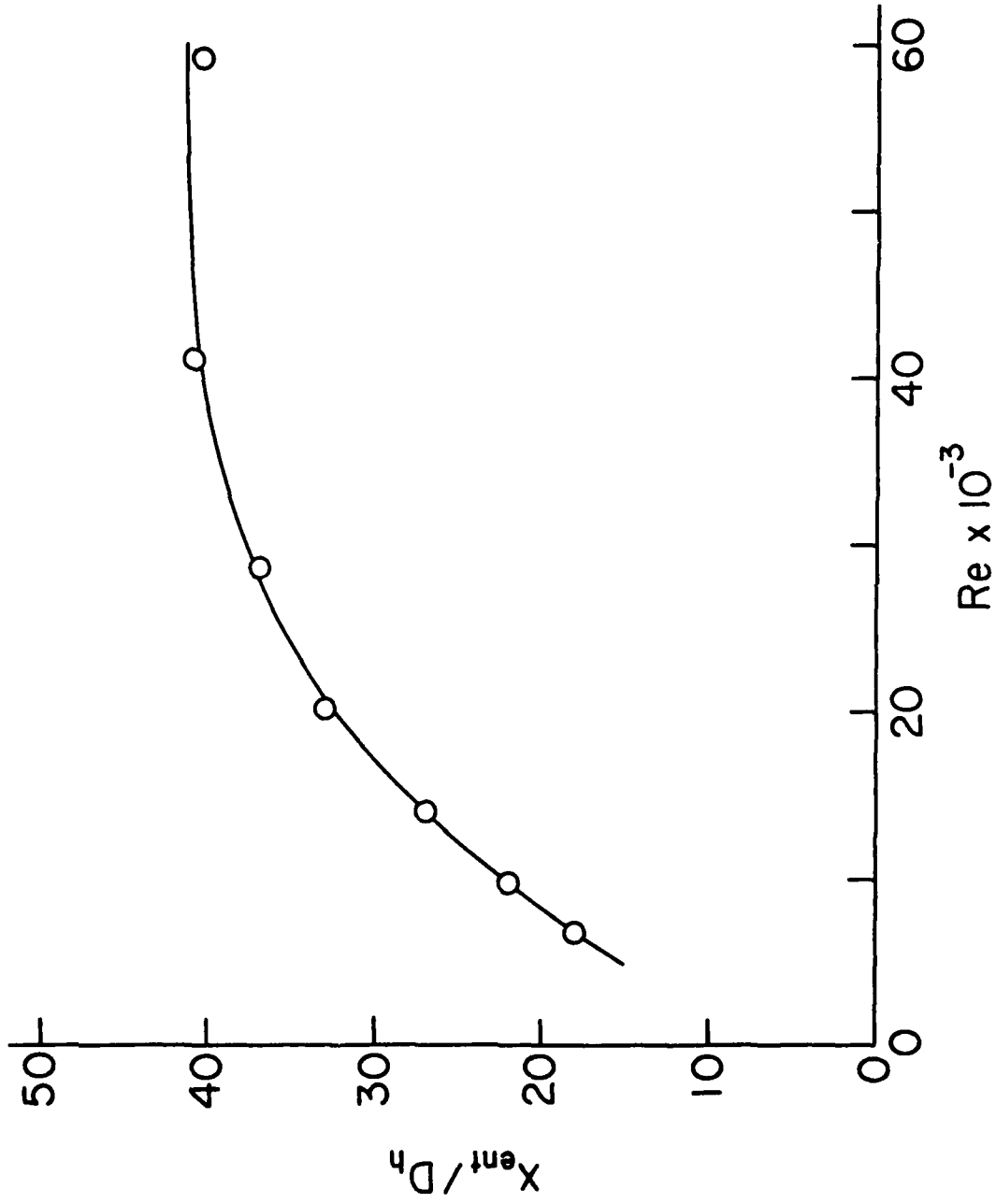

Fig. 7

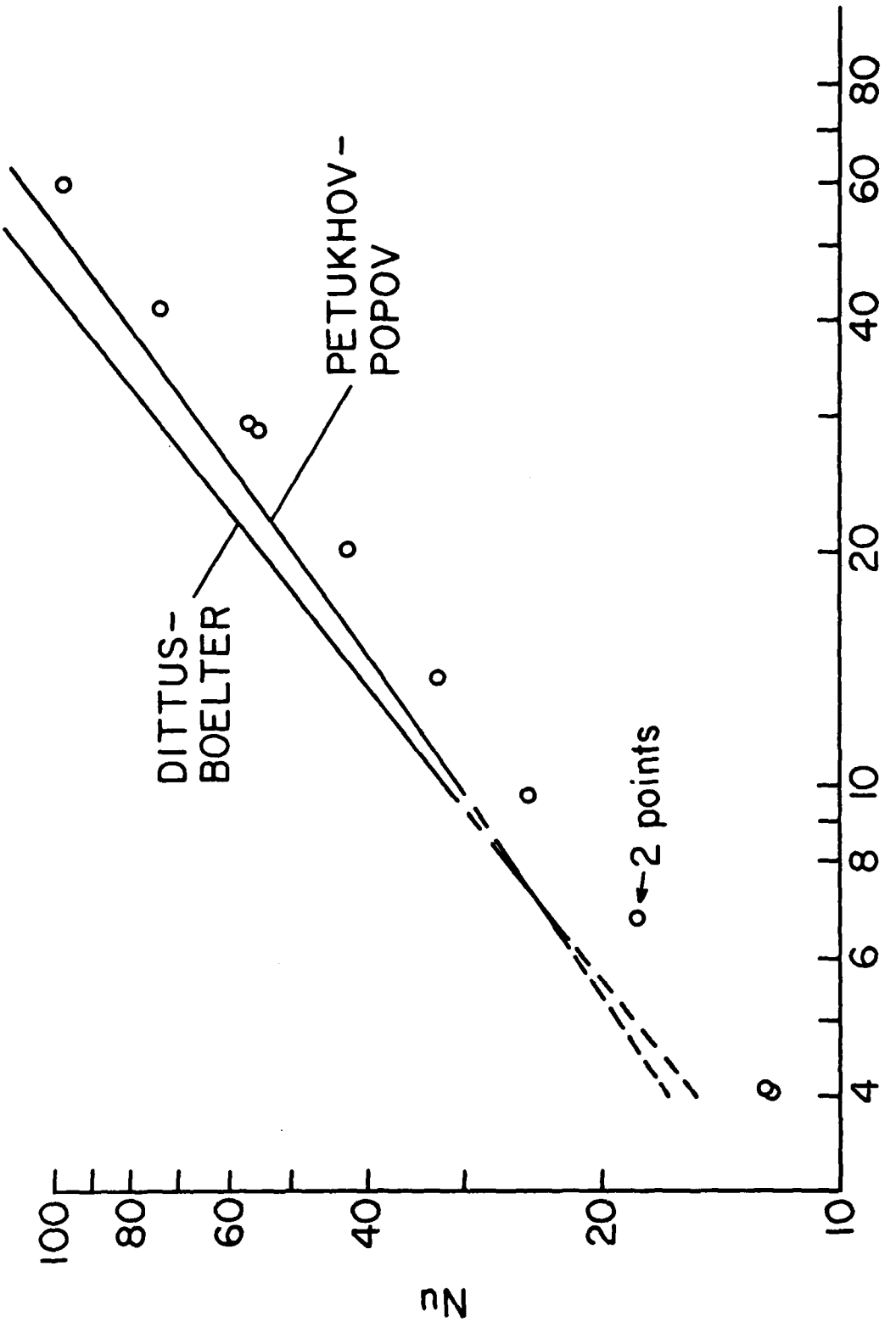
Nu
100
80
60
40
20
10
4
6
8
10
20
40
60
80
Re x 10^{-3}
DITTUS-
BOELTER
PETUKHOV-
POPOV
2 points

Fig. 8

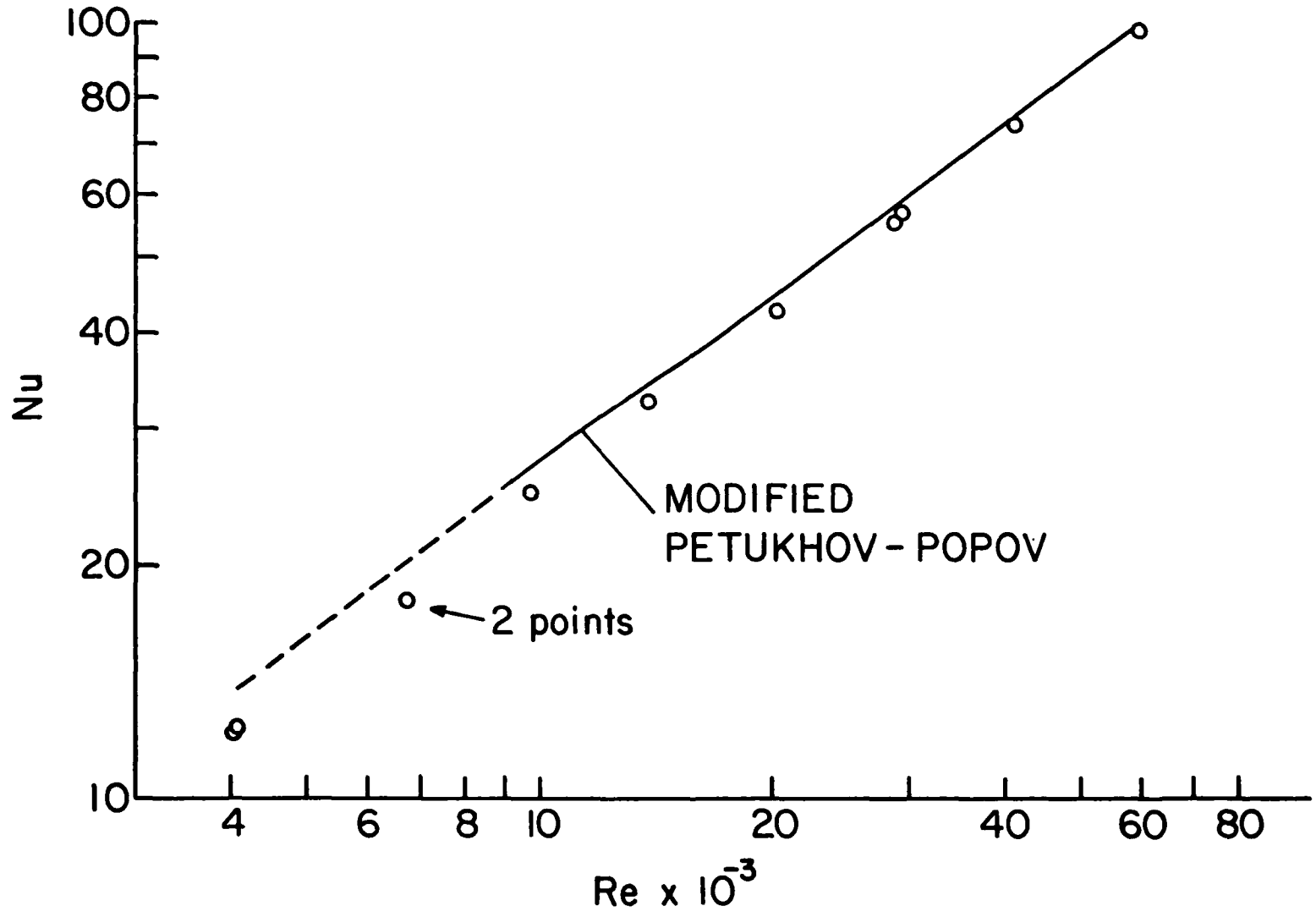
100
80
60
40
20
10
Nu
MODIFIED
PETUKHOV - POPOV
2 points
4
6
8
10
20
40
60
80
Re x 10^-3

Fig. 9

DISTRIBUTION LIST

HEAT TRANSFER

	One copy except as noted
Mr. M. Keith Ellingsworth Power Program Office of Naval Research 800 N. Quincy Street Arlington, VA 22203	5
Defense Documentation Center Building 5, Cameron Station Alexandria, VA 22314	12
Technical Information Division Naval Research Laboratory 4555 Overlook Avenue SW Washington, DC 20375	6
Professor Paul Marto Department of Mechanical Engineering US Naval Post Graduate School Monterey, CA 93940	
Professor Bruce Rankin Naval Systems Engineering US Naval Academy Annapolis, MD 21402	
Office of Naval Research Eastern/ Central Regional Office Bldg 114, Section D 666 Summer Street Boston, Massachusetts 02210	
Office of Naval Research Branch Office 536 South Clark Street Chicago, Ill. 60605	
Office of Naval Research Western Regional Office 1030 East Green Street Pasadena, CA 91106	
Mr. Charles Miller, Code 05R13 Crystal Plaza #6 Naval Sea Systems Command Washinton, DC 20362	

Heat Exchanger Branch, Code 5223
National Center #3
Naval Sea Systems Command
Washington, DC 20362

Mr. Ed Ruggiero, NAVSEA 08
National Center #2
Washington, DC 20362

Dr. Earl Quandt Jr., Code 272
David Taylor Ship R&D Center
Annapolis, MD 21402

Mr. Wayne Adamson, Code 2722
David Taylor Ship R&D Center
Annapolis, MD 21402

Dr. Win Aung
Heat Transfer Program
National Science Foundation
Washington, DC 20550

Mr. Michael Perlsweig
Department of Energy
Mail Station E-178
Washington, DC 20545

Dr. W.H. Theilbahr
Chief, Energy Conservation Branch
Dept. of Energy, Idaho Operations Office
550 Second Street
Idaho Falls, Idaho 83401

Professor Ephriam M. Sparrow
Department of Mechanical Engineering
University of Minnesota
Minneapolis, Minnesota 55455

Professor J.A.C. Humphrey
Department of Mechanical Engineering
University of California, Berkeley
Berkeley, California 94720

Professor Brian Launder
Thermodynamics and Fluid Mechanics Division
University of Manchester
Institute of Science & Technology
P088 Sackville Street
Manchester M601QD England

Professor Shi-Chune Yao
Department of Mechanical Engineering
Carnegie-Mellon University
Pittsburgh, PA 15213

Professor Charles B. Watkins
Chairman, Mechanical Engineering Department
Howard University
Washington, DC 20059

Professor Adrian Bejan
Department of Mechanical Engineering
University of Colorado
Boulder, Colorado 80309

Professor Donald M. McEligot
Department of Aerospace and Mechanical Engineering
Engineering Experiment Station
University of Arizona 85721

Professor Paul A. Libby
Department of Applied Mechanics and Engineering Sciences
University of California San Diego
Post Office Box 109
La Jolla, CA 92037

Professor C. Forbes Dewey Jr.
Fluid Mechanics Laboratory
Massachusetts Institute of Technology
Cambridge, Massachusetts 02139

Professor William G. Characklis
Dept. of Civil Engineering and Engineering Mechanics
Montana State University
Bozeman, Montana 59717

Professor Ralph Webb
Department of Mechanical Engineering
Pennsylvania State University
208 Mechanical Engineering Bldg.
University Park, PA 16802

Professor Warren Rohsenow
Mechanical Engineering Department
Massachusetts Institute of Technology
77 Massachusetts Avenue
Cambridge, Massachusetts 02139

Professor A. Louis London
Mechanical Engineering Department
Bldg. 500, Room 501B
Stanford University
Stanford, CA 94305

Professor James G. Knudsen
Associate Dean, School of Engineering
Oregon State University
219 Covell Hall
Corvallis, Oregon 97331

Professor Arthur E. Bergles
Mechanical Engineering Department
Iowa State University
Ames, Iowa 50011

Professor Kenneth J. Bell
School of Chemical Engineering
Oklahoma State University
Stillwater, Oklahoma 74074

Dr. James Lorenz
Component Technology Division
Argonne National Laboratory
9700 South Cass Avenue
Argonne, Illinois 60439

Dr. David M. Eissenberg
Oak Ridge National Laboratory
P.O. Box Y, Bldg. 9204-1, MS-0
Oak Ridge, Tennessee 37830

Dr. Jerry Taborak
Technical Director
Heat Transfer Research Institute
1000 South Fremont Avenue
Alhambra, CA 91802

Dr. Simion Kuo
Chief, Energy Systems
Energy Research Laboratory
United Technology Research Center
East Hartford, Connecticut 06108

Mr. Jack Yampolsky
General Atomic Company
P.O. Box 81608
San Diego, CA 92138

Mr. Ted Carnavos
Noranda Metal Industries, Inc.
Prospect Drive
Newtown, Connecticut 06470

Dr. Ramesh K. Shah
Harrison Radiator Division
General Motors Corporation
Lockport, New York 14094

Dr. Ravi K. Sakhuja
Manager, Advanced Programs
Thermo Electron Corporation
101 First Avenue
Waltham, Massachusetts 02154

Mr. Doug Marron
Engine R&D Branch, Code 5231
NC #4
Naval Sea Systems Command
Washington, D.C. 20362
(Tel 202-692-6874)

Mr. Richard S. Carlton
Director, Engines Division, Code 523
NC #4
Naval Sea Systems Command
Washington, D.C. 20362
(Tel. 202-692-6868)

Mr. Richard F. Wyvill
Engine Design Branch, Code 5232
NC #4
Naval Sea Systems Command
Washington, D.C. 20362
(Tel 202-692-6931)

Mr. Walter Ritz
Code 033C
Naval Ships Systems Engineering Station
Philadelphia, Pennsylvania 19112
(Tel. 215-755-3841)

Dr. Simion Kuo
United Tech. Res. Center
Silver Lane
East Hartford, Conn. 06108
(Tel. 203-727-7258)

Mr. T.M. Herder
Bldg. 464-G2
General Electric Co.
1100 Western Ave.
Lynn, Massachusettes 01910
(Tel. 617-594-3360)

Mr. Ed Strain
AiResearch of Arizona
Dept. 76, Mail Stop 301-2
P.O. Box 5217
Phoenix, Arizona 85010
(Tel 602-267-2797)

Mr. Norm McIntire
Solar Turbines International
2200 Pacific Hwy.
San Diego, CA 92101
(Tel. 714-238-6527)

Enclosure (3)

Mr. Robert W. Perkins
Turbotec Products, Inc.
533 Downey Drive
New Britain, Connecticut 06051

Dr. Keith E. Starner
York Division, Borg-Warner Corp.
P.O. Box 1592
York, PA 17405

Mr. Peter Wishart
C-E Power Systems
Combustion Engineering, Inc.
Windsor, Connecticut 06095

Mr. Henry W. Braum
Manager, Condenser Engineering Department
Delaval
Front Street
Florence, New Jersey 08518

Dr. Thomas Rabas
Steam Turbine-Generator Technical Operations Division
Westinghouse Electric Corporation
Lester Branch
P.O. Box 9175 N2
Philadelphia, PA 19113

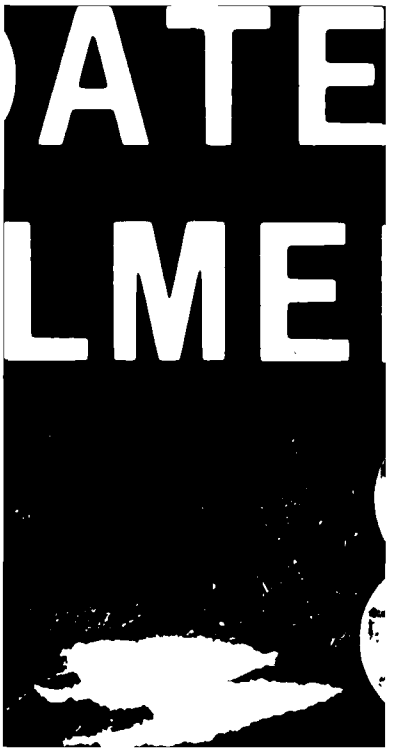
ATE
LME